RADIATION RESEARCH **177**, 398–435 (2012)
0033-7587/12 $15.00

DOI: 10.1667/RR2903.1

Magnetic Resonance Spectroscopy of Cancer Metabolism and Response to Therapy

Dominick J. O. McIntyre,[1] Basetti Madhu, Shen-Han Lee and John R. Griffiths

Cancer Research UK, Cambridge Research Institute, Li Ka Shing Centre, Robinson Way, Cambridge CB2 0RE, United Kingdom

McIntyre, D. J. O, Madhu, B., Lee, S-H. and Griffiths, J. R. Magnetic Resonance Spectroscopy of Cancer Metabolism and Response to Therapy. *Radiat. Res*. 177, 398–435 (2012).

Magnetic resonance spectroscopy allows noninvasive *in vivo* measurements of biochemical information from living systems, ranging from cultured cells through experimental animals to humans. Studies of biopsies or extracts offer deeper insights by detecting more metabolites and resolving metabolites that cannot be distinguished *in vivo*. The pharmacokinetics of certain drugs, especially fluorinated drugs, can be directly measured *in vivo*. This review briefly describes these methods and their applications to cancer metabolism, including glycolysis, hypoxia, bioenergetics, tumor pH, and tumor responses to radiotherapy and chemotherapy.

INTRODUCTION

Magnetic resonance spectroscopy (MRS) is a noninvasive and nonionizing analytical method that allows investigators to measure, and in some cases, visualize, biochemical information from living tissues. A particular strength of MRS is its applicability to a range of experimental systems, from cells and animals to humans. The past three-to-four decades have seen enormous developments in the application of MRS in studying metabolism in health and disease because it is the only method that can be used to interrogate metabolic information across these three model systems in a nondestructive manner. Additionally, observations made by *in vivo* MRS of a living tissue can be validated by *ex vivo* MRS of metabolites extracted from a sample or biopsy from that same tissue, since the latter technique has higher sensitivity and resolution.

In this article, we review studies of tumor metabolism using *in vivo* and *ex vivo* MRS methods. We have included studies ranging from cultured cells, *ex vivo* tumor tissue, experimental tumor models, and clinical data.

[1]Address for correspondence: Cancer Research UK, Cambridge Research Institute, Li Ka Shing Centre, Robinson Way, Cambridge CB2 0RE, UK; e-mail: Dominick.McIntyre@cancer.org.uk.

FUNDAMENTALS OF MAGNETIC RESONANCE SPECTROSCOPY

The signal in magnetic resonance imaging (MRI) images is derived from hydrogen nuclei found in water and fat where this is not suppressed, and are present at very high concentrations in tissue. Nuclear magnetic resonance (NMR) signals can also be detected from many other compounds present in tissue, both endogenous and exogenous compounds that are injected, ingested, or even inhaled. Measurements can be made *in vivo* with an appropriately equipped MRI scanner; useful data can also be acquired from *ex vivo* samples, including biopsies and samples of body fluids. Here, we briefly introduce metabolic MRS methodology and its key applications for various methods, to provide the reader with background for later sections arranged by MRS applications. The nuclei and key applications are summarized in Table 1.

Nuclei with odd numbers of protons, neutrons, or both, possess a magnetic moment that can be measured by magnetic resonance (MR), and metabolic studies most commonly employ MR measurements of ^{1}H, ^{19}F, ^{31}P, and ^{13}C, in descending order of sensitivity.

Nuclei in different chemical environments resonate at slightly different frequencies because local electronic distributions shield them to different degrees from the applied magnetic field; the detected signal can be Fourier-transformed to provide a spectrum containing one or more peaks from each metabolite, which may be exploited to identify and quantify the chemicals present. These peak frequencies are known as chemical shifts and are expressed as parts-per-million (ppm), because they are independent of the magnetic field used for a given scan, which simplifies comparisons between data acquired on different instruments. In addition to frequency, NMR signals are characterized by their relaxation times; T_2 is the exponential time constant for the decay of signal after excitation, and T_1 the time constant for recovery of equilibrium magnetization after it has been disturbed by excitation.

The concentrations of endogenous metabolites are much lower than water in living tissue; in different chemical environments, the resulting lower signal-to-noise ratio means that high-resolution metabolite imaging is not

TABLE 1
Summary of *In Vivo* MRS and *Ex Vivo* HR-MAS Applications in Cancer

Nucleus	Resonant frequency at 2.35T/MHz	Natural abundance of isotope (%)	Sensitivity relative to ^{1}H (%)	Application to metabolism and measurement of parameters
^{1}H	100.000	99.99	100.0	Glycolysis and end-products (lactate, pyruvate and alanine)
				Choline phospholipid metabolism (choline, PC, GPC)
				Energy metabolism (Cr and PCr)
				TCA-cycle (Glutamine, glutamate, succinate, citrate, fumarate)
				Amino acids (taurine, glycine)
				Neutral lipids (mobile lipids)
				Others (Acetate, NAA, aspartate, inositols)
				Extracellular pH (using exogenous extracellular ^{1}H probes)
^{31}P	40.517	100.0	6.65	Bioenergetics (ATP, ADP, AMP, PCr, sugar phosphates, NAD)
				Phospholipid metabolism (PME, PDE, DPDE)
				Intracellular pH (pH_i) by endogenous metabolites (intracellular phosphate)
				Extracellular pH (pH_e) by using exogenous extracellular probes
^{13}C	25.150	1.07	1.59	Metabolic flux of intermediary carbon metabolism using ^{13}C labeled probes (including hyperpolarized ^{13}C-labeled substrates)
^{19}F	94.057	100.0	83.2	Fluorinated drugs uptake (pharmacokinetics and pharmacodynamics)
				Metabolic pathways with fluorine-labeled substrates
				Oxygen tension (pO2)
				Extracellular pH (using exogenous extracellular ^{19}F probes)
^{23}Na	26.468	100.0	9.27	Ion transport mechanisms
				Edema and necrosis
^{2}H	15.35	0.01	0.96	Tissue water transport and exchange mechanisms

Note. Abbreviations used: ATP, nucleotide triphosphate; ADP, nucleotide diphosphate; AMP, adenosine monophosphate; Cr, creatine; DPDE, diphosphodiesters; GPC, glycerophosphocholine; NAD, nicotinamide adenine dinucleotide; PC, phosphocholine; PCr, phosphocreatine; PDE, phosphodiesters; PME, phosphomonoesters; TCA, tricarboxylic acid.

possible. A more acute problem for nuclei other than hydrogen is that the relative sensitivity to the applied magnetic field is lower. As a result, the spatial resolution for MR is low compared to that of MRI, with typical volumes around 1 ml for ^{1}H in a clinical setting.

NMR NUCLEI COMMONLY USED FOR METABOLIC STUDIES

^{1}H

At present, ^{1}H is the most commonly used nucleus in clinics; modern MRI systems can acquire ^{1}H MR spectra when provided with appropriate pulse sequences. Other nuclei require specialized coils as well as transmitters capable of a wide range of frequencies. However, pre-clinical systems are usually configured to be capable of multinuclear spectroscopy.

The tissue ^{1}H spectrum is dominated by signals from water and fat; other metabolites can be detected after suppression of the water signal (also, in some tissues, the signal from fat). The water signal itself may be used as a concentration reference for the other endogenous metabolites, although pathological changes in tissue water concentration and relaxation times may confound this method. There is no concentration reference equivalent to water for the other nuclei described below, for which ratio-based methods are generally used. ^{1}H data can also be presented as ratios of the common metabolites, particularly for chemical-shift imaging studies where the extra time required to obtain a water reference data set can extend the examination time beyond what is clinically acceptable.

A large number of endogenous metabolites are detectable by ^{1}H MRS, and are used to identify pathology, assess proliferation and necrosis, assess response to treatment, and differentiate tumor recurrence from radiation-induced necrosis. (These applications are discussed in greater detail later in this article.) The most prominent clinical applications at present for ^{1}H MRS are in the brain and prostate. Normal brain tissue can readily be identified by the high N-acetyl aspartate (NAA) resonance, a marker of neurones, which is reduced or absent in brain tumors; different brain tumors can be identified by differences in the presence and concentration of metabolites such as creatine (Cr), choline-containing compounds (Cho) [or total choline (tCho)], lipids, lactate (Lac), and myo-inositol (mI). Similarly, normal prostate tissue may be identified by high citrate (Cit) and polyamine resonances; Cit is drastically reduced or absent in tumor tissue.

^{31}P

A relatively small number of endogenous metabolites contain ^{31}P, including the molecules involved in energy metabolism; phosphocreatine (PCr), inorganic phosphate (P_i), and adenine triphosphate (ATP) are easily detected by

^{31}P MRS and therefore allow the energetic status of these tissues to be assessed. P_i has a pKa in the physiological range and variation in its electronic distribution with pH causes a change in shielding the phosphorus atom, resulting in a change in its chemical shift. This allows intracellular tissue pH to be measured directly from a ^{31}P spectrum, which revealed that tumor intracellular pH is normal, not acidic, as had long been believed (*1*). Additionally, magnetic resonances are visible from other metabolites including phosphomonoesters [PME: predominantly phosphocholine (PC) and phosphoethanolamine (PEth)] and phosphodiesters [PDE: glycerophosphocholine (GPC) and glycerophosphoethanolamine]. The line widths that can be obtained *in vivo* normally do not allow the ability to individually distinguish and quantify the metabolites in these peaks. 31P does not distinguish different tumor types as well as 1H MRS does (2).

^{13}C

^{1}H and ^{31}P represent 99.98 and 100% of naturally-abundant hydrogen and phosphorus. ^{13}C, however, makes up only 1.1% of naturally-abundant carbon, so that ^{13}C MRS of endogenous metabolites is two orders of magnitude less sensitive than ^{1}H, even before its lower sensitivity per nucleus is taken into account. Thus, ^{13}C studies frequently involve the administration of substrates labeled with ^{13}C, and the measurement of the incorporation of this label into other molecules, which greatly increases the signal and makes it possible to monitor, in real time, the uptake and incorporation of the ^{13}C-labeled substrate into other metabolites. Detection of the ^{13}C label is achieved using ^{13}C MRS (with ^{1}H decoupling) or heteronuclear (^{13}C-^{1}H) cross polarization, the latter technique offering higher sensitivity (*3*). Kinetic modeling of time series MRS datasets allows reconstruction of the flux through metabolic pathways (*4*). Again, this is not useful for identifying tumor types, but is perhaps the most powerful *in vivo* NMR tool for studying metabolism.

The most important development in recent years is the efficient hyperpolarization of ^{13}C-labeled small molecules, leading to 10,000-fold signal enhancements. Several hyperpolarization methods were used, with dynamic nuclear polarization (DNP) being the most successful. Ultimately, this technique is limited by longitudinal relaxation of the hyperpolarized substrate back to thermal polarization (*5*), which led to a search for compounds with relatively long value for the longitudinal relaxation rate T_1. The dominant relaxation mechanism in many small molecules is dipole-dipole interaction with adjacent ^{1}H nuclei; ^{13}C nuclei in quaternary positions, or that are part of carbonyl groups, have T_1s of tens of seconds, which is long enough to probe some metabolic effects. A commercial DNP hyperpolarizer (Oxford Instruments Hypersense) became available in 2006, and many studies on these metabolic effects have been published relating to cell systems as well as some animal measurements. The T_1 values are still short compared to conventional spectroscopic imaging methods; to minimize signal loss, rapid acquisition techniques are used at the expense of spatial resolution. It has been suggested that one way to partially compensate for this limitation is to use fast pulse sequences in combination with parallel detection methods (*6*).

A compound of particular interest is pyruvate, which is very quickly taken up into cells and converted to lactate. This process is catalyzed by lactate dehydrogenase (LDH), and depends on the presence of the NADH co-substrate. Day *et al*. (*7*) showed that hyperpolarized pyruvate-to-lactate conversion is detectable in cancers, and that the concentration of hyperpolarized lactate depends on the rate of exchange between hyperpolarized pyruvate and the endogenous pool of polarized lactate. It therefore depends on LDH activity, the presence of NADH co-substrate, and endogenous lactate concentration. A number of studies in cell systems and animals will be described later in this article.

The first clinical studies, in which prostate cancer patients were administered hyperpolarized pyruvate, began in December 2010, and can be found at this link: http://news.ucsf.edu/releases/new-prostate-cancer-imaging-shows-real-time-tumor-metabolism.

^{19}F

Unlike the nuclei described above, mammalian tissue contains no endogenous NMR-visible ^{19}F. Thus, there is no background signal to interfere with that from administered ^{19}F. A number of chemotherapeutic agents [particularly fluorouracil (5FU) and its prodrugs such as capecitabine and gemcitabine] contain ^{19}F; their biodistribution and metabolism can be mapped using ^{19}F MRS. As a result, metabolism of the parent drug can be measured *in vivo* if the products have different chemical shifts from the parent drug, which is a significant advantage over ^{18}F PET studies, which can accurately measure distribution but cannot distinguish breakdown products of the administered labeled agent.

METHODOLOGY

In Vivo Methods for Magnetic Resonance Spectroscopy

Localization

Spectra can be acquired using only the sensitive volume of the receiver coil for localization (typically referred to as nonlocalized), or using single- or multi-voxel localization methods. Single-voxel methods can give data from a small volume of better line width and lower contamination from neighboring tissue than is possible with a multi-voxel method, but provide no information on spatial variation in the metabolites being measured.

Non-localized Spectroscopy

Non-localized spectroscopy was common in early studies, but is now rarely used except for ^{19}F studies. It is typically used for metabolites with very short T_2 relaxation times, as it requires no time delay between the excitation and acquisition of signal, minimizing loss of signal to T_2 decay. Signal is detected immediately after a nonselective pulse, which excites signals from all the tissue visible to the coil. Localization to the region of interest is accomplished by the use of a receiver coil matched in size to the lesion of interest and placed directly over it. This is most successful for superficial lesions, as the sensitivity of the surface coil drops rapidly with distance. This frequently results in contamination of the data by signals from nontumor tissues (for example, extraneous signals from the high concentration of PCr in muscle in ^{31}P spectra), and localized methods are preferred.

Single-Voxel Localization Methods

A number of methods may be used to obtain a spectrum from a cuboidal region of tissue, while avoiding contamination from other tissue types nearby. PRESS (Point-RESolved Spectroscopy) and STEAM (Stimulated Echo Acquisition Mode), combined with water suppression, are used for ^{1}H spectroscopy. These methods require a delay [termed the echo time (TE)] of tens-to-hundreds of milliseconds between excitation and acquisition of the signal. TE can be chosen to optimize detection of metabolites of particular interest; for instance it may be chosen so that the spectrum from a particular coupled metabolite appears as simple as possible. Thus, long-echo ^{1}H spectra of tumors are often acquired with TE of 136 or 272 ms so that Lac appears as a doublet, inverted (at 136 ms) or in phase (at 272 ms) with respect to noncoupled peaks elsewhere in the spectrum. Long TE spectra provide information about fewer metabolites than short-TE data. However, lipid resonances and broad underlying macromolecular signals are largely eliminated; this simplifies interpretatin, and makes it easier to quantitate Lac, which is often hidden by large overlying lipid resonances in short-echo spectra. STEAM has been widely used for short-TE ^{1}H spectroscopy; however, modern scanners can achieve quite short TEs with PRESS, which also offers twice the signal of STEAM, which, as a result, is falling out of use. LASER (Localization by Adiabatic SElective Refocusing) (*8*) uses adiabatic pulses that are extremely insensitive to flip angle variation, which allows accurate localization with surface transmit-receive coils. Like PRESS and STEAM, LASER can acquire a spectrum in a single shot, though typically many averages are acquired to improve the signal-to-noise ratio. LASER uses a large number of radiofrequency pulses that reduce scalar coupling effects; the sequence can therefore be useful for quantitation of metabolites with strong couplings, such as glutamate and glutamine. Also, the pulses in this sequence give more sharply localized signals and can reduce chemical shift displacement, where the region of tissue that is actually excited changes with the chemical shift of each resonance, so that different metabolites are actually acquired from slightly different volumes of tissue. Chemical shift displacement is also a problem with the ISIS (Image-Selected *In vivo* Spectroscopy) method. This requires eight scans to provide a single localized spectrum, but acquires a signal immediately after excitation, which is suitable for short-T_2 metabolites and is routinely used for ^{31}P MRS.

Chemical Shift Imaging

Chemical shift imaging (CSI), or spectroscopic imaging, is a method for obtaining a 1D, 2D or 3D array of spectra from the tissue under investigation. Phase-encoding gradients are applied between excitation and detection of the MRS signal; multiple scans are acquired with different phase-encoding gradients in order to build up data that are Fourier transformed to obtain the grid of spectra. Typically, this may be 16×16 for a 2D scan, or $8 \times 8 \times 8$ for a 3D scan. The data may be presented as a grid of spectra, or as false-color maps of concentrations of different metabolites so as to more easily visualize the spatial variation of the metabolites. The grid may be shifted by a fraction of a voxel during reconstruction to allow the voxels to be conformed as closely as possible to the lesion of interest. Chemical shift imaging can be combined with any of the localization methods above to generate a spectral map of a region of interest within the body.

Quantitation Methods

Absolute quantitation of MRS data is difficult: the scaling factor between signal level and quantity of metabolite is unknown, and the signals depend on the sequence used and the relaxation times T_1 and T_2, as well as the number of nuclei. Often used are ratios to total signal, ratios to a single metabolite which is assumed relatively constant (often Cr in brain, for example), or to the values measured from contralateral normal-appearing tissue. ^{1}H data can be referenced to an unsuppressed water spectrum. External reference samples are sometimes used, and the ERETIC (Electronic REference To access *In vivo* Concentrations) method (*9*) employs an electronic reference signal for absolute quantitation. Computer programs are available that automatically measure individual metabolites, either by fitting to the peaks in the spectrum or to the untransformed original signal. jMRUI (*10, 11*) (which uses a range of methods from simple exponentials to quantum mechanical models to fit time domain data), and LCModel (*12*) (which uses model spectra of commonly observed metabolites to fit the spectrum), are commonly used for quantitating tumor metabolite data. A single peak in a spectrum may have multiple magnetically-equivalent nuclei contributing to it; for instance, nine protons contribute to the 3.2 ppm resonance of choline, and three protons to the 3.0 ppm

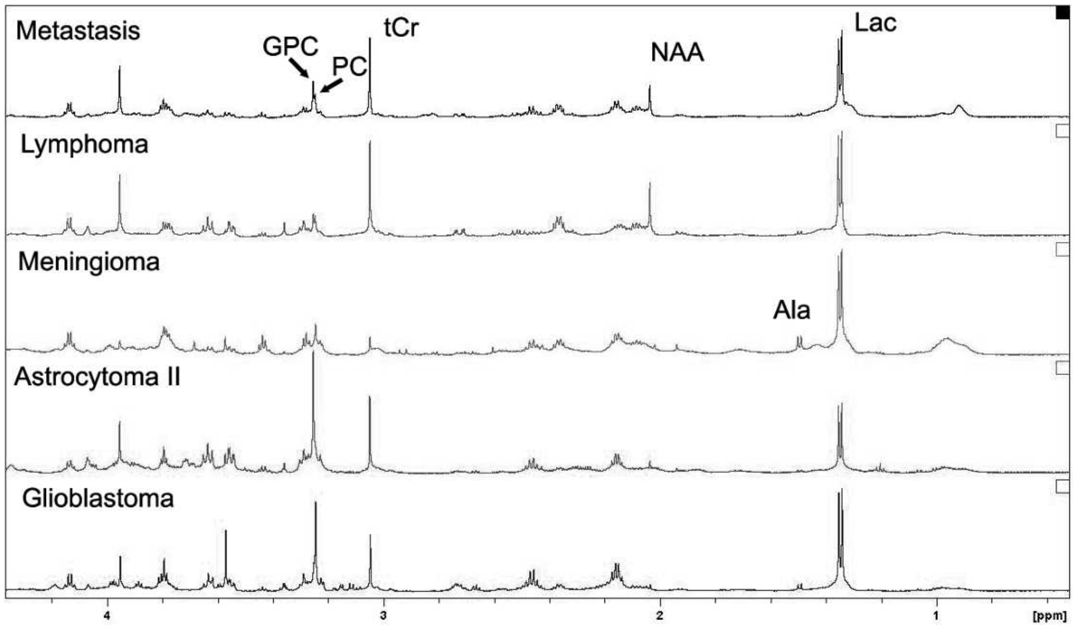

FIG. 1. Example of HR-MAS spectra from human brain tumor biopsies, showing the variation in metabolites between different tumor types and the narrow line widths obtained with this *ex vivo* method. (Image courtesy of Alan Wright, Nijmegen.)

resonance of Cr. This is a potential source of confusion when comparing studies based on simple peak area ratios with studies employing absolute concentrations, or metabolite ratios that have been corrected for the number of contributing nuclei.

In Vitro Samples: Metabolite Extracts From Cancer Cells and Tumor Tissues

To understand metabolism, cells are often used as model systems because they provide a controlled environment that can be manipulated by challenges, such as changes in temperature, pH, oxygen levels (normoxia, hypoxia), nutrient levels (ischemia), and growth factors (with or without serum in the media). Perchloric acid is used to extract water-soluble metabolites from cells and tissues (*13*); alternatively, a dual-phase chloroform/methanol extraction will yield separate aqueous and lipid fractions of metabolites (*14*). These metabolite extracts can be analyzed by high-resolution NMR spectroscopy (HR-NMR), with the resulting metabolite profiles allowing 25–40 different metabolites to be measured, either by pattern recognition methods or by estimating absolute concentrations. This rapidly-developing field of metabolomics uses solution state ^{1}H NMR spectroscopy as an analytical tool to obtain metabolic profiles from body fluids, such as plasma or urine, or from cell/tissue extracts.

Ex Vivo Samples: HRMAS of Preclinical and Clinical Biopsies

Magic angle spinning (MAS) was introduced in 1958 to remove the dipolar couplings and anisotropic interaction between spins that contribute to broad line widths observed in solid-state NMR spectroscopy (*15*). The spinning rates in solid state NMR are usually more than 10 kHz and may reach 20 kHz in some cases. Human or animal tissue can be investigated by MAS if spin rates are lowered to the range of 3–5 kHz, depending on the field strength, to ensure that spinning side bands lie outside the spectral range of interest while maintaining tissue integrity. Plant samples and lipids have been noninvasively analyzed by using MAS methods to reduce the broad line widths. This method is termed high-resolution magic angle spinning (HRMAS) to distinguish it from solid-state applications of magic angle spinning (*16–18*). In 1998, Cheng *et al*. established a correlation between quantitative neuropathology and HRMAS ^{1}H MRS data, obtaining, for the first time, useful *ex vivo* metabolic information from intact clinical biopsy samples (*19*). Subsequently, HRMAS has been applied to biopsies of human brain (*20*), breast (*21*) and prostate (*22*) tumors. Example data from brain tumors are presented in Fig. 1.

HRMAS ^{1}H MRS analysis of *ex vivo* tumor tissue has been used to validate *in vivo* observations. The Kauppinnen group applied *ex vivo* HRMAS ^{1}H MRS to validate the metabolic consequences observed *in vivo* following apoptosis induced by gene therapy in a rat glioma tumor model (*23, 24*). Another validation study of *in vivo* metabolic observations following treatment with a vascular disrupting agent in a mouse tumor model was performed by Madhu *et al*. using HRMAS ^{1}H MRS on *ex vivo* tumor samples (*25*).

As HRMAS applications of tissue analysis grew over the past 15 years, so has the demand for accurate metabolite quantitation of HRMAS NMR spectra. Several groups have used minor modifications of existing software packages such as LCModel (*26*), jMRUI (*27, 28*) and TARQUIN (*29*), to fit the observed peaks. The ERETIC method has been used for absolute quantitation of ^{13}C metabolites (*30*).

Gribbestad *et al*. have published several HRMAS ^{1}H NMR metabolomics studies of breast, brain, and prostate tumor samples (*31*). A combined transcriptomic and HRMAS ^{1}H NMR based metabolomics study in rat glioma showed the feasibility of following the molecular events that accompany metabolic perturbations during cell death processes (*32*). A recent review of HRMAS ^{1}H NMR studies on human cancer reported between 2005 and 2009, including cancers sited in lung, breast, prostate, brain, colorectal, and cervix, is available in the literature (*33*).

Although most of the HRMAS NMR applications in the last 15 years have been confined to ^{1}H NMR, owing to its high sensitivity relative to other nuclei, ^{31}P and ^{13}C NMR spectroscopic methods have been used to study bioenergetics, glycolysis, and lipid metabolism. Evaluation of ^{31}P HRMAS of intact tissue samples showed good agreement between tissue metabolite concentrations and concentrations measured from extracts of the same pieces of tissue (*34*). ^{1}H and ^{13}C HRMAS spectroscopy have been used to study intact *ex vivo* human high-grade glioma biopsies (*35*).

Advantages of HRMAS Analysis for Ex Vivo Biological Samples

Typically, HRMAS analysis uses tissue samples in the range of 10–30 mg, so it is very useful for small samples, such as clinical biopsies. Another useful application is the validation of *in vivo* metabolic observations with *ex vivo* samples, which allow much higher sensitivity and resolution of NMR signals (*23, 25*). In a recent *in vivo* ^{1}H MRS and *ex vivo* HRMAS ^{1}H NMR study on homogeneous-appearing human brain tumors, significant correlations were found between *in vivo* and *ex vivo* measurements of metabolites that are known to be metabolically stable in postmortem tissues (e.g., Cr, mI, tCho, and the 1.3 and 0.9 ppm lipid resonances). Anaerobic glycolysis during the biopsy process depletes tissue glucose, resulting in increased Lac and alanine resonances; there was no correlation between concentrations measured *in vivo* and *ex vivo* for these metabolites. It was concluded that *ex vivo* astrocytoma biopsy HRMAS ^{1}H NMR spectra have similar metabolic profiles to those obtained *in vivo*, and that detailed *ex vivo* characterization of glioma biopsies can be directly related to the original tumor within defined limitations (*36*).

HRMAS also allows the structural and metabolic integrity of samples to be preserved during analysis so they can be used further for other –omic (genomic, proteomic, etc.) analysis (*37*), and for histology, although there is inevitably some structural damage.

Cancer Metabolism

Cancer cells show several metabolic differences from normal cells. One of the earliest observed differences between tumor and normal tissue was glucose metabolism (*38*). The phenomenon of aerobic glycolysis in cancer, first described by (and later, eponymous of) Otto Warburg in the 1920s, denotes the increased propensity of tumor cells to convert glucose to lactate, even in the presence of oxygen.

In subsequent decades, studies of tumor metabolic biochemistry have revealed a diverse array of metabolic changes in cancer extending beyond the Warburg effect of aerobic glycolysis, notably alterations in the citric acid cycle, increased glutaminolysis, triglyceride biosynthesis, and choline phospholipid turnover (*39*). These metabolic changes collectively modulate levels of basic building blocks needed to give rise to new daughter cells (lipids, amino acids, and nucleic acids). In many cases, these metabolic changes are driven by increased oncogenic signaling and loss of tumor suppressive mechanisms. Thus, there is currently an increasing realization that cellular transformation and tumorigenesis involves the reprogramming of energy metabolism to meet the demands of cellular proliferation and adaptation to a hypoxic microenvironment within solid tumors (*40*).

In vivo MRS methods allow investigators to obtain quantitative information about these metabolites, which can provide a static or dynamic picture of the flux through the metabolic pathways.

MRS STUDIES OF GLYCOLYSIS IN TUMORS

The Molecular Basis of Glucose Metabolism in Tumors

The Warburg effect of aerobic glycolysis has been suggested to be a metabolic phenotype of proliferating cells in general, and of tumor cells in particular, although the reasons for this, as well as the benefits cells derive from engaging in a less-efficient form of energy metabolism still remain unclear.

Dysregulated growth-factor signal transduction pathways in human cancers, notably the phosphatidylinositol-3-kinase (PI3K)/Akt pathway, have been found to alter the central carbon metabolism of the cell and contribute to the Warburg effect. In particular, increased growth-factor signaling has been shown to promote glucose uptake into the cancer cell, and increase the activity of glycolytic enzymes. There is further evidence to suggest that growth-factor signaling can divert glycolytic intermediates into biosynthetic pathways for the production of lipids, nucleic acids, and amino acids, which are the building blocks necessary to make new daughter cells. Furthermore, in growing solid tumors, the glycolytic activity of cancer cells is enhanced where the microenvironment is hypoxic. In hypoxia, activation of the hypoxia-inducible factor (HIF) signaling pathway and transcriptional activity mediate cellular adaptation to hypoxia via the transcriptional upregulation of the expression of numerous target genes. Notably, an important subset of these genes include glycolytic enzymes such as LDH and pyruvate dehydrogenase kinase (*41, 42*).

Attempts to study the glycolytic activity of solid tumors *in vivo* by MRS have measured lactate as a surrogate marker, since this end product of glycolysis can be directly detected by ^{1}H MRS. Such studies have revealed much higher concentrations of Lac in tumors compared to normal tissues; in an experimental orthotopic rodent brain tumor model, the level of Lac was found to positively correlate with *ex vivo* histopathologically-assessed tumor cellularity (*43, 44*). The clinical application of ^{1}H MRS to measure Lac in human patients is yet to find widespread use, due to the difficulty of resolving Lac from broad overlapping lipid resonances. To overcome this technical limitation, there is currently much interest in developing Lac editing sequences for use in clinical ^{1}H MRS. In addition, there are several caveats to the use of ^{1}H MRS-detectable Lac as an indicator of glycolytic activity in cancer cells, mainly because this measurement provides only a static picture of the flux through the glycolytic pathway, and does not take into account the hemodynamics of Lac clearance, as well as the pooling of Lac in cystic or necrotic regions (*45, 46*).

To obtain a dynamic measure of glucose utilization by tumor cells, some investigators using experimental tumor models have infused 1-^{13}C glucose and monitored the production of 3-^{13}C Lac to calculate the apparent glycolytic rate (*3, 4*). This use of compartment modeling allows the precise determination of glucose uptake and Lac clearance rates. The feasibility of these strategies has been demonstrated in cancer cell lines (*47*) and in experimental tumor models (*48*). Importantly, in an orthotopic rodent glioma model, infusion of [1-^{13}C]glucose and detection by *in vivo* localized ^{1}H MRS indicated that the turnover of Lac was high (*43*). The ^{13}C label was observed only in Lac in the tumor, but not in the normal brain. Interestingly, 3-^{13}C Lac was also detected in the tissue immediately surrounding the tumor, suggesting the presence of tumor infiltration into the surrounding normal-brain parenchyma.

The robustness of the stable ^{13}C isotopic labeling strategy is reflected in its sensitivity to acute changes in glycolytic metabolism in perturbational studies (e.g., by changing tumor oxygenation using carbogen or carbon monoxide) (*49*). Importantly, this study revealed an inverse correlation between tumor oxygenation and glycolytic rate, suggesting that, at least in this tumor model, the Pasteur effect can have an impact on tumor metabolism. A limitation of this technique is the lack of information about cellular metabolic compartmentation. This may be important in human cancers since Lac may also originate from the stromal cells within the tumor, in particular, tumor-associated fibroblasts (*50, 51*) and inflammatory immune cells (*52, 53*).

Perhaps the most clinically-translatable method of assessing glycolysis *in vivo* is the use of hyperpolarized ^{13}C-pyruvate in conjunction with ^{13}C MRS, circumventing the inherently low sensitivity of standard ^{13}C MRS. A hyperpolarized ^{13}C-pyruvate study of the metabolism of a carcinosarcoma tumor model showed significantly higher Lac content than in the normal tissue (*54*). Furthermore, in a transgenic model of prostate cancer, elevated ^{13}C Lac levels have been observed in the primary and metastatic lesion, whereas normal prostate tissue was found to contain much less Lac (*55*). Hyperpolarized ^{13}C pyruvate has been reported to be sensitive to differences between tumor models with contrasting metabolic phenotypes; notably, the difference in pyruvate-to-Lac flux was shown to discriminate between two human brain tumor xenograft models with diametrically opposite metabolic and hypoxic properties (*56*).

In addition to its use as a marker of inherent metabolic differences between different tumor types, the calculated pyruvate-to-lactate flux might also serve as a suitable biomarker for tumor cell death in response to conventional chemo- and radiotherapies, in addition to new molecularly-targeted therapies. The rationale for using the pyruvate-to-Lac flux as a biomarker for cell death derives from the fact that this reaction depends on the presence of the cofactor NADH. In apoptotic cells, NADH is used to polyadenylate proteins for degradation, resulting in a depletion of the intracellular NADH pool and a reduction in the pyruvate-to-Lac flux. Reductions in pyruvate-to-Lac flux (usually by 30–50%) might be a useful surrogate of the extent of tumor cell death post-treatment (examples are discussed below in the sections on chemotherapy and radiotherapy.) Results of those preclinical studies suggest that reduction of pyruvate-to-Lac flux in a short time frame immediately after treatment, independent of changes in tumor size, might help identify patients that respond positively to these treatments.

The use of *in vivo* MRS is also important to validate the *in vivo* significance of any biochemical observations from cell culture systems, since cells might exhibit phenotypic differences when grown in culture (e.g., as the result of the routine use of 21% O_2, a concentration higher than typically experienced by tumor cells). For instance, inhibition of glycolysis by methionine is a phenomenon previously shown in transformed cells growing in culture. The inhibitory effect of methionine on glycolysis was confirmed by *in vitro* ^{1}H MRS of cell metabolite extracts, and was shown to be independent of any effect on the activity of the pentose phosphate pathway. However, *in vivo* ^{13}C MRS studies performed on experimental tumors revealed a lack of inhibitory effect of methionine on glycolysis (*57*). MRS has also been used to study the changes in intermediary carbon metabolism during cellular transformation. Hyperactivation of the Ras-MAP-kinase-signaling cascade is a critical step in cellular transformation and single-point mutations in the Ras oncoprotein family (H-Ras, K-Ras, N-Ras) is a common event in several human cancers. Aberrant Ras-MAP-kinase-signaling has been found to regulate metabolism by enhancing glycolytic flux to Lac. The effects of sequential immortalization and H-RasV12-transformation of human bronchial epithelial cells on the anabolic fate of fully-labeled ^{13}C-glucose-derived carbons was studied by using two-dimensional (2D) total correlated spectroscopic analysis NMR spectroscopy (2D TOCSY-NMR). Results of this study suggested that the oncoprotein H-RasV12 increases mitochondrial metabolism (*58*). Using ^{13}C labeled substrates in a ^{13}C NMR-based cancer cellular study, DeBerardinis *et al.* (*59*) showed that transformed cells can consume more glutamine than is required for nucleotide and protein synthesis. They proposed that this excess glutamine metabolism might facilitate the ability of transformed cells to use glucose-derived carbon and TCA cycle intermediates as biosynthetic precursors.

An *in vitro* ^{13}C MRS study of rhabdomyosarcoma (Rh30) cells and normal myocytes cultured in medium containing uniformly-labeled ^{13}C glucose revealed that the major difference between transformed and primary cells is the shift from energy and maintenance metabolism in the myocytes toward increased energy and anabolic metabolism for proliferation in the Rh30 cells. Results of this study suggest that mitochondria of the cancer cells are functional, and that Krebs cycle activity was considerably higher in cancer cells than in normal cells (*60*).

Observations from metabolic profiling of cellular extracts can also be verified by ^{13}C-isotopomer-based metabolic analysis of the extracts of tissues and blood plasma. After intravenously infusing uniformly-labeled ^{13}C-glucose to lung cancer patients prior to their surgery, ^{13}C MRS study of resected paired nonsmall-cell lung carcinoma and normal lung tissues from these patients showed that ^{13}C-enrichment of glycolytic (Lac, alanine) and the Krebs cycle metabolites succinate, glutamate, aspartate, and citrate, was higher in the tumors. This suggests that tumor tissues engage in higher rates of glycolysis and Krebs cycle compared to normal tissues (*61*).

MRS Studies of the Global Bioenergetic State of Cancer

An early application of ^{31}P MRS was in tumor metabolism; first in animals (*62, 63*), and then in humans (*64*). The early literature on MRS of experimental tumors has been reviewed by de Certaines *et al.* (*65*). In another influential early review, Negendank (*66*) analyzed a series of human studies with small cohorts. Instead of demonstrating that effective anti-cancer therapy would adversely affect tumor energy metabolism as it had in early preclinical ^{31}P MRS studies, the most significant changes in these clinical studies were in the PME and PDE peaks; they often occurred prior to any volume changes. A long-term multicenter study has been funded by the U.S. National Cancer Institute to follow up these preliminary findings. Preliminary reports indicate that low pre-treatment values for the ratio of (total phosphomonesters)/NTP are predictive of response to CHOP and RCHOP therapy for diffuse large B-cell lymphoma (*67–71*). Other studies have been reported in breast cancer (*72*) and other tissues, including sarcomas and head-and-neck cancers (*73*).

Despite the fact ^{31}P MRS was historically the first technique to be used to study tumors, this method has fallen out of favor in recent years, especially in the clinical setting, due to its relatively poor sensitivity. Nonetheless, the strength of this technique lies in its ability to directly measure signals from metabolites and breakdown products of energy metabolism, namely nucleoside triphosphate (NTP), nucleoside diphosphate (NDP), PCr, and P_i. Importantly, the levels of high-energy phosphates (NTP and PCr) depend on the availability of glucose and oxygen, both of which are delivered via the vasculature, and reflect the tight coupling between blood flow and energy metabolism. In the context of the Warburg effect and hypoxia within solid tumors, the energetic state is relatively low (*74*), and this has been confirmed using ^{31}P MRS (*75, 76*).

Perhaps the most important contribution and clinical promise of ^{31}P MRS has come from its application in the field of radiation oncology. The low energetic state of tumors and their tight coupling to oxygenation and blood flow have allowed many investigators to use ^{31}P MRS to monitor changes in tumor bioenergetics as a surrogate marker of tumor reoxygenation after radiation therapy, with the aim of detecting radiobiological hypoxia (as opposed to metabolic hypoxia) as a predictor of treatment failure (*77, 78*). This has been achieved in a number of different tumor models, where an increased energetic state was observed post-irradiation, indicative of tumor reoxygenation and response to treatment (*79*). Yet, the duration and extent of these energetic changes has varied substantially between different tumor lines (*80*). Nonetheless, an inverse association between these changes in energetic status and the fraction of radiobiologically hypoxic cells has been reported (*81*).

^{13}C MRS Studies of the TCA Cycle

The importance of the tricarboxylic acid (TCA) cycle in cancer cells and solid tumors is an area of great interest, especially because Otto Warburg erroneously proposed the absence or impairment of mitochondrial function to be the root of his eponymous effect in cancer cells. Although the assumption that mitochondrial function is impaired in cancer cells has long been disproved, the importance of the oxidative metabolism in meeting the ATP requirements of tumors is a subject of intense debate and investigation. Indeed, several metabolic balance studies performed on cancer cells in culture, and in experimental and human tumors *in vivo*, have revealed that as much as 80–90% of the ATP requirements are met by oxidative metabolism, whereas nonoxidative glycolytic metabolism contributes only 3–20% of the ATP requirements (*82–85*). In contrast, other investigators have attributed as much as 50% of ATP requirements to nonoxidative glycolysis alone (*86*). It is beyond the scope of this review to dwell on the finer points surrounding this debate, except to state that, far from being impaired, the TCA cycle is functionally active within cancer cells, and that there are particular tumor types that have high rates of oxidative metabolism (*82*). More importantly, the recent discoveries of neomorphic oncogenic point mutations in isocitrate dehydrogenase enzymes in human cancers by whole genome sequencing imply that the changes in the TCA cycle might have a pro-oncogenic role extending beyond its traditional function of generating ATP (*87, 88*). Thus, MRS techniques that allow the measurements of flux through the TCA cycle may find a use in distinguishing different tumor metabolic profiles, and in assessing treatment response to therapeutics that impact the TCA cycle.

Strategies to study the TCA cycle by *in vivo* MRS resemble those employed to study the glycolytic pathway. Several studies have reported the use of 1-^{13}C glucose and dynamic monitoring of the incorporation of the ^{13}C label into glutamate as a measure of the flux through the TCA cycle in cancer cells and *in vivo* tumors, and the results of these studies have revealed a significantly high flux, underscoring the importance of oxidative metabolism under these conditions (*89, 90*). Thus far, there have not been any reports of the use of hyperpolarized ^{13}C-labeled substrates to measure the TCA cycle in tumors *in vivo*. Nevertheless, this remains feasible in theory, at least according to extrapolated evidence originating from the field of cardiovascular biology. A recent study performed on perfused rodent hearts *in vivo* found that infusion of hyperpolarized 2-^{13}C pyruvate and its conversion to ^{13}C glutamate and citrate gives a direct measure of the TCA cycle flux (*91*). Importantly, acute ischemic challenge of the heart was shown to result in a reduction of ^{13}C glutamate and citrate, with an accompanying increase in ^{13}C-Lac, confirming a reduction in oxidative metabolism and an increase in nonoxidative glycolysis when the heart is subjected to ischemia (*91*). It remains to be seen if such a principle can be applied to study the TCA cycle in solid tumors.

Phospholipid Metabolism

In vivo ^{1}H spectra of tumors often show a large resonance at 3.2 ppm. This consists of free choline, PC, and GPC, and is often referred to as total choline (*66, 92*). It has been shown that the profile of choline compounds GPC and PC is drastically altered in malignantly-transformed mammary epithelial cells (*93, 94*). Further, in high-resolution ^{1}H and ^{31}P MRS of metabolite extracts of ovarian and breast cells, it was found that GPC was higher than PC in normal cells, but lower than PC in cancer cells (*93, 94*). Human breast, brain, and prostate tumor biopsies also demonstrated elevated choline signals in HRMAS ^{1}H NMR spectra (*31, 95, 96*). Elevated choline signals are observed by *in vivo* ^{1}H MRS in many human cancers. *In vivo* ^{1}H MRS of human breast tumors showed enhanced choline resonances (*97, 98*), and clinical trials are under way to establish *in vivo* ^{1}H MRS choline signals as a metabolic marker for chemotherapy in breast tumors (*97, 99*). Heerschap *et al.* (*100*) studied prostate cancer by *in vivo* ^{1}H MRS, finding that the average Cit/Cho signal ratio was significantly lower than for benign prostatic hyperplasia, and for noncancerous peripheral and central zone tissue, though this is in part due to reduction in Cit. An *in vivo* ^{1}H MR spectroscopy study of human head and neck lymph node metastasis found Cho signal intensity to be poorly correlated with pO_2, although it appeared to decrease at higher oxygenation levels (*101*). An *ex vivo* ^{1}H MRS study of gastric cancer lesions showed decreased levels of lipid peaks, elevated Lac doublet peaks, and increased intensity of Cho when compared with noncancerous gastric tissue (*102*). A combined proton-decoupled *in vivo* ^{31}P MRS and ^{1}H MRS study of untreated pediatric brain tumors measured total phosphorylated cholines (PC+GPC)/ATP with ^{31}P MRS and tCho with ^{1}H MRS; the authors found that, in these tumors, a large fraction of tCho-signal was not accounted for by PC and GPC (*103*), perhaps because partially-mobile cholines in membranes contribute to signal. *In vivo* ^{1}H MRS at 1.5T of primary and metastatic melanoma showed high levels of Cho, which was later validated with *ex vivo* ^{1}H MRS biopsy analysis at 8.5T (*104*). *In vivo* ^{1}H MRS of solid thyroid carcinoma detected Cho in all tumors, but no Cho in normal thyroid tissues. The mean tumor Cho/Cr ratio was 4.3 at TE 136 ms and 5.4 at TE 272 ms. Cho/Cr ratios for malignant tumors at TE 136 ms ranged from 1.6 in well-differentiated follicular carcinoma to 9.4 in anaplastic carcinoma (*105*). A longitudinal *in vivo* ^{1}H MRS study of a mouse model of brain metastasis from breast cancer cells found that Cho rose and Cr decreased as the lesions developed (*106*).

Much of the research on phospholipids carried out in the 1990s has been well summarized in reviews by de Certaines (*65*) and Podo (*92*). Choline metabolites are involved in the membrane biosynthetic and degrading pathways known as the Kennedy pathway (*92*), and these pathways have been studied to understand the biochemical and mechanistic nature of the increase in choline compounds found in cancer cells (*107*). Enzymes in this pathway are responsible for biosynthetic and breakdown products of the membrane phospholipid phosphatidyl choline (PtdCho). Free choline, PC and GPC are precursors of PtdCho, and may also be observed as catabolic breakdown products of PtdCho. Higher rates of choline transport, over-expression and activity of choline kinase, and increased phospholipase C and D activities, are found in some cancer cells (*107*).

The earliest *in vivo* clinical ^{31}P MRS cancer studies showed elevation of the phospholipid signals from both PME and PDE (*62, 64, 66*). It was not clear exactly which metabolites were responsible for this elevation, as these spectral peaks contain signal from several metabolites that cannot be resolved *in vivo* due to the broad line widths. In the last two decades, *in vivo* and *ex vivo* ^{1}H MRS observations have found enhanced tCho in premalignant and malignant tumors (*108, 109*). Gillies *et al.* (*110*) investigated the endogenous choline pathway by following the metabolic fate of ^{13}C-labeled methionine in 9L glioma tumors *in vivo*; this indicated that there was a significant amount of *de novo* choline synthesis *in vivo*. However, similar experiments performed *in vitro* using ^{13}C and ^{31}P NMR on glioma cells cultured in bioreactors indicated that glioma cells themselves are unable to synthesize choline *de novo*.

Some groups have studied the relationship between the level of choline observed in tumors by MRS and indices of either proliferation or malignancy. Miller *et al*. (*111*) found that the intensity of Cho resonances measured by *in vivo* ^{1}H MRS of human brain lesions was correlated with the cellular density of the tumor. In an *in vivo* ^{1}H MRS study of human brain tumors, a highly-significant positive correlation was found between the tCho-concentration and the immunohistochemical marker of cell proliferation, the Ki-67 labeling index. Melanoma cells treated with chloroethylnitrosourea *in vitro* have shown a strong phospholipid metabolism alteration involving a decrease of PC, and a dramatic and irreversible increase of PEth signal in 2D-TOCSY spectra obtained using HRMAS ^{1}H MRS (*112*). Water-soluble metabolites extracted from surgically excised samples of glioblastoma (GBM) tumors were measured quantitatively using *in vitro* HR-NMR; the tCho, inositol, alanine, glycine, and phosphorylethanolamine, all increased with the degree of malignancy (*113*).

Studies have been published that link the choline pathway to other altered biochemical and signaling pathways, such as HIF-1, fatty acid synthase, PI3K, and mitochondrial activity. Single-voxel *in vivo* localized ^{1}H spectra from HT-29 xenografts showed that the tCho resonance was significantly decreased 12 and 24 h after treatment with the HIF-1 inhibitor PX-478, later confirmed with high-resolution ^{1}H and ^{31}P MRS analysis of tissue metabolite extracts (*114*). A combined ^{1}H, ^{31}P, and ^{13}C MRS study of PC-3 prostate cancer cells, SKOV-3 ovarian cancer cells, and MCF-7 breast cancer cells treated with a fatty acid synthase inhibitor, showed a significant correlation between reduction in PC and the treatment-induced drop in *de novo* synthesized fatty acid levels (*115*). The PI3K/Akt oncogenic pathway is critical in cancers including GBMs. Loss of PTEN is observed in 70–80% of malignant gliomas; this is a negative regulator of the PI3K pathway or activated PI3K/Akt pathway, and its loss therefore enables increased proliferation, survival, neovascularization, glycolysis, and invasion. Thus, PI3K is an attractive therapeutic target for malignant glioma. ^{1}H MRS data from tumor models of GBM showed that treatment with the PI3K inhibitor PX-866 caused a significant reduction in the Cho/NAA ratio, reduction in growth, and increase in survival time (*116*). In a metabolomics study, Baykal *et al*. found that dramatic elevation in the levels of PtdCho metabolites could be induced by the inhibition of individual ETS (electron transport system) complexes, suggesting that the inhibition of each of the five ETS complexes might differentially regulate phospholipase activities within choline metabolic pathways in neuronal cells (*117*).

Choline kinase is overexpressed in breast cancer cells, and activated by oncogenes and mitogenic signals, making it a potential target for cancer therapy. Glunde *et al*. (*118*) showed that RNA interference-mediated choline kinase suppression in breast cancer cells induces differentiation and reduces proliferation. *In vivo* ^{31}P spectra of chk-shRNA-transduced tumors showed lower PC and PME levels that were associated with reduced tumor growth and proliferation (*119*). MN58b is a novel anticancer drug that inhibits choline kinase, resulting in inhibition of PC synthesis. In a study of human HT29 colon and MDA-MB-231 breast carcinoma cells by ^{1}H and ^{31}P MRS before and after treatment with MN58b both in culture and in xenografts, a decrease in PC and tCho levels was observed *in vitro* in both cell lines after MN58b treatment (*120*).

The presence of MRI contrast agents can cause changes in Cho signal estimations due to differential relaxation of the signal. Sijens *et al*. (*121*) observed reduced Cho signal in brain tumors after contrast agent administration, whereas Lin *et al*. (*122*) observed elevated Cho/Cr ratio at short TE in the presence of gadolinum. Madhu *et al*. (*123*) studied the effect of neutral contrast agent Gd-DTPA-BMA on the estimation of Cho concentration by *in vivo* ^{1}H MRS, and showed it varied with the dose of contrast agent, the TE, and the time-after-contrast-agent administration in HT29 tumors. It was later found, in a study on the effect of contrast agents on ^{1}H MRS-measured Cho signals, that the use of negatively-charged chelates may lead to an underestimation of the levels of Cho present in human breast cancers, since most studies use MRS post-contrast administration. The same study recommended the use of neutral chelates in MRI/MRS studies of the breast to minimize loss of Cho signal (*124*).

In vivo and *in vitro* ^{31}P MRS analysis of docetaxel-treated tumors showed significant decreases in intracellular PC and increases in GPC. It was also found that these decreases coincided with other tumor and cellular responses, such as tumor growth delay, cell-cycle arrest, and modes of cell death, such as mitotic catastrophe, necrosis, and apoptosis, with mitotic catastrophe predominating (*125, 126*). In another study of patients receiving neoadjuvant chemotherapy, absence/reduction in tCho was observed in 89% of patients. tCho was also detected in 2 of 14 benign lesions. The sensitivity and specificity of *in vivo* ^{1}H MRS in detecting tCho in human malignant tumors was found to be 78 and 86%, respectively (*97*).

From a systems biological view, the elevation or reduction of choline-containing compounds in cancer cells during tumor progression, or in response to therapy, may reflect a complex multiplicity of alterations taking place at the genomic, epigenetic, transcriptional, post-transcriptional, and translational levels. Although the exact mechanism behind the observation of elevated Cho levels in tumors cells is still not fully understood, it continues to be empirically useful in research and potentially useful in the clinic.

Lipid Metabolism

Lipid molecules in cells perform several activities including energy storage, signaling mechanisms, apoptosis, necrosis and inflammation. MRS-visible mobile lipids are considered important markers in diagnosis of human cancer and are thought to be closely involved in various aspects of tumor transformation, such as cell proliferation, necrosis, apoptosis, hypoxia, and drug resistance. In this section, we review fatty acid metabolism in relationship to cancer. The lipid metabolism associated with cell death process can be found in the subsequent sections on apoptosis and necrosis.

Lipid droplets have been observed in histological sections of preclinical glioma tumor models and in human brain tumors. *In vivo* ^{1}H MRS signals in these gliomas have shown methylene (1.3 ppm) and methyl (0.9 ppm) signals from free fatty acyl chains of triglycerides that formed these mobile lipids (*127*). There was controversy over whether these lipids originate from the cytoplasm or the cell membrane (*128, 129*). Polyunsaturated fatty acyl-chain signals can also be detected at 5.4 and 2.8 ppm, and can be used to assess the degree of polyunsaturation. The mobile lipid signals in ^{1}H MRS have been observed to change with apoptosis, necrosis, and lipid droplet formation. Several biological processes like hypoxia, growth arrest, apoptosis, differentiation, and degeneration of mitochondria have been cited as possible causes for accumulation of cytoplasmic triacylglycerides (*130–132*). These lipid droplets also have been shown to correlate with drug resistance or response.

Lower levels of MRS-visible mobile neutral lipids were unexpectedly detected in ras-transformed, *in vivo* tumorigenic fibroblasts, relative to their untransformed and nontumorigenic parental cells, suggesting altered lipid metabolism in transformed cells (*133*). HRMAS ^{1}H MRS studies of normal tissue from patients with squamous cell carcinoma (SCC) showed significantly higher triglycerides than normal tissue from patients with benign uterine disease, but significantly lower triglycerides than SCC tissue (*134*). The HRMAS ^{1}H MRS spectra of human normal cortex and medulla showed the presence of organic osmolytes. A marked decrease or disappearance of these metabolites and a high lipid content (triglycerides and cholesteryl esters) were typically observed in clear cell renal cell carcinomas (RCCs), while papillary RCCs were characterized by the absence of lipids and very high amounts of taurine (*135*). Using *in vivo* ^{1}H MRS, Griffitts *et al.* (*136*) showed that alterations in the integral ratios of the bis-allyl to vinyl hydrogen protons in unsaturated lipid fatty acyl groups correlate with the development of neoplasms *in vivo* in a TGFα/c-myc mouse hepatocellular carcinoma model.

A diffusion-edited sequence, based on stimulated echo and bipolar gradient pulses, was used to characterize molecules with low diffusion rates, arising from mobile lipid components in *ex vivo* malignant gliomas, RCCs, and colorectal adenocarcinoma tissues. Cholesterol, triglycerides, and PtdCho were simultaneously detected, and all these lipids contribute to the mobile lipid resonances present in malignant glioma and clear cell RCC spectra. Conversely, PtdCho resonances dominated the spectrum of papillary cell RCC, and that of colorectal adenocarcinoma was characterized by signals arising from triglycerides (*137*). Polyunsaturated omega-6 fatty acids (PUFAs) have been shown to promote prostate cancer; an HRMAS ^{1}H NMR study detected omega-6 PUFA in 15% of human malignant prostate tumors (*138*).

MRS Studies of Tumor pH

Warburg's description of aerobic glycolysis in tumors led to the erroneous assumption that lactate produced by cancer cells would tend to acidify cytoplasm and lower intracellular pH (pH_i) (*1, 139*). This dogma persisted for nearly half a century until the first ^{31}P MR spectra of solid tumors in rodents and humans revealed that the pH_i of tumors was, in fact, neutral to alkaline, which is very similar to that of normal tissues (*62, 64*). Subsequent development of MRS-detectable pH-sensitive indicators used to probe the extracellular pH of tumors firmly established that the extracellular interstitial space of tumors is acidic (not the cancer cell cytoplasm) with typical extracellular pH (pH_e) values in the range of 6.3– 6.99 (*140, 141*).

A contributing factor to the acidic tumor microenvironment is production of excess acids by cancer cells as a result of their abnormal intermediary metabolism (*74*). Whether cancer cells engage in aerobic glycolysis or oxidative metabolism, the end products of both processes are acids, respectively lactic acid and CO_2 (carbonic acid when dissolved in water) (*142*). Tight regulation of pH_i within a narrow range is essential for the proper functioning of cellular biochemical processes (*143*). In addition, a slightly alkaline pH_i has also been suggested to be permissive for cellular proliferation (*144–146*). To counter the acidifying effect of these acidic waste products on the intracellular pH, cancer cells are able to subvert a variety of physiologic mechanisms to extrude H^+ equivalents into the extracellular space (*147–149*). Since cancer cells maintain relatively constant pH_i, any changes to the intermediary metabolism of tumors are expected to affect pH_e to a greater extent than pH_i. This is because the tumor interstitium is poorly buffered, and the abnormally-organized tumor vasculature inefficiently clears H^+ (*139*).

Since pH_e reflects the metabolism of tumors, and may directly influence many aspects of primary tumor growth (*150–152*) and the invasion-metastasis cascade (*153, 154*), independent measurements of pH_e and pH_i can illuminate tumor biology and treatment response. Single-voxel and CSI MRS methods have been used for this purpose, yielding noninvasive *in vivo* measurements that are both accurate and precise with reasonable spatial resolution. Strategies to measure pH by MRS are varied, and can use ^{31}P, ^{19}F or ^{1}H nuclei. Typically, these depend on a group with a pKa in the physiological pH range; the protonated and nonprotonated forms of the group will resonate at slightly different frequencies relative to others in the spectrum, due to changes in the electronic shielding of the nucleus. The proportion of protonated and nonprotonated forms will change with pH. Exchange between the protonated and nonprotonated forms is fast on the NMR time-scale; within a single compartment, a single peak will be seen at a frequency that is the weighted average of the frequencies of the protonated and nonprotonated forms. The pH can be calculated from this frequency. Multiple peaks may be observed where barriers, such as cell membranes, prevent such rapid exchange. To measure extracellular pH by MRS, it is necessary to introduce into the tissue interstitial space an exogenous MR-detectable pH-sensitive compound that is impermeable to the cell surface membrane.

^{31}P MRS

The earliest attempts to study the pH of tumors *in vivo* by MRS utilized the ^{31}P nucleus. These experiments revealed that the pH_i of tumors were neutral to alkaline, which overturned the long-held dogma that the pH_i of tumor cells were acidic as a consequence of the Warburg effect (*62, 64*). In these experiments, the frequency of the endogenous P_i signal was used to measure pH, with the P_i chemical shift being referenced to either (GPC) (0.49 ppm) or the α-peak of nucleoside triphosphate (α-NTP) (10.05 ppm). The P_i signal in tumors has been found to be mainly intracellular, based in part on the assumption that volume of the intracellular compartment is greater than 50% of total tumor volume (*155*). The reliability of the resonance frequency of P_i as a measure of pH_i was confirmed through comparisons with pH values measured by intracellularly-trapped 2-deoxyglucose-6-phosphate (*156*). The measurement of pH_e was achieved with the development of nontoxic, membrane-impermeant exogenous phosphonate indicators, of which the most widely used is 3-aminopropylphosphonate (3-APP), though its toxicity limits its use, particularly for clinical applications. The administration of 3-APP in conjunction with ^{31}P MRS allows the simultaneous measurement of both intra- and extracellular pH. Such a technique has been used to measure the pH_e of several experimental tumor models, and these studies have revealed the acidic nature of the tumor interstitial space (*140*). Clinically, ^{31}P studies of brain tumors (*157–159*) have consistently shown that their pH_i is more alkaline than the adjacent normal brain, with low-grade gliomas, glioblastomas, and meningiomas showing progressively higher pH values.

Overall, investigations into tumor pH by MRS have greatly advanced the understanding of tumor pathophysiology by firmly establishing the concept of a neutral/alkaline pH_i and an acidic tumor pH_e. Nonetheless, like other uses of ^{31}P MRS, pH measurement with ^{31}P MRS suffers from the same problem of low sensitivity due to the low signal-to-noise ratio of ^{31}P, which precludes the acquisition of ^{31}P MR spectra at high spatial resolution. Currently, it is only possible to acquire a ^{31}P MR spectrum from 3–4-mm thick tumor slices or from large voxels of approximately $6 \times 6 \times 6$ mm^3 localized to the tumor for preclinical studies (*160*).

^{19}F MRS

Measurements of pH can also be performed using ^{19}F-containing probes, and compared to ^{31}P, ^{19}F MRS benefits from higher sensitivity, allowing for quicker spectral data acquisition from a smaller voxel size. Yet, because of the limited concentration of probe molecule that is physiologically acceptable in a tumor, pH measurements with ^{19}F MRS still have limited spatial resolution even at high magnetic field strengths; relatively less work has been done on measuring pH in tumors using this approach. The first exogenous ^{19}F pH probes were in the form of fluorinated vitamin B6 derivatives, which could permeate across the cell membrane and provide measurements of pH_i and pH_e gradients (*161, 162*). Subsequently, the membrane-impermeant ^{19}F MRS probe, 3-[N-(4-fluor-2-trifluoromethylphenyl)-sulphamoyl]-propionic acid (ZK-150471) was shown to produce consistent pH_e values in a number of different tumor models when compared with those obtained using ^{31}P MRS with 3-APP (*163*).

^{1}H MRS

The ^{1}H nucleus offers slightly higher sensitivity, even greater than ^{19}F. The acquisition of spectral data from a matrix of voxels using ^{1}H CSI enables pH measurements in multiple voxels and the generation of pH maps (*164*). This spectroscopic imaging technique has been used in conjunction with extrinsic ^{1}H MR pH_e indicators to map the pH_e of tumors in a number of experimental xenograft models.

The extrinsic ^{1}H MR pH_e indicators are aromatic compounds, such as imidazoles, that resonate at higher frequencies compared to endogenous metabolites, and appear downfield in the ^{1}H MR spectrum. The use of imidazoles as extrinsic pH probes was first reported by Rabenstein and Isab (*165*), who incubated imidazole with erythrocytes and measured intracellular pH of erythrocytes from pH-sensitive frequencies of protons on positions 2, 4 and 5 on the imidazole ring (H2, H4 and H5) (*165*). The protonation of the imidazole N3 atom affects distribution of delocalized π-orbital electrons on the ring structure, resulting in a change in the degree of shielding of the H2, H4 and H5 atoms (*166*). In a more acidic environment, the H2, H4 and H5 resonance peaks will be displaced further downfield in the spectrum. Several chemical modifications were made to the side chain on the imidazole ring to modulate its lipophilicity and membrane permeability, to ensure that the probe remains extracellular (*166*). This led to the development of IEPA (imidazol-1-yl-ethoxycarbonyl propionic acid), the first probe used to spatially map the distribution of pH_e in tumors using ^{1}H CSI (*141*). To generate such pH_e maps with IEPA, ^{1}H CSI is performed using a relatively short TE to measure the chemical shift of the H2 proton in a matrix of voxels. These chemical-shift values are transformed into their corresponding pH values to generate pH_e maps. Using this approach, tumor pH_e maps have been generated in experimental tumor models of breast (*141*) and brain (*167*) cancers, with a spatial resolution as high as $1 \times 1 \times 1$ mm^3 (*167*). An improvement in the use of imidazoles as pH probes was made through the development of ISUCA (2-imidazol-1-yl succinic acid), a probe based on the structure of IEPA with a more physiological pKa and better pharmacokinetic profile (*168*). The use of imidazole probes to spatially map the pH_e of tumors has illuminated the cellular energetics and pH regulation of cancers; these studies reveal that tumor pH_e is heterogeneous, with a spatial variation of up to 0.5 pH units across a distance of 8 mm (*168*). Furthermore, the relationship between regions of low pH_e and poor blood perfusion has been studied through co-registration of these pH maps with contrast-enhanced MR images. Importantly, results of these studies suggest that the relationship between pH_e and Lac concentration might not be as simple as previously thought. A comparison of the distribution of pH_e and metabolites by ^{1}H CSI in a glioma model revealed a lack of correlation between low pH_e and high Lac levels (*168*).

^{13}C MRS Hyperpolarized Bicarbonate

The reversible hydration of CO_2 in a reaction catalyzed by carbonic anhydrase provides another means of measuring pH, since the Henderson-Hasselbalch equation allows the calculation of pH from known concentrations of bicarbonate and carbon dioxide. Thus, in principle, ^{13}C MRS measurements of the concentration of these carbon species can be used to calculate pH. This was first demonstrated by Hoffman and Henkens (*169*) who used ^{13}C MRS to measure the kinetics of CO_2 hydration and HCO_3^- dehydration in erythrocytes. Nonetheless, the low natural abundance of the ^{13}C isotope (1.1%) and the low gyromagnetic ratio of the ^{13}C nucleus mean that such a technique would have very low sensitivity. The first measurements of pH using the detection of CO_2 and HCO_3^- by ^{13}C MRS was performed in superfused frog muscle using administration of high concentrations of labeled bicarbonate (*170*). A recent study improved sensitivity by employing hyperpolarized HCO_3^- (*171*). Administration of hyperpolarized HCO_3^- and monitoring of the conversion of $H^{13}CO_3^-$ to $^{13}CO_2$ by ^{13}C MRS allowed mapping of tumor pH in a lymphoma tumor model (*171*). Since the cell membrane is permeable to HCO_3^-, dynamics of its distribution across the cell membrane means that the measured pH is not solely confined to the extracellular compartment and might include contributions from the intracellular compartment. However, in the same study, a comparison of the measured tumor pH values using hyperpolarized HCO_3^- and those using 3-APP and ^{31}P MRS found them to be similar, implying that most of the ^{13}C signal was extracellular, at least in that particular tumor model (*171*).

Tissue Oxygenation

^{19}F MRS has been employed to estimate the tissue oxygenation in rodent tumors. Two approaches were followed in preclinical studies. The first attempted to improve the nitroimidazole agents that had previously been shown (in the 1980s) to bind to hypoxic tissue, so that these agents could be used in patients (*172, 173*). The second approach was to use perfluorocarbon molecules, in which the T_1 of the ^{19}F signal is reduced by binding to oxygen. Hexafluorobenzene, for instance, was extensively studied by Mason and co-workers (*174*), and a perfluoro-15-crown-5-ether was introduced by Sotak and co-workers (*175*).

CELL DEATH (APOPTOSIS AND NECROSIS)

Apoptosis

When cells undergo abnormal stress, apoptotic pathway signals can be activated, which then induce programed cell death. This process needs sufficient energy to be available in the cell and sufficient time for its execution. Necrosis is the violent death of cells and can be caused by sudden lack of supply of nutrients or exposure to a toxic environment. The pathway of cell death after anti-cancer treatment is often apoptosis, which leads to accumulation of mobile lipids detectable by ^{1}H MRS *in vivo*. Cell death processes can be observed in cell cultures by employing histological, biophysical, and biochemical methods. Some groups have tried to observe these cell death processes in solid tumors *in vivo* by employing diffusion-weighted ^{1}H MRS methods.

^{31}P and ^{13}C NMR spectroscopy have been applied to study cellular metabolism of MCF7 cells during tumor necrosis factor (TNF)-induced apoptosis, and a decrease in the level of PC was found (*176*). Hakumaki *et al.* (*127*) detected accumulation of PUFA during gene therapy of gliomas by using *in vivo* ^{1}H MRS. Early changes in glycolytic and phospholipid metabolites were detected in the ^{1}H and ^{31}P HR-NMR data of metabolites extracted from HT29 cells undergoing apoptosis after treatment with interferon-γ (IFN-γ) and TNF-α (*177*). ^{1}H MRS of neuroblastoma cells treated with COX inhibitors, which induce apoptosis, has demonstrated accumulation of PUFA and depletion of choline compounds (*178*).

Drug resistance in neuroblastoma cells was investigated by using the ^{1}H MRS lipid signals. Cytotoxic drug treatment of drug-sensitive SH-SY5Y neuroblastoma cells resulted in increased methylene and PUFA resonances, and a decreased choline resonance. The methylene/Cho ratio was correlated with cell death, and increased in cisplatin-treated drug-sensitive (SH-SY5Y, IMR-32) cell lines, but not in drug-resistant [SK-N-BE2, SK-N-FI, SK-N-AS] cell lines. Response or resistance to chemotherapy were accurately predicted by ^{1}H-MRS in experimental neuroblastoma models *in vivo* (*179*).

^{1}H-decoupled ^{31}P MRS was used to examine the metabolic changes associated with FK866-induced tumor cell death in a mouse mammary carcinoma. There were significant increases in the ^{31}P MR signal in the PME region, and a decrease in NAD^{+} levels, pH, and bioenergetic status. These results suggested that FK866 interferes with multiple biochemical pathways that contribute to increased cell death (apoptosis) and the subsequent radiation sensitivity observed in the mammary carcinoma, and that they could be serially monitored by ^{31}P MRS (*180*).

^{1}H MR spectra [both diffusion-weighted (DW) and unweighted] showed an increase in lipid signals during apoptosis of lymphoma cells. However, the methylene/methyl peak ratio showed only minimal changes. Localized *in vivo* ^{1}H MRS of EL-4 tumors also showed an increase in lipid signals, including a signal from polyunsaturated lipid at 2.8 ppm, after 16–24 h of drug treatment. Again, there was no significant change in the methylene/methyl peak ratio (*181*).

An HRMAS ^{1}H MRS study on clinical glioma biopsies showed that taurine was significantly correlated with apoptotic cell density (TUNEL) in both nonnecrotic and necrotic biopsies (*182*). In a rodent tumor model [ganciclovir-treated herpes simplex thymidine kinase (HSV-tk) gene-transfected BT4C gliomas], water diffusion and water-referenced concentrations of mobile lipids showed clearly increasing and interconnected trends during treatment by using *in vivo* ^{1}H MRS (*183*).

Necrosis

MR-visible lipids were detected in 87% of 64 tumor samples from six grade-4 astrocytomas investigated *ex vivo* by ^{1}H MRS, and subsequently by histopathology to obtain percentages of viable and necrotic tumors and grey and white matter (*184*). ^{1}H MRS data from C6 rat brain glioma suggested that mobile lipids detected at long TE *in vivo* by ^{1}H MRS in C6 tumors arise mainly from lipid droplets located in necrotic tissue (*132*). The correlation between HRMAS ^{1}H MRS-observed lipid signals and number of Nile Red-stained droplets in histological sections, and the presence of lipid droplets in the nonnecrotic human brain tumor biopsy specimens, provided good evidence that the *in vivo* NMR-visible lipid signals were cytoplasmic in origin, and that formation of lipid droplets preceded the necrosis (*130*).

MRS IN TUMOR DIAGNOSIS

The brain is the easiest organ to study by ^{1}H MRS, and brain cancers give detailed spectra that can be used to assist both diagnosis and grading. Using a standard 1.5T clinical instrument, it is usually possible to resolve signals from NAA (indicating the presence of normal neuronal tissue in the region of interest), Cr, Cho, and myo-inositol plus glycine. Small peaks assigned to alanine, glutamine plus glutamate, and glutathione are also often resolvable, and there are a number of peaks due to lipids and macromolecules (*185*). The two major tumor classes (gliomas and meningiomas) have characteristic metabolite patterns that are easily distinguished from normal brain. In gliomas it is also possible to differentiate between different grades of malignancy; for instance, glioma grade II (slow-growing) has a very different spectrum from the highly-malignant glioblastoma (*185*).

Two European Union-funded collaborations (INTERPRET, 2000–2002 and eTumor, 2004–2009) have developed large databases of tumor spectra and automated decision support systems (DSSs) that utilized pattern recognition algorithms (*186*). These DSSs can be used by clinicians to assist in making diagnoses of brain tumors from ^{1}H MR spectra. A small study using the INTERPRET method demonstrated that, for certain tumor types (notably gliomas) provision of MRS-derived information significantly improved diagnosis by neuroradiologists (*187*); improved discrimination is likely to be possible as databases obtained using instruments with 3T, and even more powerful magnets, become generally available.

The prostate is the other organ in which MRS study of cancer is relatively easy. It is possible to detect citrate, choline, creatine, and polyamines, although at 1.5T the peaks for choline, creatine, and polyamines overlap (*188*). Citrate signals are unique to normal prostate, whereas they are reduced or eliminated in prostate cancer. In contrast, like many other cancers, prostate tumors display tCho peaks, and their intensity correlates approximately with the Gleason score (standard index of prostate cancer malignancy). Thus, the ratio tCho/citrate is often used as a biomarker for the presence of prostate cancer.

In tumor sites other than the brain and the prostate, 1H MRS mainly gives a tCho resonance along with intense lipid signals. However, this tCho resonance can be used both for diagnosis and grading of cancer, and also to monitor response. Breast cancer has been most intensively studied, and the size of the tCho peak has been found to correlate with grade of malignancy (*189*).

As with the single-voxel studies mentioned thus far, multivoxel ^{1}H MRS studies of cancer can also be performed, giving crude images of the concentration of each metabolite that can be overlaid onto the anatomical image of a tumor. It is also possible to use a pattern recognition algorithm (such as those used by the INTERPRET and eTumor DSSs) to assign a tumor type and grade on the basis of the spectrum in each voxel. The resulting nosologic image can then be coregistered with the anatomical image (*190*).

The vast majority of diagnostic clinical MRS has employed the ^{1}H nucleus. A number of ^{31}P studies of a range of brain tumors have been able to distinguish between tumor types, and to differentiate them from normal brain (*157–159*). In addition to the pH_i differences mentioned above, differences are observed in PCr, PDE, and PME, with reduced PCr observed in GBM and meningiomas, perhaps reflecting tissue necrosis.

MRS MEASUREMENTS OF RESPONSE TO RADIOTHERAPY

Radiotherapy induces many physiological changes, including increased blood flow, reoxygenation (*77*), energetic status changes, and necrosis, all of which can occur rapidly after the start of therapy, but are not immediately reflected in changes in tumor volume. MRS has been applied to measure these physiological changes. In particular, since radiobiological hypoxia by definition represents regions of tissue that will not respond to radiotherapy, detection of reperfusion and improved oxygenation in these tissues would be of great interest.

^{31}P MRS in Radiotherapy

^{31}P MRS gives information on tissue phospholipids, intracellular pH, and energetic status, from the chemical shift of the P_i peak, from changes in PME or PDE peaks, and by alteration in tumor energetics. Reoxygenation due to increased tissue perfusion has been observed after radiotherapy, and this can potentially improve energetics (by improving the supply of glucose and oxygen) and increase pH (by indirectly reducing lactate). In contrast, necrosis resulting from radiotherapy results in degraded energetic status, and potentially in a dramatic increase in P_i if large numbers of dead cells are present (though this is not typically observed with current fractionated clinical strategies). Thus, different doses of radiotherapy or different scan timings can result in opposing changes in ^{31}P MRS. Ng *et al.* (*191*) studied a range of murine tumor types, investigating changes with tumor size and with treatment by cyclophosphamide, BCNU, hyperthermia, or radiotherapy. As tumors grew, bioenergetic status became poorer, which was subsequently found to be common to many models: PCr/P_i, NTP/P_i, and $(PCr+NTP)/P_i$ ratios fall, reflecting reduction in aerobic metabolism. Treatment of a mammary 16/C tumor with 14 Gy caused the PCr resonance to disappear completely at 15 min; at 24 h, large increases in PCr and ATP showed evidence of high aerobic metabolism. Tozer *et al.* (*192*) measured pH, PCr/P_i and NTP/Pi ratios in RIF-1 tumors grown in C3H mice after treatment with 2, 5, 10 or 20 Gy of X irradiation. PCr/P_i was significantly elevated at 1 day after treatment for doses of 10 Gy and above, and at 2 days after treatment for all doses; NTP/P_i was elevated at both time points at all doses. Pre-treatment pH_i was 7.09, increasing significantly at 1 and 2 days after treatment for doses above 5 Gy. These observations are consistent with improved energetic status and reperfusion. Reperfusion was confirmed using 4-iodo [N-methyl-^{14}C]antipyrine; significant tumor blood flow improvement was observed at days 1–3 after 20 Gy, but not after 2 Gy. Necrosis increased only transiently over the period of observation. Response was dose-dependent, with 20 Gy giving 75% regression at 2 days, while 2 Gy arrested growth over that period. The authors concluded that ^{31}P MRS was unlikely to act as an early predictor of tumor cell reproductive death, and that changes in the radiobiologically hypoxic fraction were not enough to account for the up to twofold changes observed in PCr/P_i, which might in part be due to reduced accumulation of P_i by improved circulation, or increases in PCr and NTP due to improved overall tumor oxygenation. Evanochko *et al.* (*193*) studied the rapidly-growing 16/C mammary adenocarcinoma, showing that high-energy phosphate metabolites decreased with tumor mass; they studied the acute response to radiotherapy, and observed complete disappearance of the PCr resonance within 15 min of treatment with 14 Gy ($n = 5$), followed by a return at 9 h, eventually reaching higher levels relative to ATP than pre-treatment. This spectral pattern suggests aerobic metabolism consistent with reperfusion or reduction in hypoxia due to the reduction in tumor volume; these tumors were reduced in volume by almost half within 1.7 days, unlike the RIF-1 tumors observed by Tozer *et al.* Similarly, Koutcher *et al.* (*194*) observed lower PCr/P_i ratios in large FSaII mouse fibrosarcomas compared with small (<250 mm^3) tumors; treatment with a single dose of 70–100 Gy resulted in growth arrest followed by tumor shrinkage in the small tumors, in which no significant change was observed in the NMR spectrum. In the larger tumors, the radiotherapy resulted in increased ATP and PCr, and reduced P_i and PME at 44 h post-treatment; at 96 h, regrowth had begun and the spectrum had returned to pre-treatment status. Koutcher's group published more papers on radiotherapy response, including studies of the response of hypoxic murine mammary carcinomas to doses of 32 and 65 Gy (*81*) and lower doses of 4, 8 and 17 Gy (*195*), and a study of the response of RIF-1 tumors *in vivo* and RIF-1 cultured cells *in vitro* over 7 days after a dose of 17 Gy to investigate direct cellular effects versus systemic effects of the radiation dose (*196*). The changes in PME (primarily in PEth) and PDE (primarily GPC) were similar in the two systems, but energetic status changes were confined to the *in vivo* model; the authors infer that these are primarily due to systemic changes, such as altered blood flow, while the PME and PDE changes are a direct cellular response to radiation. Sijens *et al.* (*197*) studied the effects of whole-body irradiation of mice bearing syngeneic NU-82 mammary tumors with 10 or 20 Gy. At 20 Gy, tumor ATP/P_i fell steadily for 48 h; at 10 Gy, ATP/P_i fell, with only a transient increase at 10 h after treatment. pH_i was unchanged. PDE decreased at both doses, which they ascribed to increased uptake of PDE for repair of damaged membranes. Up to

90% of tumor tissue was necrotic 48 h after treatment, and they found a linear relationship between the fraction of non-necrotic cells and the ATP/P_i ratio.

Some groups have attempted to use ^{31}P MRS to predict radioresistance of preclinical models. For example, Rofstad *et al.* (*198*) investigated four tumor types of varying hypoxic fraction at volumes from 200-2000 mm^3 using ^{31}P MRS in parallel with HbO2 cryophotospectroscopy. While they found a clear relationship between oxygen saturation status and tumor bioenergetic status, neither was predictive of radiobiological hypoxia. Similarly, Fu *et al.* (*199*) noted striking variations with tumor volume in metabolite ratios, pH_i, the surviving fraction, and the hypoxic fraction in SCCVII/SF tumors post-radiotherapy; again, highly-significant correlations did not result in strong predictive power because of the heterogeneity of the MRS parameters. Koutcher *et al.* (*200*) studied changes in ^{31}P MRS with administration of intravenous Fluosol DA and inhaled carbogen, an intervention intended to reduce the radiobiologically hypoxic fraction of murine MCa tumors. Mice receiving carbogen or Fluosol alone showed no significant changes in tumor MRS; mice receiving both carbogen and Fluosol and bearing tumors less than ~900 mm^3 showed significant increases in PCr/P_i ratio, and these changes were strongly correlated with increases in radiosensitivity with carbogen and Fluosol.

There have been relatively few clinical studies of the response of ^{31}P MRS to radiotherapy. Heindel *et al.* (*2*) acquired ^{31}P spectra from intracranial tumors including meningiomas, malignant gliomas, and low-grade astrocytomas, noting that low-grade pre-treatment spectra were very similar to those from normal brain, and that in one patient responding to treatment, the PCr peak grew dramatically, suggesting an improvement in tumor energetic status. Semmler *et al.* (*201*) examined 23 patients with a variety of superficial tumors, including serial studies of two receiving radiotherapy. One subject who had a partial response to combined radio- and chemotherapy, followed by tumor regrowth, showed an increase in PCr/P_i followed by a decrease, paralleling the changes in tumor size. Ng *et al.* (*202*) presented case studies of three women receiving various chemo- and radiotherapeutic treatments for breast cancer, noting that the PME/ATP and PDE/ATP ratios fell with treatment in all three, but pH_i was not significantly changed. The same group examined pH_i measured by ^{31}P MRS in 35 tumors of various types undergoing radiotherapy, observing values in the neutral-to-mildly alkaline range, occasionally rising as high as 8.0; fluctuations were not correlated with response to radiotherapy. They concluded that only a small fraction of cells in tumors studied were chronically hypoxic, and that the fluctuations might be related to variations in cell-cycle phase. Leach *et al.* (*203*) presented a clinical study of breast tumors, including an examination of the PME and PDE resonances. Serial studies using ISIS localization were carried out in 19 patients, 8 receiving radiotherapy and the remainder receiving either mitozantrone, methotrexate, and mitomycin C; cyclophosphamide, methotrexate, 5FU; or tamoxifen. The data were studied as a single group, as individually the treatment groups were too small to obtain meaningful results. Changes in PME at week 3 were found to be associated with volume response at that time, with higher PME value being associated with poor response. Prescott *et al.* (*204*) carried out a ^{31}P study in humans and dogs where they measured the response to combined hyperthermia and radiation treatment. The results were not consistent between humans and canines; a reduction in ATP/PME ratios was associated with necrosis levels $> 95\%$ in resected human tumors, but there was no association between phosphorus metabolites and time-to-local failure in dogs. Changes in PME and ATP signal-to-noise ratios correlated with cumulative thermal descriptors in both groups, perhaps suggesting that fully quantitative measures of ^{31}P would be more predictive of response. Interestingly, tumors with good energetics as assessed by NTP/P_i ratios also showed efficient heating, which is perhaps unexpected because large vessels tend to remove heat efficiently from tissue; easily heated regions might be expected to be poorly vascularized and thus poorly supplied with nutrients. The authors suggest this is because heat transport is dominated by large vessels, whereas nutrient supply depends on a good capillary network.

One early study by Szigety *et al.* (*205*) examined the effect of brain tumor radiotherapy on both ^{31}P and ^{1}H MRS of normal brain. While the pre-treatment metabolite levels observed by ^{31}P were abnormal compared to healthy brains, radiotherapy did not alter pH or the metabolite ratios; changes were, however, detected by ^{1}H MRS, particularly in the Cho/NAA ratio, and this was more marked in regions receiving higher doses of radiation.

In summary, larger tumors show lower values of PCr/P_i and NTP/P_i ratios. High doses of radiation result in transient disappearance of PCr, but at 24 h PCr is typically elevated, perhaps because reperfusion improves the energetic status. High PME post-therapy may be a marker of poor response.

^{1}H MRS in Radiotherapy

^{1}H MRS is predominantly applied clinically in brain and prostate cancers to assess response to therapy. In addition, it is applied to differentiation of recurrent glioma from treatment effects of radiotherapy or chemoradiotherapy. These include pseudoprogression and radiation necrosis, which are increasingly common in combined chemoradiotherapy with temozolomide [reviewed by Brandsma *et al.* (*206*), who place MRS studies in context with other imaging methods for management of GBM treated by radiotherapy and chemotherapy]. These are primarily distinguished by the higher level of Cho in recurrent disease (*207–209*).

Heesters *et al.* (*210*) used long-echo (TE 272ms) single-voxel, or 1D or 2D CSI, to investigate response of a range of gliomas to radiotherapy. In all cases, NAA was lower in tumor than normal contralateral tissue; this was not altered by radiotherapy. Cho was elevated in tumors, and five subjects showed reduced Cho post-therapy, accompanied by reduction in the diameter of the tumor measured by MRI. However, two subjects showed sustained high Cho and reduced tumor diameter. Lac was detected in high-grade astrocytomas, and was generally absent in low-grade gliomas; in three patients, the Lac signal disappeared after radiotherapy, and this was accompanied by decreases in Cho and tumor diameter. Lac persisted in the other four patients in which it was detected pre-therapy.

Bizzi *et al*. (*211*) published a case study of a patient with a cerebral nonHodgkins lymphoma, whose response to treatment was reflected in reductions in Cho and lipid resonances measured by CSI. Thirty-three months later, on diagnosis of recurrence, CSI showed normal spectral patterns throughout the brain volume examined.

Usenius *et al*. (*212*) used quantitative PRESS-localized ^{1}H MRS with normalization-to-water concentration and correction for T_2 relaxation to measure NAA, Cho and Cr between 6 months and 13 years after radiotherapy treatment of intracranial tumors. They found that normal brain exposed to high (59–62 Gy) doses of radiation during treatment showed around 30% reduction in NAA due to neuronal damage, but this was not observed at doses up to 43 Gy. These data showed no signs of cerebral necrosis in normal brain resulting from the radiation dose, detection of which has since become a major application for ^{1}H MRS in radiotherapy. For example, Taylor *et al*. (*213*) used long-TE STEAM-localized MRS to measure Cho, Cr and NAA in post-radiotherapy lesions in children previously treated for primary brain tumors; those lesions shown histologically to be delayed necrosis had lower Cho and Cr concentrations than recurrent tumor. They suggested use of an index based on the vector sum of the Cho and Cr peak areas to identify necrosis. The long TE method applied here could not detect lipid in the lesions. Wald *et al*. (*214*) used a shorter TE of 60 ms and PRESS-localized 3D CSI spectroscopy for a serial study of 12 patients with GBM who underwent subtotal resection, external beam radiotherapy, and brachytherapy. Patients received an average of 4.8 scans at 8-week intervals. The investigators noted heterogenous spectra, including spectra consistent with tumor in nonenhancing regions, and in enhancing regions where no metabolites were observed in the spectra, assigning the latter as enhancing necrosis. They hypothesised that ^{1}H CSI might be useful for planning radiotherapy and identifying radiation-induced necrosis in regions where MR-visible metabolites disappear post-therapy. Preul *et al* (*208*) used CSI in two brain tumor patients with recurrent symptoms to study regions of interest that were ambiguous by MRI post-contrast and CT, showing that Cho levels were high in tissue histologically identified as tumor and low in radiation necrosis. Esteve *et al*. (*215*) applied long-echo (272 ms) PRESS-localized CSI to study the time-course over eight months of metabolite changes in contralateral brain of patients being treated for grade II, III and IV gliomas and brain metastases of kidney cancer; results were consistent with reduction in NAA and increase in Cho up to four months post-irradiation. These changes were sustained in 3/11 patients, metabolite levels in the remaining eight returning to normal by eight months post-irradiation.

Waldrop *et al*. (*216*) carried out an extensive single-voxel long-TE PRESS study of uninvolved brain far from the tumor site in 70 children who were undergoing a variety of radio- and chemotherapeutic regimes. The tumors were mainly primitive neuroectodermal tumors or low-grade astrocytomas. Metabolite ratios were consistent with reduced NAA in patients versus normal controls; data were suggestive of greater reductions in NAA with whole-brain irradiation versus focal irradiation, and greater reductions when chemotherapy was administered before radiotherapy, but these results were not statistically significant. As with the study of Esteve *et al*. (*215*), no radiation necrosis was detected in uninvolved brain, and no lactate was observed in the spectra. Lazareff *et al*. (*217*) also studied children with brain tumors, but focused on response of tumors to chemotherapy or radiotherapy, and not uninvolved brain. They observed sustained reduction up to 40 months in tumor Cho relative to values in uninvolved brain post-treatment in responding patients, and increased Cho post-treatment in progressive disease.

Chan *et al*. (*218*) studied long-term effects on normal brain of radiotherapy for nasopharyngeal cancer; in this group there was no brain pathology other than iatrogenic radiation necrosis, and patients whose tumor had progressed into the brain were excluded. These subjects were up to 10 years post-RT and had previous diagnosis of temporal lobe radiation injury by CT or MRI. They noted reductions in NAA/Cr relative to pre-treatment controls even in temporal lobes appearing normal by MRI. The most severe cases were characterized by increases in Cho/Cr and detectable Lac levels. Chong *et al*. (*219*) carried out a similar study of 18 patients previously treated with RT for nasopharyngeal cancer, though this study used water quantitation rather than metabolite ratios. They observed reduced NAA in almost all subjects, even when T_2w MRI appeared normal. Abnormal regions on T_2w MRI represent tumor, edema, and microscopic infiltration, and are often regarded as a good guide to the volume to be irradiated, whereas surgery would be performed on a smaller volume. Cho values were higher than normal in three subjects with contrast-enhancing lesions (which were radiation necrosis rather than tumor), but were generally lower than normal. Spectra from regions of cystic encephalomalacia showed no detectable metabolites. Schlemmer *et al*. (*209*) measured metabolite ratios using single-voxel long-echo (TE 135ms) PRESS in progressive tumor, radiation injury, stable disease, and contralateral uninvolved brain, in 56 patients who had previously undergone RT for primary brain tumors (and in some cases a second cycle to treat recurrent disease). NAA/

Cr ratios distinguished uninvolved brain from all disease, while linear discriminant analysis of Cho/Cr and Cho/NAA ratios could distinguish progressive tumor (in which both ratios were elevated) from the other pathologies with better than 80% accuracy. However, radiation injury could not be differentiated from stable disease. The same group presented a case report (*220*) of a patient whose PET and MRI scans suggested high-grade tumor progression, while MRS suggested radiation necrosis, a diagnosis subsequently confirmed by histology.

Graves *et al*. (*221*) studied the response to gamma-knife radiosurgery of 18 patients with recurrent malignant brain tumors. They used 3D PRESS-CSI (TE 65, 144 or 272 ms in different patients) to investigate the high-dose region as well as the uninvolved tissue remote from this region, measuring Cho, NAA, Cho/NAA, and lipids + lactate (Lip+Lac) normalized to metabolite peak areas in uninvolved tissue prior to radiosurgery and for up to 14 months afterwards. Patients showing no local recurrence showed reduced Cho/NAA in the high-dose region. Recurrence as measured by contrast enhancement (whether local or remote) was always preceded by an increase in Cho/NAA, although median Cho in the high-dose regions could decrease due to dilution of the tumor signal by radiation necrosis. Apparent increases in NAA in some high-dose regions were ascribed to loss of tumor cells resulting in a higher proportion of neurons in the voxel. They speculated that, ''The presence of tumor-suggestive voxels beyond the regions of contrast enhancement implies the presence of a more aggressive or infiltrative variety of tumor that will respond poorly regardless of the treatment applied''. Dowling *et al*. (*222*) obtained 79 biopsies accurately positioned by a surgical navigation system from 29 patients undergoing surgery for newly-diagnosed or recurrent tumor. Histology results were compared with the corresponding voxel in MRS data acquired with a 3D PRESS-CSI sequence, TE 144 ms. Cho/NAA ratios, and Cho and NAA normalized to peak areas in uninvolved brain were analyzed. The $2 \times 2 \times 3$ mm^3 biopsies were found to be heterogeneous (implying that the 1 ml MRS voxels were also heterogenous), and contained tumor, necrosis, and other tissues including white and grey matter, astrogliosis, and macrophage infiltration. Cho elevated more than two standard deviations (2SD) above uninvolved brain, and NAA more than 2SD below uninvolved brain were shown to be an invariable marker of tumor; elevated Cho with Cho/NAA > 1 normally implied tumor. Voxels with decreased Cho and NAA corresponded to radiation necrosis, astrogliosis, macrophage infiltration, and mixtures including all grades of tumor. MRS data were more specific than MRI data alone. An early 3T study on patients with brain tumors of grade II or higher who had received at least 54 Gy of radiotherapy at least three months prior to MRS, was carried out by Rabinov *et al*. (*207*); they used PRESS-144 CSI with voxel size 1.5 or 0.6 ml, and calculated ratios of NAA and Cho peak areas to Cr in the same voxel and in an equivalent uninvolved contralateral voxel. The ratio of Cho in the lesion to Cr in uninvolved brain differentiated lesions that were assessed by histology to be predominantly radiation effect on normal brain from those that were predominantly tumor ($P < 0.003$), with tumor typically having ratios >1.3; in biopsies that contained predominantly radiation effect, three of the four highest Cho/Cr ratios were from voxels also containing foci of residual tumor. Similarly, Rock *et al*. (*223*) found that pure tumor was associated with high Cho:normal Cr and low Lip+Lac:Cho values, and pure necrosis was associated with low Cho:normal Cr, low Cho:normal Cho and high ratios of Lip+Lac to Cho and normal Cr. However, specimens that were identified by biopsy as mixed radiation necrosis and tumor could not reliably be identified by any MRS ratio. In the study by Rabinov *et al*., NAA, lipid, and Lac had no predictive value. In contrast, Tarnawski *et al*. (*224*) found the Lac/NAA and Lip/NAA ratios to be highly predictive of survival in a short-TE (35 ms) single-voxel study of a group of patients receiving radiotherapy after partial or total resection of high-grade brain tumors, with peak area ratios >2 being strongly associated with poorer survival. It is unclear whether this represented higher levels of residual tumor, or whether radiobiological hypoxia was associated with high Lac levels. Weybright *et al*. (*225*) used 2D PRESS CSI (TE 144 ms) to study 28 patients showing new enhancing lesions on MRI at least two months after radiotherapy for brain tumors. Lesions were subsequently identified as tumor or radiation necrosis either by biopsy or autopsy, or by their behavior on long-term follow-up. Cho/Cr and Cho/NAA ratios were significantly higher in radiation necrosis than in uninvolved brain, and significantly higher in recurrent tumor than in radiation necrosis. Similarly, NAA/Cr was lower in radiation necrosis than in uninvolved brain, and lower still in recurrent tumor. NAA/Cr ratios were generally lower in uninvolved brain than the literature values for normal brain, possibly as a side-effect of the radiotherapy. Lac and Lip were not useful for distinguishing radiation injury from tumor. Metabolically abnormal voxels consistent with tumor were observed outside the enhancing region, which was consistent with a number of previous studies comparing CSI and MRI. For example, Pirzkall *et al*. (*226, 227*) used 3D PRESS CSI to investigate the mismatch between metabolic abnormality and apparent tumor boundaries on T_2W MRI in high-grade and low-grade gliomas, using z-scores for Cho/NAA as an index (CNI) of active tumor metabolism, Lac as an index of hypoxia (and a marker of regions potentially requiring higher RT dose), and Cr/NAA as an index of healthy respiration. This study was later extended to patients with high-grade gliomas post-surgery, but prior to radiotherapy (*228*). Many patients showed CNI values indicative of tumor outside the area of T_2W abnormality, with this being greater for high-grade tumors. However, the extent of this was not uniform, suggesting an application for CSI in setting more useful boundaries for RT than a simple boundary around the MRIdelineated tumor. In post-surgical patients showing no contrast enhancement, there was an inverse correlation between the volume of high CNI and the time-to-onset of contrast enhancement. The same group (*229*) studied eight children with diffuse intrinsic pontine gliomas with 3D CSI and also, in some cases, 2D CSI, with a TE of 144 ms and a voxel size of 1 ml or 1.85 ml. Five patients underwent CSI both before and after radiotherapy, allowing comparison of diagnostic, response, and recurrence spectra. The small size of the study limits the conclusions that can be drawn, but a number of patients showed CSI changes indicative of progression (increased Cho:NAA or Lac+Lip) prior to clinical or imaging changes, and two responders showed resolution of Lac+Lip peaks after RT. Responders to RT appeared to show a decrease in Cho:NAA with a P value of 0.06 which may have appeared significant in a larger study. Overall, reductions in Cho, Lac or Lip may indicate response to radiotherapy. MRS can play a useful role in differentiating progressive tumor from radiation necrosis; and NAA reveals subtle damage to irradiated normal brain, which is not visible by MRI.

A number of prostate cancer studies have also been carried out. Interpretation of data post-radiotherapy is challenging, because radiation reduces Cit and polyamine levels (*230*) in the normal gland. Post-irradiation changes can also confound MRI assessment of the prostate. Coakley *et al*. (*230*) presented a CSI study of prostate post-RT (mean dose 74.7 Gy) in a group of men who showed biochemical treatment failure as assessed by three consecutive rises in PSA (prostate-specific antigen), and identified tumor voxels by a Cho/Cr ratio > 5, or Cho SNR > 5 in voxels where Cr could not be identified. Voxels containing no Cho or Cit were identified as metabolic atrophy. Diagnoses were confirmed by sextant biopsy. In this study, the area under the receiver operating characteristic curve for CSI detection of local recurrence was 0.81, where by MRI alone the areas under the ROC for two independent readers were 0.49 and 0.51. Metabolic mapping is also used in the planning of radiotherapy. For example, Pouliot *et al*. (*231*) used a scoring system devised by Jung *et al*. (*232*) to identify the dominant intraprostatic lesion for planning brachytherapy. Pickett *et al*. (*233*) monitored 70 patients up to 72 months after brachytherapy, with subgroups also receiving external beam RT and hormone therapy. Time-to $> 95\%$ metabolic atrophy (that is, 95% of voxels containing no metabolite with SNR > 5) was measured and compared with the time-to-PSA-nadir. Patients not receiving hormone therapy showed 95% metabolic atrophy up to 18 months earlier than PSA nadir. Thirty-one percent of patients showed transient blips in PSA until a final nadir; the fraction of metabolic atrophy increased monotonically with no blips. The authors suggest the blips are due to PSA being released as cells die, delayed death of epithelial cells, or radiation-induced prostatitis. The same group (*234*) also studied 55 patients who underwent external beam RT but did not receive brachytherapy, with similar results; mean time-to-disease-resolution assessed by CSI was 40.3 months, and to PSA nadir was 50 months. Eleven patients undergoing biopsy showed complete agreement between biopsy and CSI, but not with PSA, seven subjects with negative biopsy and CSI showing positive PSA results. Pucar *et al*. (*235*) studied nine patients showing increased PSA after RT, including six in biochemical failure as defined by three consecutive increases in PSA after a nadir. Patients underwent MRI, a single 3D CSI exam, digital rectal exam (DRE), and sextant biopsy prior to salvage radical prostatectomy and definitive diagnosis by step-section pathology of the resected gland. Voxels were classified as suspicious for tumor if the (Cho+Cr)/Cit ratio was greater than 0.5, or if the SNR of Cho was > 3 and that for Cit was < 3. On this basis, CSI was more sensitive (77% compared to 68% for MRI, 45% for sextant biopsy, and 16% for DRE) but less specific (78% compared to better than 90% for all other techniques) than the other techniques. False-negative voxels were, ''unusable or had nondiagnostic levels of metabolites''; false-positives had (Cho+Cr)/Cit > 0.5, perhaps because of metabolic atrophy of Cit in normal gland post-RT. A biopsy study by Menard *et al*. (*236*) noted the complete absence of Cit in almost all post-radiotherapy samples, whether benign or malignant, though increased Cho and reduced Cr remained diagnostic of malignant disease.

King *et al*. (*237*) studied the response of head and neck squamous cell carcinoma (HNSCC) to radiotherapy by ^{1}H MRS. Good-quality data in this area of the body are hard to obtain for technical reasons. Pre- and post-treatment MRS data were obtained from 30 patients with post-treatment masses, of which nine were residual cancer as defined either by biopsy or continued growth. Cho was detected post-treatment in five of the residual cancers, and in none of the noncancerous post-treatment masses. While the association of Cho with residual cancer was statistically strong, the high false-negative rate limits use of the technique in HNSCC.

A number of preclinical studies have also been carried out. Bhujwalla *et al*. (*238*) applied long-TE (TE $=$ 272 ms) ^{1}H CSI in RIF-1 mouse tumors to investigate their response to radiotherapy. This long TE was combined with outer volume suppression via the BASSALE sequence (*239*) to minimize the intense subcutaneous lipid signals and improve detection of Lac. MRS data were acquired before, and at 24 and 48 h after doses of 2, 4 and 20 Gy of γ radiation. The spectra were dominated by Cho and Lac. All groups showed significantly decreased Lac at 48 h post-treatment, and the 20 Gy group at 24 h post-treatment; this was consistent with the earlier ^{31}P study of Tozer *et al*. (*192*). Aboagye *et al*. (*240*) followed up this study using multiple-quantum coherence methods to measure Lac in untreated RIF-1 and in the more radioresistant EMT6 model, which was treated with up to 20 Gy of radiation. Pre-treatment Lac/water ratios were compared, and data from treated EMT6 were compared with the previous RIF-1 data. Despite the difference in hypoxic fraction between the two models, Lac/water ratios were not significantly different. Significant decreases were observed 48 h after 10 Gy (–21%) and 20 Gy (–40%); there was no decrease in tumor volume. Lac decreases were smaller than those observed in RIF-1, and significant decreases were only observed at higher doses. These caused initial optimism that Lac would be an early indicator of early response to RT. Interestingly, a more recent publication (*241*) using bioluminescence to measure Lac in excised tumors saw no correlation between hypoxic fraction and Lac, but a strong association ($P < 0.003$) between Lac and TCD50 in a panel of HNSCC tumors grown in nude mice.

Dyke *et al*. (*242*) studied the CWR22 murine prostate cancer model, which was treated with 20 Gy of radiation in a single dose, and used BASSALE (*239*) localized CSI with 136 ms TE and high-resolution spectroscopy of perchloric acid extracts of tumors. Metabolite ratios were calculated relative to water in the same voxel obtained from a separate nonwater-suppressed acquisition. This dose resulted in a regrowth delay of 15.8 ± 4.8 days in treated mice ($n = 8$) relative to untreated controls ($n = 22$). Spectra were assessed for Cho:water ratio and for presence of mI, Cr and Cit resonances. Treatment caused a reduction in Cho at 24 h, with signs of subsequent recovery. Typically, other metabolites were reduced below detectable levels post-treatment. Cit was detected in some tumors. PSA was correlated with tumor volume in the untreated cohort, but not in the treated cohort. Lac was not detected *in vivo*.

^{13}C MRS Studies of Radiotherapy

Recently, Day *et al*. (*243*) applied the emerging technique of hyperpolarized ^{13}C MRS to investigate the response to radiotherapy of the C3 glioma model grown intracranially in rats. Hyperpolarized [1-^{13}C] pyruvate was injected and an 11 s CSI acquisition was used to assess its exchange with Lac. Observed Lac levels were much higher in untreated tumor than in normal brain. The highest pyruvate signals were detected from blood vessels. Tumor Lac normalized to the highest blood pyruvate fell by 30% ($P < 0.05$) by 72 h post-treatment with 15 Gy of radiation to the whole head; earlier time points with fewer tumor measurements were consistent with this reduction happening as early as 24 h, but this was not statistically significant. Animal survival was substantially increased by treatment, despite apparent increases in size of tumors; this may have been pseudo-progression, suggesting potential clinical utility for the method in the important question of distinguishing pseudoprogression from true disease progression.

CHEMOTHERAPY RESPONSE BY MRS

As well as revealing the effect of chemotherapy on endogenous metabolites, in some cases MRS can also directly measure the pharmacokinetics and distribution of administered agents, especially fluorinated agents such as 5FU, capecitabine, and gemcitabine. For the first two, MRS can differentiate the administered agent and a number of its metabolites, allowing detailed pharmacokinetic measurements. Similarly, ^{31}P MRS can detect ifosfamide directly.

^{31}P MRS in Chemotherapy

While clinical use of ^{31}P MRS is presently much smaller than might have been hoped for 20 years ago, pre-clinical studies investigating its potential continue, in particular for agents targeting choline kinase. An NHL study has been described above. Other clinical studies include the work of Semmler *et al*. (*244*), who examined the response of a malignant melanoma on the sole of a patient's foot to isolated limb perfusion, observing transient depletion of high-energy phosphates and increases in P_i, PME, and PDE. The spectrum at one week post-treatment resembled the pre-treatment spectrum, but with lower overall peak areas. In 2002, Kettelhack *et al*. (*245*) used a 1.5T Siemens instrument to perform a clinical ^{31}P study of isolated limb perfusion treatment of patients with locally advanced, unresectable soft tissue sarcomas, and bulky melanomas. Post-treatment, PME/PCr and PME/β-ATP ratios were reduced in all patients except one that showed no decrease in PME/PCr only. Fifteen of the 32 subjects had partial responses, and these were significantly associated ($P = 0.02$) with greater decreases in PME/β-ATP. Importantly, the PME/β-ATP ratio was strongly related to high levels of necrosis, suggesting it is measuring this directly, and is potentially a useful marker for treatments that cause necrosis without immediate reduction in tumor size.

Shukla-Dave *et al*. (*246*) used proton-decoupling and the Nuclear Overhauser Effect for maximum sensitivity and optimized resolution of overlapping resonances in a 1.5T study of the association between PME pre-treatment and response to chemotherapy and radiotherapy of squamous cell head and neck carcinomas. They found that the pre-treatment PME/β-NTP ratio was significantly smaller in complete responders than in the group comprising partial responders and nonresponders ($P = 0.004$).

Preclinical ^{31}P MRS studies are much more common. Proietti *et al*. (*247*) used ^{31}P MRS of freshly-excised tumor tissue to investigate the effects of intratumoral injection of IFN and X irradiation on IFN-sensitive and resistant FLC tumors grown in mice. Both lines showed increased pH and reductions in the ratios of PC, GPC, and GPE to P_i with IFN before the onset of necrosis, which may have been a host-mediated effect; the same changes were not observed after radiotherapy, despite induction of necrosis and 50% reduction in tumor volume. Similarly, Allavena *et al* (*248*), measured changes in ^{31}P MRS of highly-vascular, well-oxygenated DMBA-induced fibrosarcomas in rats with growth and on treatment with 5FU and radiotherapy, alone and in combination; while the individual treatments in this case caused no significant changes in the spectra, the combination treatment resulted in significant increases in

PDE/total phosphate and P_i/total phosphate ratios, and a reduction in pH_i, accompanied by an 80% reduction in tumor volume. The majority of ^{31}P MRS responses to chemotherapy show similar results; for instance, Beauregard *et al*. (*249*) treated murine sarcoma F tumors with the vascular disrupting agent combretastatin A4 phosphate (CA4P) and observed reduction in the NTP/P_i ratio and acidification of pH over 150 min from treatment; PME was unchanged over this time period. The same group (*250*) treated HT29 and LS174 colon adenocarcinomas in SCID mice with CA4P and the small-molecule cytokine-inducing vascular disrupting agent DMXAA, and found that HT29 responded to DMXAA but not to CA4P as assessed by changes in the P_i/NTP ratio measured by ISIS-located ^{31}P MRS, while LS174 tumors responded to both agents. Similar results were obtained by McPhail *et al*. (*251*), who used ^{31}P and ^{1}H spectroscopy *in vivo* to investigate the effect of DMXAA in HT29 xenografts. ISIS localization was used for ^{31}P and PRESS with TEs of 20, 68, 136, 272, and 408 ms for ^{1}H, together with a multiple quantum coherence-edited sequence for Lac detection. *In vivo* data were acquired before and 6 h post-treatment with vehicle and doses of DMXAA up to 21 mg/kg, as well as 24 h post-treatment with 21 mg/kg. High-resolution ^{31}P and ^{1}H spectroscopy were carried out on tumor perchloric acid (PCA) extracts. ^{31}P MRS showed massive decreases in tumor bioenergetics at doses of 15 mg/kg and above, with reductions in high-energy phosphates and PDE, and increases in P_i, consistent with nutrient starvation resulting from vascular shutdown. Cho decreased significantly 24 h after 21 mg/kg of DMXAA. Substantial increases in Lac were observed in individual tumors after 21 mg/kg DMXAA, but this was not statistically significant across the group. High-resolution MRS showed significant increases in free Cho and P_i, and decreases in GPC, GPE, and PDE at the highest dose. These data were interpreted as reduction in membrane synthesis that resulted in loss of membrane breakdown products and increased free Cho. High-resolution MRS detects opposing changes in metabolites, which contribute to the total Cho resonance observed by ^{1}H MRS *in vivo*, which may limit its sensitivity to response to DMXAA compared to ^{31}P MRS. The work of Madhu *et al*. demonstrating reduced Cho and unchanged Lac on treatment with the VDA ZD6126 is covered in the HRMAS section.

Koutcher *et al*. (*252*) carried out an *in vivo* study in MCa mouse tumors of the effects of treatment order for combined bryostatin-1 and paclitaxel treatment, based on cell studies that implied that treatment with paclitaxel first might be more effective; not only was this the case, but pre-treatment with bryostatin-1 was actually less effective than paclitaxel alone. ^{31}P and DCE-MRI studies demonstrated reduced tumor pH, impaired energetics as assessed by PCr/P_i ratio, and reduced tumor blood flow at 12 h post-treatment with bryostatin-1. These factors may have reduced the effectiveness of paclitaxel. A recent study by the same group (*253*) showed that ^{31}P measures of PME predicted response to an oncolytic virus. A water bath immersion system was used to optimize field homogeneity, allowing the PME region of the spectrum to be resolved into PEth and PC. The sensitivity of five different tumor models to two oncolytic viruses was investigated, and it was noted that the PEth/PC ratio was lower in virus-sensitive models; low PEth/PC was also associated with shorter doubling times.

Klawitter *et al*. (*254*) used ^{1}H, ^{13}C and ^{31}P HR-NMR of PCA cell extracts to compare metabolic responses to imatinib in imatinib-sensitive and resistant cell lines; the main difference was greater reductions in PC in the sensitive lines, followed by a decrease in PtdCho measured in lipid fractions. Increases in GPC and GPE were also observed in sensitive cells. Glycolytic activity, as assessed by production of [3-^{13}C]Lac after addition of [1-^{13}C]glucose, was inhibited by imatinib in the sensitive lines only.

Koutcher *et al*. (*255*) showed a more specific response to inhibition of the pentose phosphate pathway (PPP) by 6-aminonicotinamide (6AN); 10 h after administration, this resulted in a large 6-phosphogluconate peak, not normally visible in ^{31}P spectra, indicative of PPP inhibition. Additionally, 6AN had a synergistic effect on radiotherapy response in the mammary carcinoma model in this study. Al-Saffar *et al*. (*120*) used ^{31}P and ^{1}H MRS *in vivo* in xenografts, on tumor extracts, and on cell culture extracts of HT29 and MDA-MB-231 lines to evaluate response to the choline kinase inhibitor NM58b. This agent has the effect of reducing PC synthesis, which should be reflected directly in the ^{31}P spectrum. Statistically-significant reductions were seen in PME *in vivo*, and in PC in extracts; free choline, GPC, and PtdCho levels were not significantly altered. The same team (*256*) later published a similar study of response to the phosphoinositide 3-kinase inhibitor PI-103, and demonstrated that it down-regulated choline kinase, reflected in reductions in PC and tCho as measured in cell culture by ^{31}P and ^{1}H MRS.

Chung *et al*. (*257*) demonstrated with ^{31}P and ^{1}H MRS that the heat shock protein inhibitor 17AAG altered phospholipid metabolism in cultured colon cancer cell lines and xenografts; strikingly, response to this agent resulted in significant increases in the PME/PDE ratio *in vivo* and in PC, PEth, and valine levels in tumor extracts. Brandes *et al*. (*258*) subsequently measured the response of MCF7 cells to 17AAG with ^{1}H, ^{31}P and ^{13}C MRS of cells and extracts, again observing significant increases in Cho, PC, and GPC. Cho and PC increases were correlated with increases in expression of the choline transporter SLC44A1 and phospholipase A2. Therefore, it cannot be blindly assumed that Cho will be reduced in response to all chemotherapeutic agents. Similar results have been observed with histone deacetylase (HDAC) inhibitors; Chung *et al*. (*259*) published data on the HDAC inhibitors LAQ824 and suberoylanilide hydroxamic acid, demonstrating that LAQ824 treatment compromised the tumor bioenergetics and altered phospholipid metabolism, resulting in reduced tissue pH, increases in P_i and PME, and decreases in NTP, expressed as fractions of total phosphorus signal. In an *in vitro* study, Sankaranarayanapillai *et al.* (*260*) studied the response of PC3 cells to *p*-fluorosuberoylanilide hydroxamic acid by ^{31}P MRS and ^{19}F MRS of the fluorinated lysine derivative Boc-Lys-(Tfa)-OH (BLT). Since BLT is cleaved to trifluoroacetic acid by HDAC, the level of BLT measured by ^{19}F MRS was higher in cells treated with the HDAC inhibitor. Increases in PC were also observed by ^{31}P MRS of the treated cells, possibly resulting from the observed depletion of the Hsp90 client proteins c-Raf-1 and cdk4. Sterin *et al.* (*261*) measured ^{31}P spectra in a range of breast cancer cell lines varying in estrogen dependence, estrogen responsiveness, metastatic potential, and estrogen receptor status, that were treated with antimicrotubule agents, as well as doxorubicin and methotrexate. Baseline GPC levels were low for the ER negative, metastatic MDA-MB231 and MDA-MB435 lines. Intracellular GPC rose dramatically on treatment with the antimicrotubule agents, but not with doxorubicin or methotrexate.

The alkylating agents ifosfamide and cyclophosphamide contain ^{31}P with resonances downfield of the endogenous ^{31}P-containing metabolites. Both clinical and pre-clinical ^{31}P MRS studies have been carried out to monitor these agents. Rodrigues *et al.* (*262, 263*) measured ifosfamide uptake *in vivo* in rat tumors. They detected ifosfamide within a few minutes of injection; AUC and growth delays were increased by simultaneous breathing of hypercapnic gas mixtures of 2.5–5% carbon dioxide with oxygen and 5% CO_2 with air. However, clinical studies did not progress beyond a feasibility study in which Payne *et al.* (*264*) demonstrated large gains in SNR using decoupling and polarization transfer techniques on a phantom, and then used these methods to detect ifosfamide and cyclophosphamide in the livers of patients. The same group (*265*) carried out CSI-localized studies in guinea pigs, finding long-lived ifosfamide signals in the gall bladder as well as the liver; they used high-resolution NMR of bile (*266*) to identify metabolic products including parent drug, carboxyifosfamide and the glutathione conjugate of ifosfamide.

In summary, ^{31}P MRS of chemotherapeutic response broadly shows degraded energetics, reduced PC, and reduced pH_i. However, some responses to agents targeting Cho-related pathways can be reflected in increases in PC.

^{1}H MRS Studies of Chemotherapy

Due to the large number of endogenous signals, ^{1}H MRS is not useful for assessing the pharmacokinetics of chemotherapeutic agents. However, it is useful for detecting the pharmacodynamic response to treatment. *In vivo* studies typically focus on Cho and Lac resonances as markers for cell proliferation and glycolysis, respectively. Most pre-clinical work has been carried out in subcutaneous transplanted tumors using surface coils, which are more sensitive than volume coils and allow easier localization. Some orthotopic studies have also been carried out for example, Fricke *et al.* (*267*) demonstrated ^{1}H MRS of the TRAMP prostate cancer model.

Shungu *et al.* (*268*) demonstrated that 5FU treatment reduced Cho relative to tumor water, and that acute tumor blood-flow reduction by hydralazine increased Lac in RIF-1 tumors. Mardor *et al.* (*269*) used a method devised by van Zijl *et al.* (*270*) to address the problem of distinguishing intracellular and extracellular metabolites in a high-field 600 MHz *in vitro* study of melanoma and breast cancer cells in alginate beads. They used diffusion-weighted spectroscopy to eliminate the signal from mobile metabolites in perfusate and beads, while retaining the bulk of the signal from intracellular metabolites whose diffusion is restricted by cellular structures and membranes. They demonstrated that treatment with lonidamine resulted in increased intracellular Lac and reduced extracellular Lac, which was consistent with previous data showing that lonidamine reduced Lac transport.

Natarajan *et al.* (*271*) used ^{1}H MRS to study PCA extracts from malignant and nonmalignant human mammary epithelial cells after treatment with the COX inhibitor indomethacin. PC/GPC ratios were reduced by treatment, and COX-1 levels were significantly correlated with the PC/GPC ratio and tCho; lower levels of all three were observed in the nonmalignant cell lines, which were more sensitive to treatment. Jordan *et al.* (*114*) used PRESS-localized 136 ms TE ^{1}H MRS as well as ^{1}H and ^{31}P NMR of tumor extracts to evaluate response of HT29 xenografts after treatment with PX-478 to inhibit HIF-1α. Cho was significantly reduced after treatment, but there was no significant change in Lac+Lip, which appears, from the figures, to have been dominated by lipid resonances despite the long TE. High-resolution data showed significant reductions in PC, GPC, and mI, but no significant change in Lac; *in vitro* cell studies showed significant reduction in Lac under hypoxic conditions, where HIF-1α levels would be high in the absence of PX-478. *In vivo* data may be confounded by reduced perfusion post-treatment.

The Glickson group carried out a series of chemotherapy studies of the DLCL2 human diffuse large-B-cell lymphoma model in SCID mice. Initially (*272, 273*), they used both ^{1}H MRS sequences edited to measure Cho and lactate selectively, and ^{31}P MRS to measure response to the CHOPB and CHOP regimes. CHOPB resulted in significant reductions in Cho, Lac, and the PME/βNTP ratio, which was consistent with responders in clinical MRS studies of nonHodgkins lymphoma (*274, 275*). CHOP, on the other hand, resulted in no reduction in Cho or PME/βNTP, though there was a significant reduction in Lac, reduction in PE, and increase in GPE; the authors ascribed this to poor response, with the treatment resulting only in growth arrest, which was not sustained after treatment was halted. Subsequently (*276*), the same group compared changes in ^{1}H MRS in response to rituximab alone and rituximab combined with CHOP, finding a significant reduction in

Lac with CHOP treatment and a small but significant reduction in Cho with rituximab, alone or in combination with CHOP. The tCho reduction was not correlated with reduction in proliferation as assessed by Ki67 staining, which was significantly reduced by RCHOP but not by rituximab alone. RCHOP treatment resulted in 20% reduction in tumor volume. These studies are unusual in following a regime similar to that used clinically.

In a clinical study, Jagannathan *et al.* (*97*) found that Cho was reduced or absent in 89% of breast cancer patients after neoadjuvant chemotherapy. A number of studies have found MRS to be predictive of response; Meisamy *et al.* (*99*) found that reduction in Cho 24 h post-treatment was predictive of objective response to neoadjuvant chemotherapy with doxorubicin, and that the fractional change in Cho at 24 h was strongly correlated with the change in lesion diameter after four cycles of treatment. Reduction in Cho preceded reduction in tumor volume. However, Baek *et al.* (*277*) found that pathological complete responders could only be identified by Cho after four cycles of neoadjuvant therapy on a regime beginning with doxorubicin and cyclophosphamide. Tozaki *et al.* (*278*) observed a strong correlation between changes with treatment in Cho and changes in ^{18}FDG (fluorodeoxyglucose) PET. [More information on breast MRS of therapy response is available in a recent review by Sharma *et al.* (*279*).] Schwarz *et al.* acquired short-echo single-voxel MRS data from extracranial tumors including malignant lymphomas and germ-cell tumors, and found that the Cho:water ratio was reduced after the first cycle of chemotherapy in partial responders, and was unchanged in patients with progressive disease; these changes preceded significant reductions in tumor volume. Several studies of the response of gliomas to chemotherapy have been published; Balmaceda *et al.* (*280*) studied low-grade gliomas being treated with chemotherapy alone, finding that, where Lac was detectable in the tumors, decreases in Lac/Cr post-treatment were associated with response, and that increased Cho/Cr and reduced NAA/Cr in peritumoral brain post-treatment were associated with nonresponse. Dyke *et al.* (*281*) used CSI to study peritumoral brain in three patients with recently diagnosed GBM before and after surgery, and implantation of Gliadel wafers in the resection cavity. Two of the three patients showed reduced NAA/Cho and increased NAA/Cr ratios in the peritumoral brain 3–5 weeks after treatment, which the authors ascribe to the effect of Gliadel, since the surgery would not be expected to affect the peritumoral area directly. The usual pattern of reduced Cho in responders was not observed by Sankar *et al.*, who performed serial studies of patients undergoing tamoxifen treatment for GBM or anaplastic astrocytoma (*282*), in a follow-up to earlier work showing that linear discriminant analysis of pre-treatment CSI data could predict response to tamoxifen (*283*). Cho did not differ between responders and nonresponders either before, or during, the first 8 weeks of treatment. However, responders had significantly higher Cr and NAA, and significantly lower Lac, Lip, Cho/NAA, and Lac/NAA ratios; Lac and Lip levels fell over those first 8 weeks. Increases in Cho, Lip, Lac/NAA, and Cho/NAA preceded clinical failure.

As well as the Cho and Lac resonances that are the focus of the studies above, the mobile lipid signal has been investigated as a marker of response to chemotherapy. Hakumäki *et al.* (*127*) studied the rat BT4C brain tumor model treated with herpes simplex thymidine kinase (HSV-tk)/ganciclovir gene therapy as a model of apoptotic response to therapy; Cho fell significantly 6 days into treatment, but increases in lipid resonances were visible as early as 2 days into treatment, which correlated with increases in lipid droplets visible by electron microscopy. In particular, levels of PUFA increased. Total lipid levels measured *in vitro* were unchanged, suggesting that changes in MR visibility contribute to the increase of the *in vivo* signal. Lehtimäki *et al.* (*23*) studied the same model by *in vivo* MRS, MAS of biopsies, and high-resolution MRS of PCA extracts. Glycine, taurine, and Cr fell with treatment, but Cho remained constant with falling cell density until extremely late stages; MRS-detectable levels rose as previously reported. Liimatainen *et al.* (*183*) measured changes in mobile lipids and in tissue water apparent diffusion coefficient (ADC) in the same model *in vivo*; they found increases in lipid levels and ADC with the apoptotic response to this treatment, and a positive correlation between increased lipid levels and increased ADC for ADC levels below 100×10^{-5} mm^2/s, and ascribed the breakdown above this point to a large decrease in cell density and integrity. Schmitz *et al.* (*181*) observed similar lipid changes in EL4 tumors undergoing etoposide-induced apoptosis *in vivo*, and detected increased lipids in cell culture as early as 4 h post-treatment. Again, Cho levels *in vivo* showed no early changes with treatment.

Some clinical studies of breast cancer response to therapy have shown diagnostic value in the water/lipid ratio pre- and post-therapy. Jagannathan *et al.* (*284*) noted a significant reduction in the water/lipid ratio measured by long-echo (TE = 135 ms) spectroscopy between pre-treatment and the end of the chemotherapy course. Manton *et al.* (*285*) found percentage change with treatment in the water-to-lipid ratio measured at TE = 135 ms to be predictive of partial response, but not when the ratio was measured at TE = 30 ms; this was attributed primarily to changes in water T_2, which was also predictive of response.

In summary, response is generally reflected in reduced Cho, reduced Lac, and/or reduced Lip, though some evidence suggests apparent reductions in Lip may be confounded by changes in water T_2.

^{19}F MRS Studies of Chemotherapy

^{19}F MRS, for which there are no endogenous signals, is used to follow the pharmacokinetics of chemotherapeutic agents incorporating ^{19}F atoms. For example, Kristjansen *et* *al*. (*286*) monitored the time course of gemcitabine after injection of a single high dose to nude mice bearing CPH SCCLA 54A and 54B small cell lung cancer xenografts. The mean AUC for the 54B tumors was almost double that for the 54A ($P < 0.05$), and longer growth delays were observed for 54B tumors than 54A, reflecting greater exposure of the 54B cells to chemotherapy. The cytotoxic activity of gemcitabine depends on it being converted by phosphorylation to dFdCTP, which is incorporated into DNA. Deoxycytidine kinase (dCK) activity is the rate-limiting step in this process, and Blackstock *et al*. (*287*) used HPLC and *in vivo* ^{19}F MRS to investigate the effect of increased dCK expression on pharmacokinetics and tumor response to gemcitabine. The dCK tumors were more sensitive to treatment than wild-type, and the ^{19}F spectra showed signal persisting much longer in the dCK tumors, which was consistent with the enhanced levels of dFdCTP measured by HPLC. The authors suggested that ^{19}F MRS peak lifetime might be used clinically to predict response. Similarly, Cron *et al*. (*288*), used ^{19}F MRS to study changes in gemcitabine kinetics on treatment with the vascular modifiers BQ123, thalidomide, and Botulinum neurotoxin type A (BoNT-A); BoNT-A improved response, with a 1.7 day growth delay, and was also the only agent to increase gemcitabine uptake. The resonances of gemcitabine and its main catabolites, dFdCTP and dFdUrd, were not distinguishable in these *in vivo* experiments; Olive *et al*. (*289*) used ^{19}F MRS of tissue extracts to demonstrate that, in the genetically modified KPC mouse model of pancreatic cancer, pre-treatment with gemcitabine combined with IPI-926 (which inhibits the Hedgehog pathway and depletes tumor-associated stromal tissue, thus enhancing drug delivery), increased levels of gemcitabine and its metabolites by 60% after a single dose, compared with controls and with pre-treatment with gemcitabine or IPI-926 alone.

5FU was arguably the first rationally-designed anti-cancer agent; its structure is sufficiently similar to uracil to enter the same pathways, but sufficiently different to halt progression far down the pathways. It is converted to fluoronucleotides (FNuct) *in vivo*, in particular in rapidly-dividing cells; the key fluoronucleotides are FDUMP (which results in inhibtion of thymidylate synthase, leading to inhibition of DNA synthesis), and FUTP (which is incorporated into RNA, and disrupts normal RNA function) [usefully reviewed by Pinedo (*290*)]. Normal liver catabolizes a large proportion of the injected dose of 5FU to FBAL; FBAL detected in-tumor may be recirculated from the liver (*291, 292*). Unlike gemcitabine and its metabolites, the wider spread of the chemical shifts of the species involved in 5FU allows the resonances to be readily distinguished. 5FU can be given either as a bolus or by continuous infusion; it is simpler to measure the kinetics of a bolus dose, and this leads to transiently-higher levels of 5FU and its metabolites, and higher signal-to-noise ratio. The high sensitivity and absence of background signal for ^{19}F mean that it is, in principle, possible to image different chemical species, as Doi *et al*. (*293*) demonstrated in a mouse model giving oral 5FU at up to 260 mg/kg. In the model they used, FNuct levels were high enough to be imaged; in general, FNuct can be difficult to detect even with bolus doses, because the tissue concentrations are low, even at cytotoxic levels, and FNuct incorporated into RNA or DNA is unlikely to be visible by NMR. 5FU and FBAL (in liver) are readily detected *in vivo*, and resonances ~2 ppm downfield of FBAL are sometimes observed more frequently in experimental animals than in man. These may emanate from FUPA, carboxy-FBAL, or FBAL conjugated with bile acids in the gall bladder (*294*). In 1984, Malet-Martino *et al*. (*295*) used ^{19}F NMR to study 5FU metabolism in blood, plasma, and urine of patients treated with 5FU; in the same year, Stevens *et al* (*296*) performed the first *in vivo* MRS studies of 5FU metabolism in livers and tumors of C57 mice bearing Lewis lung carcinomas, detecting 5FU and FNuct in tumor, and 5FU, FBAL, and other products of the catabolic pathway in liver. They showed that a higher dose of 5FU led to FNuct concentrations elevated relative to the injected dose, and that were prolonged in lifetime. The first *in vivo* human study was performed in 1987 by Wolf *et al*. (*297*), who made measurements at 1.5T from the livers of three patients receiving bolus administration of 5FU. Wolf *et al*. later produced an extremely influential publication in the field (*298*), studying 5FU kinetics in human tumors as well as in rabbit VX2 carcinomas. Their initial results suggested a correlation between 5FU half-life in the tumor and tumor response, with those tumors with half-lives much longer than the plasma half-life being termed ''trappers.'' The clinical work was followed-up (*299, 300*), with over 100 patients eventually being studied. Seventy percent of trappers with 5FU half-lives greater than 20 min showed objective clinical responses, and all nontrappers were nonresponders. They concluded from pharmacokinetic modeling (*301*) that the bulk of 5FU visible at 20 min post-bolus injection was intracellular. In a later study (*302*), they used smaller surface coils, that were matched to the size of the individual patient's liver tumor, to investigate changes in 5FU half-life when the treatment was modulated with IFN-α or methotrexate in patients not responding to therapy with 5FU and leucovorin alone. Only five patients were studied, with four showing increased 5FU half-life with modulation, and two showing partial response to the IFN-5FU combination, with 41% and 30% increases in 5FU half-life, respectively. A comparison of 5FU half-life (*303*) in the presence and the absence of leucovorin showed no significant differences, consistent with the potentiating effect of leucovorin depending only on its effect on cellular metabolism. The methotrexate data are consistent with a rat study by El-Tahtawy *et al*. (*304*), which found reduced rates of elimination of 5FU from tumors, and elevated levels of FNuct on pre-treatment with methotrexate; similarly, the IFN-α data are consistent with a pre-clinical study by McSheehy *et al*. (*291*), which showed 5FU tumor half-life increasing almost 2-fold with co-administration of IFN-α. IFN also had the effect of increasing the ΔpH across the tumor cell membrane, as measured by ^{31}P MRS. A number of other studies have also combined ^{31}P and ^{19}F MRS to investigate the relationships between 5FU kinetics, tumor energetics, and pH. Guerqin-Kern *et al*. (*305*) used a dual-tuned surface coil to demonstrate a correlation between low intracellular pH as measured by ^{31}P MRS and extended 5FU half-life in tumor and muscle, and observed increases up to 2.5-fold at pH_i values below 6.9. While tumor pH_i is typically well-regulated, they employed a rat tumor model in which pH_i can drop as low as 6.8 in larger tumors; additionally, they employed ketamine or glucose infusion to induce intracellular acidosis. Extracellular pH was not measured in this study, but glucose-induced acidosis has been shown to cause even greater acidosis of pH_e, increasing the ΔpH (*306*). This is consistent with cell culture studies, such as those of Ojugo *et al*. (*307*), who used radiolabeled 5FU to show that 5FU uptake and retention improved with larger ΔpH across the cell membrane, as well as with lower pH_i. McSheehy *et al*. (*308*) used bafilomycin to reduce ΔpH without affecting pH_i, and showed that this reduced the half-life of 5FU in GH3 rat prolactinomas. They hypothesized that ΔpH determines 5FU membrane transport. Lemaire *et al*. (*309*) performed similar studies of the response of MNU chemically-induced rat tumors to 5FU, and found no relationship between 5FU half-life, FNuct levels, or pre-treatment pH and response; in that study, pre-treatment values of 0.9 or higher for the NTP/P_i ratio were the only significant predictor of tumor response.

Semmler *et al*. (*310*) measured half-lives of 5FU and FBAL in the livers of patients receiving intra-arterial 5FU chemotherapy for liver metastases ($n = 7$) and primary tumors ($n = 1$), finding 5FU half-lives from 8–75 min, and FBAL half-life values clustering around either 15 or 50 min, and observing a broad FNuct resonance in one patient. A number of later studies have been carried out on patients with liver tumors, despite the difficulty of separating metabolism in tumors from that in normal liver. For instance, Findlay *et al*. (*311*) studied patients receiving continuous infusion of 5FU, with IFN-α added to the regime when the disease became refractory to 5FU alone; they observed better response to 5FU alone when it was detectable by ^{19}F MRS, and that patients showing new or increased signals on IFN-α treatment were more likely to show response to IFN. Schlemmer *et al*. (*312*) noted higher- and longer-lasting 5FU levels in responders than in nonresponders; they also observed a correlation between 5FU levels and metastasis volume, estimating absolute concentrations of FBAL at 1–2 μmol/g liver tissue, and observing saturation of FBAL kinetics at doses above 1g 5FU. Li *et al*. (*313*) performed a feasibility study for 3D ^{19}F CSI of liver in patients with no liver disease, detecting 5FU and FBAL in 64ml voxels with 8.5 min time resolution; the same group (*314*) demonstrated improved resolution and SNR from proton-decoupled ^{19}F spectra of liver 5FU metabolism, especially for FBAL whose signal is a complex multiplet. Li *et al*. (*315*) elegantly acquired simultaneous ^{31}P and ^{19}F CSI data from the liver of a patient receiving 5FU chemotherapy, which reduced total scan time by half an hour, but this has not been followed-up.

The relatively low SNR of these studies has led to more recent CSI studies being carried out on 3T instruments where possible, although Klomp *et al*. (*316*) demonstrated approximately doubled sensitivity at 1.5T by using quadrature receive coils with integrated pre-amplifiers, and optimized excitation and data acquisition protocols. Dzik-Jurasz *et al*. (*294*) carried out CSI studies of the livers of patients receiving 5FU bolus or continuous infusion, observing a resonance 2.2 ppm downfield of FBAL localized to the gallbladder, and absent in patients whose gallbladders could not be identified. No other resonances were observed in patients receiving continuous infusion, and all other resonances disappeared at 4 h post-treatment in patients receiving bolus 5FU. They hypothesized that continuous infusion was resulting in a recirculating pool of catabolite maintaining detectable levels of FBAL conjugated with bile acids in the gallbladder. van Laarhoven *et al*. (*317*) correlated 5FU CSI data and DCE-MRI parameters with outcomes, finding a strong negative correlation between 5FU half-life and the DCE-MRI parameter K_{trans} (*318*); this suggests that 5FU wash-out is accelerated by high tumor blood flow and/or vessel permeability. None of the parameters were predictive of outcome, though the 5FU half-lives were all shorter than those defined as trappers by Wolf *et al*.

Griffiths *et al*. (*319*) published a study of the effect of breathing carbogen (95% O_2/5% CO_2) (which causes vasodilation and increased perfusion), during 5FU bolus administration in normal rats, and in the livers of two patients with colorectal primary tumors, but with no liver metastases. The preliminary clinical data of Griffiths *et al*. showed FNuct signals in normal liver, which had not previously been observed, and suggested that carbogen breathing might enhance FNuct levels. However, a later publication from the same group (*320*) showed no consistent changes in liver 5FU kinetics with carbogen breathing, which may, in part, be due to normal liver metabolism masking changes in tumor tissue. They confirmed detection of FNuct in the livers of patients with no liver disease, and showed that high levels of FNuct in patients with liver disease were associated with poor outcomes, possibly because the high FNuct signal resulted from high metastatic load. McSheehy *et al*. and Kamm *et al*. have published pre-clinical data on the effect of carbogen breathing on 5FU uptake and tumor response, which varies for different tumor models. For example, McSheehy *et al*. (*321*) found 5FU uptake and retention, and tumor response measured by initial decrease in volume and growth delay, were all significantly increased by carbogen breathing in the RIF-1 murine model, and that 5FU kinetics were unchanged in the GH3 prolactinoma (*322*), while in the rat H9618A hepatoma, FNuct increased despite a reduction in the 5FU half-life. Kamm *et al*. (*323*) in C38 murine colon tumors found increased levels of 5FU and its metabolites, but no increase in 5FU half-life; these effects were not reflected in improved tumor response. Kamm *et al*. (*324*) also compared two colon carcinoma lines with different sensitivity to 5FU; the more sensitive line showed higher levels of FNuct. Carbogen breathing during 5FU bolus increased the growth delay in the sensitive line, but made no significant changes to 5FU kinetics. van Laarhoven *et al*. (*325*) found carbogen increased 5FU uptake, decreased pH_e measured by ^{31}P MRS, and increased plasma volume measured using an intravascular contrast agent in C38 and C26a murine tumors; the more poorly perfused C26a line showed a greater improvement in response to chemotherapy with carbogen. McSheehy (*322*) assessed the results to date, together with ^{31}P data from the lines studied in that paper, as suggesting that the effects of carbogen breathing are a combination of increased blood flow, improved energy status, and increased transmembrane pH gradient, and that only in tumors where these combine to enhance FNuct production will carbogen improve response. These data suggest that the ability of MRS to distinguish FNuct from parent drug is potentially a significant advantage over PET.

McSheehy *et al*. also carried out a number of chemotherapy studies in mouse tumors; in 1989 (*326*), they used HPLC to validate *in vivo* measurements of FNuct levels in Walker carcinomas treated with different doses of 5FU and with allopurinol to inhibit conversion of 5FU to FNuct. They concluded that there was a correlation between FNuct levels measured by ^{19}F MRS and tumor response, and that at higher doses of 5FU the cytotoxic FUTP formed a higher proportion of the detected FNuct. They later showed (*327*) that pre-treatment with methotrexate (which increases levels of 5-phosphoribosyl-1-pyrophosphate, which favors conversion of 5FU to FUMP, and subsequently to FNuct) significantly increased FNuct formation in the same model and caused growth delay compared to treatment with 5FU followed 24 h later by methotrexate. Prior *et al*. (*328*) measured kinetics of 5FU and its analogues – 2′-deoxy-5-fluorouridine (2′FdURD), 5′-deoxy-5-fluorouridine (5′FdURD), and R,S-1-(tetrahydro-2-furyl)-5-fluorouracil (Ftorafur) – in rat liver and subcutaneous prolactinomas, noting that 2′FdURD and 5FU led to tumor growth delays when administered either as bolus or continuous infusion, although continuous infusion of 2′FdURD did not give detectable levels of FNuct. Similarly, Holland *et al*. (*329*) demonstrated increased formation and retention of FNuct in colon 38 xenografts when 5FU was combined with the uridine phosphorylase inhibitor 5-benzylacyclouridine.

Some preliminary studies have been carried out on capecitabine, an oral pro-drug of 5FU. It is metabolized to 5′-deoxy-5-fluorocytidine (5′DFCR) by hepatic carboxylesterase, and then to 5′-deoxy-5-fluorouridine (5′DFUR) by cytidine deaminase in liver and tumor tissue. 5′DFUR is converted to 5FU by thymidine phosphorylase (TP), which is highly active in tumor tissue; 5FU is therefore produced preferentially in tumor cells. Capecitabine thus has a higher therapeutic window than 5FU itself. Since the first two metabolic stages are active in the liver, measurements from this organ can be useful even in the absence of liver disease. van Laarhoven *et al*. (*330*) carried out liver CSI examinations in patients with liver and lung metastases of colorectal cancer at 1.5T and 3T, detecting the parent drug, 5′DFCR, 5′DFUR, FBAL, and FBAL-bile acid conjugates. 5FU, which is rapidly converted to FBAL or FNuct as it is produced, and FNuct, were below the limit of detection, even using the higher-field magnet, which gave SNR values between 1.3–3-fold higher, and better spectral resolution. The same group, in 2007 (*331*), published a feasibility study for absolute quantification of ^{19}F CSI using a coil detunable to ^{1}H to obtain a water reference, with results consistent with literature values, and demonstrating different distributions for capecitabine and FBAL in normal liver. Chung *et al*. (*332*) studied the metabolism of capecitabine and 5′DFUR by murine bladder tumor models with different levels of TP, observing higher degradation rates of 5′DFUR with higher TP levels, as expected.

^{13}C MRS Studies of Chemotherapy

Carbon spectroscopy has been applied in pharmacodynamic and metabolic studies of chemotherapy for many years. For example, Poptani *et al*. (*333*) measured [3-^{13}C] Lac production in RIF-1 tumors during infusion of [1-^{13}C] glucose with proton-decoupled NOE-enhanced nonlocalized spectroscopy at 5 min time resolution, demonstrating a significant reduction of >50% in glycolytic rate constant 24 h post treatment with cyclophosphamide, consistent with a shift towards oxidative metabolism. Fluorescence measurements showed NADH levels to be increased post-treatment. Rivenzon-Segal *et al*. (*4, 334*) infused ^{13}C-glucose in breast cancer models, demonstrating reduction in glycolysis in response to tamoxifen treatment. Many recent works have employed hyperpolarization of ^{13}C for rapid, sensitive metabolic measurements. For example, Day *et al*. (*7*) investigated the effect of etoposide on the flux of hyperpolarized [1-^{13}C] pyruvate-to-Lac in EL-4 lymphoma cells in culture and grown as xenografts in mice, obtaining CSI data in 5 s with sufficient resolution to differentiate tumor- and normal-tissue metabolism. Reduction of NADH activity (which reduces pyruvate-Lac exchange) and of endogenous Lac by etoposide, results in substantial reduction of the hyperpolarized Lac signal, which is a potential biomarker of etoposide activity. This was followed up (*335*) by a comparison of the flux of hyperpolarized [1-^{13}C] pyruvate-to-Lac in the same models, with scintillation counting of [^{14}C]FDG as a surrogate for PET imaging. The etoposide-induced fall in the pyruvate-Lac exchange rate constant paralleled the reduction in FDG uptake, although FDG uptake fell more rapidly after treatment. This is potentially useful as a clinical response biomarker, particularly in the brain, where FDG is taken up avidly in uninvolved tissue as well as in viable tumor tissue. Similarly, Seth *et al*. (*336*) studied changes in pyruvate-to-Lac flux with inhibition of LDH by dichloroacetate. Response has also been observed with other chemotherapeutic agents and hyperpolarized substrates. Park *et al* (*337*) showed reduction in the Lac/pyruvate ratio in a rat brain tumor model as early as 1 day post-treatment with temozolomide. Gallagher *et al*. (*338*) demonstrated that conversion of hyperpolarized [1,4-$^{13}C_2$]fumarate to malate is enhanced in EL4 cells, and in tumors undergoing necrosis after etoposide treatment, due to membrane breakdown in necrosis, and allows the fumarate easy access to the intracellular enzyme fumarase, which catalyzes this reaction. Bohndiek *et al*. (*339*) used hyperpolarized pyruvate and fumarate, as well as DCE-MRI and diffusion-weighted imaging (DWI), to assess EL4 tumors 6 and 24 h after treatment with the vascular-disrupting agent combretastatin-A4-phosphate; tumor volumes were unaltered by this treatment. DWI showed no change; DCE-MRI showed a reduction in AUC at 6 h, which was gone by 24 h as perfusion was restored. However, the reduction in pyruvate-lactate exchange at 6 h was sustained at 24 hours, and malate production rose at 6 h and rose further at 24 h, representing increased necrosis at this time point, giving metabolic information not evident with the more conventional MRI techniques. Witney *et al*. (*340*) showed similar MRS results in MDA-MB-231 cells and xenografts after treatment with doxorubicin. Ward *et al*. (*341*) used hyperpolarized pyruvate in cultured cells and xenografts to investigate inhibition of PI3K by LY294002, and inhibition of mTOR by everolimus. Reduced HIF-1 activity led to reduction in LDH, and significant reductions of the flux from hyperpolarized pyruvate-to-Lac in GS2 cells and tumors, and MDA-MB-231 cells.

CONCLUSIONS

NMR spectroscopy is a useful tool for probing tumor metabolism and response to treatment, with wide applications. As is evident from the vast number of studies presented in this review, *in vitro* and *ex vivo* NMR spectroscopic analysis of cells and biopsies is widely applied in basic scientific research of cancer to investigate tumor metabolism, response to treatment, and cancer biology. On the other hand, successful preclinical *in vivo* MR applications can be readily translated into clinical cancer research studies with minor modifications. The field of MRS applications is well suited for carrying out translational (''bench to bed side'' and vice versa) research. At present, ^{1}H MRS is the most common method in clinical use. This is, in part, because standard hospital scanners are capable of acquiring MRS data from this nucleus, but require specialized additional hardware to work with other nuclei. Clinical translation of the rapidly-expanding field of hyperpolarized ^{13}C spectroscopy may, in the future, see wider use of nonproton spectroscopy.

ACKNOWLEDGMENTS

We would like to acknowledge the support of The University of Cambridge, Cancer Research UK and Hutchison Whampoa Limited.

Received: December 14, 2011; accepted: February 8, 2012; published online: March 8, 2012

REFERENCES

1. J. R. Griffiths, Are cancer cells acidic? Br J Cancer **64**, 425–427 (1991).

2. W. Heindel, J. Bunke, S. Glathe, W. Steinbrich and L. Mollevanger, Combined H1 MR imaging and localized P31 spectroscopy of intracranial tumors in 43 patients. Journal of Computer Assisted Tomography **12**, 907–916 (1988).

3. D. Artemov, Z. M. Bhujwalla and J. D. Glickson, In vivo selective measurement of (1-13C)-glucose metabolism in tumors by heteronuclear cross polarization. Magn Reson Med **33**, 151–155 (1995).

4. D. Rivenzon-Segal, R. Margalit and H. Degani, Glycolysis as a metabolic marker in orthotopic breast cancer, monitored by in vivo C-13 MRS. American Journal of Physiology-Endocrinology and Metabolism **283**, E623–E630 (2002).

5. J. H. Ardenkjaer-Larsen, B. Fridlund, A. Gram, G. Hansson, L. Hansson, M. H. Lerche, R. Servin, M. Thaning and K. Golman, Increase in signal-to-noise ratio of $>$ 10,000 times in liquid-state NMR. Proc Natl Acad Sci U S A **100**, 10158–10163 (2003).

6. A. I. Hashim, X. Zhang, J. W. Wojtkowiak, G. V. Martinez and R. J. Gillies, Imaging pH and metastasis. NMR Biomed **24**, 582–591 (2011).

7. S. E. Day, M. I. Kettunen, F. A. Gallagher, D. E. Hu, M. Lerche, J. Wolber, K. Golman, J. H. Ardenkjaer-Larsen and K. M. Brindle, Detecting tumor response to treatment using hyperpolarized C-13 magnetic resonance imaging and spectroscopy. Nature Medicine **13**, 1382–1387 (2007).

8. M. Garwood and L. DelaBarre, The Return of the Frequency Sweep: Designing Adiabatic Pulses for Contemporary NMR. Journal of Magnetic Resonance **153**, 155–177 (2001).

9. L. Barantin, A. Le Pape and S. Akoka, A new method for absolute quantitation of MRS metabolites. Magn Reson Med **38**, 179–182 (1997).

10. A. Naressi, C. Couturier, J. M. Devos, M. Janssen, C. Mangeat, R. de Beer and D. Graveron-Demilly, Java-based graphical user interface for the MRUI quantitation package. MAGMA. **12**, 141–152 (2001).

11. L. Vanhamme, A. van den Boogaart and S. Van Huffel, Improved method for accurate and efficient quantification of MRS data with use of prior knowledge. Journal of Magnetic Resonance **129**, 35–43 (1997).

12. S. W. Provencher, Estimation of metabolite concentrations from localized in vivo proton NMR spectra. Magn Reson Med **30**, 672–679 (1993).

13. J. E. Le Belle, N. G. Harris, S. R. Williams and K. K. Bhakoo, A comparison of cell and tissue extraction techniques using high-resolution 1H-NMR spectroscopy. NMR Biomed **15**, 37–44 (2002).

14. R. K. Tyagi, A. Azrad, H. Degani and Y. Salomon, Simultaneous extraction of cellular lipids and water-soluble metabolites: evaluation by NMR spectroscopy. Magn Reson Med **35**, 194–200 (1996).

15. A. B. E. R. Andrew, R. G. Eades Nuclear magnetic resonance spectra from a crystal rotated at high speed. Nature **182**, 1659 (1958).

16. R. Haberkorn, J. Herzfeld and R. Griffin, High resolution phosphorus-31 and carbon-13 nuclear magnetic resonance spectra of unsonicated model membranes. J Am Chem Soc **100**, 1296–1298 (1978).

17. J. D. Gross, P. R. Costa, J. P. Dubacq, D. E. Warschawski, P. N. Lirsac, P. F. Devaux and R. G. Griffin, Multidimensional NMR in lipid systems. Coherence transfer through J couplings under MAS. J Magn Reson B **106**, 187–190 (1995).

18. J. H. Davis, M. Auger and R. S. Hodges, High resolution 1H nuclear magnetic resonance of a transmembrane peptide. Biophys J **69**, 1917–1932 (1995).

19. L. L. Cheng, M. J. Ma, L. Becerra, T. Ptak, I. Tracey, A. Lackner and R. G. Gonzalez, Quantitative neuropathology by high resolution magic angle spinning proton magnetic resonance spectroscopy. Proc Natl Acad Sci U S A **94**, 6408–6413 (1997).

20. L. L. Cheng, I. W. Chang, D. N. Louis and R. G. Gonzalez, Correlation of high-resolution magic angle spinning proton magnetic resonance spectroscopy with histopathology of intact human brain tumor specimens. Cancer Res **58**, 1825–1832 (1998).

21. L. L. Cheng, I. W. Chang, B. L. Smith and R. G. Gonzalez, Evaluating human breast ductal carcinomas with high-resolution magic-angle spinning proton magnetic resonance spectroscopy. J Magn Reson **135**, 194–202 (1998).

22. L. L. Cheng, C. Wu, M. R. Smith and R. G. Gonzalez, Non-destructive quantitation of spermine in human prostate tissue samples using HRMAS 1H NMR spectroscopy at 9.4 T. FEBS Lett **494**, 112–116 (2001).

23. K. K. Lehtimaki, P. K. Valonen, J. L. Griffin, T. H. Vaisanen, O. H. J. Grohn, M. I. Kettunen, J. Vepsalainen, S. Yla-Herttuala, J. Nicholson and R. A. Kauppinen, Metabolite changes in BT4C rat gliomas undergoing ganciclovir-thymidine kinase gene therapy-induced programmed cell death as studied by H-1 NMR spectroscopy in vivo, ex vivo, and in vitro. Journal of Biological Chemistry **278**, 45915–45923 (2003).

24. P. K. Valonen, J. L. Griffin, K. K. Lehtimaki, T. Liimatainen, J. K. Nicholson, O. H. Grohn and R. A. Kauppinen, High-resolution magic-angle-spinning 1H NMR spectroscopy reveals different responses in choline-containing metabolites upon gene therapy-induced programmed cell death in rat brain glioma. NMR Biomed **18**, 252–259 (2005).

25. B. Madhu, J. C. Waterton, J. R. Griffiths, A. J. Ryan and S. P. Robinson, The response of RIF-1 fibrosarcomas to the vascular-disrupting agent ZD6126 assessed by in vivo and ex vivo 1H magnetic resonance spectroscopy. Neoplasia **8**, 560–567 (2006).

26. K. S. Opstad, B. A. Bell, J. R. Griffiths and F. A. Howe, Toward accurate quantification of metabolites, lipids, and macromolecules in HRMAS spectra of human brain tumor biopsies using LCModel. Magn Reson Med **60**, 1237–1242 (2008).

27. H. Rabeson, F. Fauvelle, G. Testylier, A. Foquin, P. Carpentier, F. Dorandeu, D. van Ormondt and D. Graveron-Demilly, Quantitation with QUEST of brain HRMAS-NMR signals: application to metabolic disorders in experimental epileptic seizures. Magn Reson Med **59**, 1266–1273 (2008).

28. H. Ratiney, M. J. Albers, H. Rabeson and J. Kurhanewicz, Semi-parametric time-domain quantification of HR-MAS data from prostate tissue. NMR Biomed **23**, 1146–1157 (2010).

29. M. Wilson, G. Reynolds, R. A. Kauppinen, T. N. Arvanitis and A. C. Peet, A constrained least-squares approach to the automated quantitation of in vivo (1)H magnetic resonance spectroscopy data. Magn Reson Med **65**, 1–12 (2011).

30. O. Risa, T. M. Melo and U. Sonnewald, Quantification of amounts and (13)C content of metabolites in brain tissue using high-resolution magic angle spinning (13)C NMR spectroscopy. NMR Biomed **22**, 266–271 (2009).

31. S. Moestue, B. Sitter, T. F. Bathen, M. B. Tessem and I. S. Gribbestad, HR MAS MR spectroscopy in metabolic characterization of cancer. Curr Top Med Chem **11**, 2–26 (2010).

32. J. L. Griffin, C. Blenkiron, P. K. Valonen, C. Caldas and R. A. Kauppinen, High-resolution magic angle spinning 1H NMR spectroscopy and reverse transcription-PCR analysis of apoptosis in a rat glioma. Anal Chem **78**, 1546–1552 (2006).

33. E. M. DeFeo and L. L. Cheng, Characterizing human cancer metabolomics with ex vivo 1H HRMAS MRS. Technol Cancer Res Treat **9**, 381–391 (2010).

34. G. S. Payne, H. Troy, S. J. Vaidya, J. R. Griffiths, M. O. Leach and Y. L. Chung, Evaluation of 31P high-resolution magic angle spinning of intact tissue samples. NMR Biomed **19**, 593–598 (2006).

35. M. C. Martinez-Bisbal, L. Marti-Bonmati, J. Piquer, A. Revert, P. Ferrer, J. L. Llacer, M. Piotto, O. Assemat and B. Celda, 1H and 13C HR-MAS spectroscopy of intact biopsy samples ex vivo and in vivo 1H MRS study of human high grade gliomas. NMR Biomed **17**, 191–205 (2004).

36. K. S. Opstad, A. J. Wright, B. A. Bell, J. R. Griffiths and F. A. Howe, Correlations between in vivo (1)H MRS and ex vivo (1)H HRMAS metabolite measurements in adult human gliomas. J Magn Reson Imaging **31**, 289–297 (2010).

37. A. A. Tzika, L. Astrakas, H. Cao, D. Mintzopoulos, O. C. Andronesi, M. Mindrinos, J. Zhang, L. G. Rahme, K. D. Blekas, et al., Combination of high-resolution magic angle spinning proton magnetic resonance spectroscopy and microscale genomics to type brain tumor biopsies. Int J Mol Med **20**, 199–208 (2007).

38. O. Warburg, The Metabolism of Tumors. Constable, London, 1930.

39. R. J. DeBerardinis, J. J. Lum, G. Hatzivassiliou and C. B. Thompson, The biology of cancer: metabolic reprogramming fuels cell growth and proliferation. Cell Metab **7**, 11–20 (2008).

40. G. Kroemer and J. Pouyssegur, Tumor cell metabolism: cancer's Achilles' heel. Cancer Cell **13**, 472–482 (2008).

41. J. W. Kim, I. Tchernyshyov, G. L. Semenza and C. V. Dang, HIF-1-mediated expression of pyruvate dehydrogenase kinase: a metabolic switch required for cellular adaptation to hypoxia. Cell Metab **3**, 177–185 (2006).

42. I. Papandreou, R. A. Cairns, L. Fontana, A. L. Lim and N. C. Denko, HIF-1 mediates adaptation to hypoxia by actively downregulating mitochondrial oxygen consumption. Cell Metab **3**, 187–197 (2006).

43. M. Terpstra, R. Gruetter, W. B. High, M. Mescher, L. DelaBarre, H. Merkle and M. Garwood, Lactate turnover in rat glioma measured by in vivo nuclear magnetic resonance spectroscopy. Cancer Res **58**, 5083–5088 (1998).

44. M. Terpstra, W. B. High, Y. Luo, R. A. de Graaf, H. Merkle and M. Garwood, Relationships among lactate concentration, blood flow and histopathologic profiles in rat C6 glioma. NMR Biomed **9**, 185–194 (1996).

45. D. Ott, J. Hennig and T. Ernst, Human brain tumors: assessment with in vivo proton MR spectroscopy. Radiology **186**, 745–752 (1993).

46. H. Kugel, W. Heindel, R. I. Ernestus, J. Bunke, R. du Mesnil and G. Friedmann, Human brain tumors: spectral patterns detected with localized H-1 MR spectroscopy. Radiology **183**, 701–709 (1992).

47. A. K. Bouzier, R. Goodwin, F. M. de Gannes, H. Valeins, P. Voisin, P. Canioni and M. Merle, Compartmentation of lactate and glucose metabolism in C6 glioma cells. A 13c and 1H NMR study. J Biol Chem **273**, 27162–27169 (1998).

48. D. Artemov, Z. M. Bhujwalla, U. Pilatus and J. D. Glickson, Two-compartment model for determination of glycolytic rates of solid tumors by in vivo 13C NMR spectroscopy. NMR Biomed **11**, 395–404 (1998).

49. F. U. Nielsen, P. Daugaard, L. Bentzen, H. Stodkilde-Jorgensen, J. Overgaard, M. R. Horsman and R. J. Maxwell, Effect of changing tumor oxygenation on glycolytic metabolism in a murine C3H mammary carcinoma assessed by in vivo nuclear magnetic resonance spectroscopy. Cancer Res **61**, 5318–5325 (2001).

50. G. Migneco, D. Whitaker-Menezes, B. Chiavarina, R. Castello-Cros, S. Pavlides, R. G. Pestell, A. Fatatis, N. Flomenberg, A. Tsirigos, et al., Glycolytic cancer associated fibroblasts promote breast cancer tumor growth, without a measurable increase in angiogenesis: evidence for stromal-epithelial metabolic coupling. Cell Cycle **9**, 2412–2422 (2010).

51. S. Pavlides, D. Whitaker-Menezes, R. Castello-Cros, N. Flomenberg, A. K. Witkiewicz, P. G. Frank, M. C. Casimiro, C. Wang, P. Fortina, et al., The reverse Warburg effect: aerobic glycolysis in cancer associated fibroblasts and the tumor stroma. Cell Cycle **8**, 3984–4001 (2009).

52. C. M. Cham and T. F. Gajewski, Glucose availability regulates IFN-gamma production and p70S6 kinase activation in CD8+ effector T cells. J Immunol **174**, 4670–4677 (2005).

53. K. A. Frauwirth and C. B. Thompson, Regulation of T lymphocyte metabolism. J Immunol **172**, 4661–4665 (2004).

54. K. Golman, R. I. Zandt, M. Lerche, R. Pehrson and J. H. Ardenkjaer-Larsen, Metabolic imaging by hyperpolarized 13C magnetic resonance imaging for in vivo tumor diagnosis. Cancer Res **66**, 10855–10860 (2006).

55. M. J. Albers, R. Bok, A. P. Chen, C. H. Cunningham, M. L. Zierhut, V. Y. Zhang, S. J. Kohler, J. Tropp, R. E. Hurd, et al., Hyperpolarized 13C lactate, pyruvate, and alanine: noninvasive biomarkers for prostate cancer detection and grading. Cancer Res **68**, 8607–8615 (2008).

56. I. Park, P. E. Larson, M. L. Zierhut, S. Hu, R. Bok, T. Ozawa, J. Kurhanewicz, D. B. Vigneron, S. R. Vandenberg, et al., Hyperpolarized 13C magnetic resonance metabolic imaging: application to brain tumors. Neuro-Oncology **12**, 133–144 (2010).

57. V. Collet, D. Carrez, A. Croisy and J. L. Dimicoli, Effect of methionine on glycolysis in tumor cells: in vivo and in vitro NMR studies. NMR Biomed **9**, 47–52 (1996).

58. S. Telang, A. N. Lane, K. K. Nelson, S. Arumugam and J. Chesney, The oncoprotein H-RasV12 increases mitochondrial metabolism. Mol Cancer **6**, 77 (2007).

59. R. J. DeBerardinis, A. Mancuso, E. Daikhin, I. Nissim, M. Yudkoff, S. Wehrli and C. B. Thompson, Beyond aerobic glycolysis: transformed cells can engage in glutamine metabolism that exceeds the requirement for protein and nucleotide synthesis. Proc Natl Acad Sci U S A **104**, 19345–19350 (2007).

60. T. W. Fan, M. Kucia, K. Jankowski, R. M. Higashi, J. Ratajczak, M. Z. Ratajczak and A. N. Lane, Rhabdomyosarcoma cells show an energy producing anabolic metabolic phenotype compared with primary myocytes. Mol Cancer **7**, 79 (2008).

61. T. W. Fan, A. N. Lane, R. M. Higashi, M. A. Farag, H. Gao, M. Bousamra and D. M. Miller, Altered regulation of metabolic pathways in human lung cancer discerned by (13)C stable isotope-resolved metabolomics (SIRM). Mol Cancer **8**, 41 (2009).

62. J. R. Griffiths, A. N. Stevens, R. A. Iles, R. E. Gordon and D. Shaw, 31P-NMR investigation of solid tumors in the living rat. Biosci Rep **1**, 319–325 (1981).

63. W. T. Evanochko, T. C. Ng, J. D. Glickson, J. R. Durant and T. H. Corbett, Human tumors as examined by in vivo 31P NMR in athymic mice. Biochem Biophys Res Commun **109**, 1346–1352 (1982).

64. J. R. Griffiths, E. Cady, R. H. Edwards, V. R. McCready, D. R. Wilkie and E. Wiltshaw, 31P-NMR studies of a human tumor in situ. Lancet **1**, 1435–1436 (1983).

65. J. D. de Certaines, V. A. Larsen, F. Podo, G. Carpinelli, O. Briot and O. Henriksen, In vivo 31P MRS of experimental tumors. NMR Biomed **6**, 345–365 (1993).

66. W. Negendank, Studies of human tumors by MRS: a review. NMR Biomed **5**, 303–324 (1992).

67. F. Arias-Mendoza, K. Zakian, A. Schwartz, F. A. Howe, J. A. Koutcher, M. O. Leach, J. R. Griffiths, A. Heerschap, J. D. Glickson, et al., Methodological standardization for a multi-institutional in vivo trial of localized 31P MR spectroscopy in human cancer research. In vitro and normal volunteer studies. NMR Biomed **17**, 382–391 (2004).

68. F. Arias-Mendoza, G. S. Payne, K. Zakian, M. Stubbs, J. G. Cruz-Lobo, A. J. Schwarz, A. Shukla-Dave, F. Howe, N. R. Maisey, et al., Treatment response predictor using 31P MRS for chop and R-chop therapy in diffuse large B-cell lymphoma. Annals of Oncology **19**, 147–147 (2008).

69. F. Arias-Mendoza, G. S. Payne, K. L. Zakian, A. J. Schwarz, M. Stubbs, R. Stoyanova, D. Ballon, F. A. Howe, J. A. Koutcher, et al., In vivo 31P MR spectral patterns and reproducibility in cancer patients studied in a multi-institutional trial. NMR Biomed **19**, 504–512 (2006).

70. F. Arias-Mendoza, M. O. Leach, J. A. Koutcher, J. R. Griffiths, A. Heerschap, J. D. Glickson, O. A. O'Connor, T. R. Brown and M. R. A. C. Cooperat Grp, Prediction of treatment response in subtypes of non-Hodgkin's lymphoma by in vivo P-31 MR spectroscopy before treatment. Journal of Clinical Oncology **27**, 8565 (2009).

71. F. Arias-Mendoza, M. R. Smith and T. R. Brown, Predicting treatment response in non-Hodgkin's lymphoma from the pretreatment tumor content of phosphoethanolamine plus phosphocholine. Academic Radiology **11**, 368–376 (2004).

72. R. Kalra, K. E. Wade, L. Hands, P. Styles, R. Camplejohn, M. Greenall, G. E. Adams, A. L. Harris and G. K. Radda, Phosphomonoester is associated with proliferation in human breast cancer: a 31P MRS study. Br J Cancer **67**, 1145–1153 (1993).

73. X. Maldonado, J. Alonso, J. Giralt, M. G. Cucurella, J. M. del Campo, A. Rovira, E. Felip, J. Capellades, E. Grivé, et al., 31Phosphorus magnetic resonance spectroscopy in the assessment of head and neck tumors. Int J Radiat Oncol Biol Phys **40**, 309–312 (1998).

74. M. G. Vander Heiden, L. C. Cantley and C. B. Thompson, Understanding the Warburg effect: the metabolic requirements of cell proliferation. Science **324**, 1029–1033 (2009).

75. S. J. Li, J. P. Wehrle, S. S. Rajan, R. G. Steen, J. D. Glickson and J. Hilton, Response of radiation-induced fibrosarcoma-1 in mice to cyclophosphamide monitored by in vivo 31P nuclear magnetic resonance spectroscopy. Cancer Res **48**, 4736–4742 (1988).

76. P. G. Okunieff, J. A. Koutcher, L. Gerweck, E. McFarland, B. Hitzig, M. Urano, T. Brady, L. Neuringer and H. D. Suit, Tumor size dependent changes in a murine fibrosarcoma: use of in vivo 31P NMR for non-invasive evaluation of tumor metabolic status. Int J Radiat Oncol Biol Phys **12**, 793–799 (1986).

77. R. F. Kallman, The phenomenon of reoxygenation and its implications for fractionated radiotherapy. Radiology **105**, 135–142 (1972).

78. G. M. Tozer and J. R. Griffiths, The contribution made by cell death and oxygenation to 31P MRS observations of tumor energy metabolism. NMR Biomed **5**, 279–289 (1992).

79. D. R. Olsen and E. K. Rofstad, Monitoring of tumor reoxygenation following irradiation by 31P magnetic resonance spectroscopy: an experimental study of human melanoma xenografts. Radiother Oncol **52**, 261–267 (1999).

80. H. Lyng, D. R. Olsen, T. E. Southon and E. K. Rofstad, 31P-nuclear magnetic resonance spectroscopy in vivo of six human melanoma xenograft lines: tumor bioenergetic status and blood supply. Br J Cancer **68**, 1061–1070 (1993).

81. J. A. Koutcher, A. A. Alfieri, M. L. Devitt, J. G. Rhee, A. B.

Kornblith, U. Mahmood, T. E. Merchant and D. Cowburn, Quantitative changes in tumor metabolism, partial pressure of oxygen, and radiobiological oxygenation status postradiation. Cancer Res **52**, 4620–4627 (1992).

82. X. L. Zu and M. Guppy, Cancer metabolism: facts, fantasy, and fiction. Biochem Biophys Res Commun **313**, 459–465 (2004).

83. P. Vaupel, F. Kallinowski and P. Okunieff, Blood flow, oxygen and nutrient supply, and metabolic microenvironment of human tumors: a review. Cancer Res **49**, 6449–6465 (1989).

84. M. Guppy, P. Leedman, X. Zu and V. Russell, Contribution by different fuels and metabolic pathways to the total ATP turnover of proliferating MCF-7 breast cancer cells. Biochem J **364**, 309–315 (2002).

85. M. Stubbs and J. R. Griffiths, The altered metabolism of tumors: HIF-1 and its role in the Warburg effect. Adv Enzyme Regul **50**, 44–55 (2010).

86. H. Schmidt, W. Siems, M. Muller, R. Dumdey and S. M. Rapoport, ATP-producing and consuming processes of Ehrlich mouse ascites tumor cells in proliferating and resting phases. Exp Cell Res **194**, 122–127 (1991).

87. D. W. Parsons, S. Jones, X. Zhang, J. C. Lin, R. J. Leary, P. Angenendt, P. Mankoo, H. Carter, I. M. Siu, et al., An integrated genomic analysis of human glioblastoma multiforme. Science **321**, 1807–1812 (2008).

88. L. Dang, D. W. White, S. Gross, B. D. Bennett, M. A. Bittinger, E. M. Driggers, V. R. Fantin, H. G. Jang, S. Jin, et al., Cancer-associated IDH1 mutations produce 2-hydroxyglutarate. Nature **462**, 739–744 (2009).

89. A. K. Bouzier, B. Quesson, H. Valeins, P. Canioni and M. Merle, [1-(13)C]glucose metabolism in the tumoral and nontumoral cerebral tissue of a glioma-bearing rat. J Neurochem **72**, 2445–2455 (1999).

90. J. C. Portais, R. Schuster, M. Merle and P. Canioni, Metabolic flux determination in C6 glioma cells using carbon-13 distribution upon [1-13C]glucose incubation. Eur J Biochem **217**, 457–468 (1993).

91. M. A. Schroeder, H. J. Atherton, D. R. Ball, M. A. Cole, L. C. Heather, J. L. Griffin, K. Clarke, G. K. Radda and D. J. Tyler, Real-time assessment of Krebs cycle metabolism using hyperpolarized 13C magnetic resonance spectroscopy. FASEB J **23**, 2529–2538 (2009).

92. F. Podo, Tumor phospholipid metabolism. NMR Biomed **12**, 413–439 (1999).

93. E. O. Aboagye and Z. M. Bhujwalla, Malignant transformation alters membrane choline phospholipid metabolism of human mammary epithelial cells. Cancer Res **59**, 80–84 (1999).

94. E. Iorio, D. Mezzanzanica, P. Alberti, F. Spadaro, C. Ramoni, S. D'Ascenzo, D. Millimaggi, A. Pavan, V. Dolo, et al., Alterations of choline phospholipid metabolism in ovarian tumor progression. Cancer Res **65**, 9369–9376 (2005).

95. J. L. Griffin and R. A. Kauppinen, A metabolomics perspective of human brain tumors. FEBS J **274**, 1132–1139 (2007).

96. C. F. Santos, J. Kurhanewicz, Z. L. Tabatabai, J. P. Simko, K. R. Keshari, A. Gbegnon, R. D. Santos, S. Federman, K. Shinohara, et al., Metabolic, pathologic, and genetic analysis of prostate tissues: quantitative evaluation of histopathologic and mRNA integrity after HR-MAS spectroscopy. NMR Biomed **23**, 391–398 (2010).

97. N. R. Jagannathan, M. Kumar, V. Seenu, O. Coshic, S. N. Dwivedi, P. K. Julka, A. Srivastava and G. K. Rath, Evaluation of total choline from in-vivo volume localized proton MR spectroscopy and its response to neoadjuvant chemotherapy in locally advanced breast cancer. Br J Cancer **84**, 1016–1022 (2001).

98. P. J. Bolan, S. Meisamy, E. H. Baker, J. Lin, T. Emory, M. Nelson, L. I. Everson, D. Yee and M. Garwood, In vivo quantification of choline compounds in the breast with 1H MR spectroscopy. Magn Reson Med **50**, 1134–1143 (2003).

99. S. Meisamy, P. J. Bolan, E. H. Baker, R. L. Bliss, E. Gulbahce, L. I. Everson, M. T. Nelson, T. H. Emory, T. M. Tuttle, et al., Neoadjuvant chemotherapy of locally advanced breast cancer: Predicting response with in vivo H-1 MR spectroscopy - A pilot study. Radiology **233**, 424–431 (2004).

100. A. Heerschap, G. J. Jager, M. van der Graaf, J. O. Barentsz, J. J. de la Rosette, G. O. Oosterhof, E. T. Ruijter and S. H. Ruijs, In vivo proton MR spectroscopy reveals altered metabolite content in malignant prostate tissue. Anticancer Res **17**, 1455–1460 (1997).

101. J. M. Star-Lack, E. Adalsteinsson, M. F. Adam, D. J. Terris, H. A. Pinto, J. M. Brown and D. M. Spielman, In vivo 1H MR spectroscopy of human head and neck lymph node metastasis and comparison with oxygen tension measurements. AJNR Am J Neuroradiol **21**, 183–193 (2000).

102. C. W. Mun, J. Y. Cho, W. J. Shin, K. S. Choi, C. K. Eun, S. S. Cha, J. Lee, Y. I. Yang, S. H. Nam, et al., Ex vivo proton MR spectroscopy (1H-MRS) for evaluation of human gastric carcinoma. Magn Reson Imaging **22**, 861–870 (2004).

103. M. J. Albers, M. D. Krieger, I. Gonzalez-Gomez, F. H. Gilles, J. G. McComb, M. D. Nelson, Jr. and S. Bluml, Proton-decoupled 31P MRS in untreated pediatric brain tumors. Magn Reson Med **53**, 22–29 (2005).

104. R. M. Bourne, P. Stanwell, J. R. Stretch, R. A. Scolyer, J. F. Thompson, C. E. Mountford and C. L. Lean, In vivo and ex vivo proton MR spectroscopy of primary and secondary melanoma. Eur J Radiol **53**, 506–513 (2005).

105. A. D. King, D. K. Yeung, A. T. Ahuja, G. M. Tse, A. B. Chan, S. S. Lam and A. C. van Hasselt, In vivo 1H MR spectroscopy of thyroid carcinoma. Eur J Radiol **54**, 112–117 (2005).

106. R. V. Simoes, A. Martinez-Aranda, B. Martin, S. Cerdan, A. Sierra and C. Arus, Preliminary characterization of an experimental breast cancer cells brain metastasis mouse model by MRI/MRS. MAGMA **21**, 237–249 (2008).

107. F. Podo, S. Canevari, R. Canese, M. E. Pisanu, A. Ricci and E. Iorio, MR evaluation of response to targeted treatment in cancer cells. NMR Biomed (2011).

108. S. S. Gill, D. G. Thomas, N. Van Bruggen, D. G. Gadian, C. J. Peden, J. D. Bell, I. J. Cox, D. K. Menon, R. A. Iles, et al., Proton MR spectroscopy of intracranial tumors: in vivo and in vitro studies. J Comput Assist Tomogr **14**, 497–504 (1990).

109. C. Remy, M. Von Kienlin, S. Lotito, A. Francois, A. L. Benabid and M. Decorps, In vivo 1H NMR spectroscopy of an intracerebral glioma in the rat. Magn Reson Med **9**, 395–401 (1989).

110. R. J. Gillies, J. A. Barry and B. D. Ross, In vitro and in vivo 13C and 31P NMR analyses of phosphocholine metabolism in rat glioma cells. Magn Reson Med **32**, 310–318 (1994).

111. B. L. Miller, L. Chang, R. Booth, T. Ernst, M. Cornford, D. Nikas, D. McBride and D. J. Jenden, In vivo 1H MRS choline: correlation with in vitro chemistry/histology. Life Sci **58**, 1929–1935 (1996).

112. D. Morvan, A. Demidem, J. Papon and J. C. Madelmont, Quantitative HRMAS proton total correlation spectroscopy applied to cultured melanoma cells treated by chloroethyl nitrosourea: demonstration of phospholipid metabolism alterations. Magn Reson Med **49**, 241–248 (2003).

113. Y. Kinoshita and A. Yokota, Absolute concentrations of metabolites in human brain tumors using in vitro proton magnetic resonance spectroscopy. NMR Biomed **10**, 2–12 (1997).

114. B. F. Jordan, K. Black, I. F. Robey, M. Runquist, G. Powis and R. J. Gillies, Metabolite changes in HT-29 xenograft tumors following HIF-1 alpha inhibition with PX-478 as studied by MR spectroscopy in vivo and ex vivo. NMR Biomed **18**, 430–439 (2005).

115. J. Ross, A. M. Najjar, M. Sankaranarayanapillai, W. P. Tong, K. Kaluarachchi and S. M. Ronen, Fatty acid synthase inhibition results in a magnetic resonance-detectable drop in phosphocholine. Mol Cancer Ther **7**, 2556–2565 (2008).

116. D. Koul, R. J. Shen, Y. W. Kim, Y. Kondo, Y. L. Lu, J. Bankson, S. M. Ronen, D. L. Kirkpatrick, G. Powis and W. K. A. Yung, Cellular and in vivo activity of a novel PI3K inhibitor, PX-866, against human glioblastoma. Neuro-Oncology **12**, 559–569 (2010).

117. A. T. Baykal, M. R. Jain and H. Li, Aberrant regulation of choline metabolism by mitochondrial electron transport system inhibition in neuroblastoma cells. Metabolomics **4**, 347–356 (2008).

118. K. Glunde, V. Raman, N. Mori and Z. M. Bhujwalla, RNA interference-mediated choline kinase suppression in breast cancer cells induces differentiation and reduces proliferation. Cancer Res **65**, 11034–11043 (2005).

119. B. Krishnamachary, K. Glunde, F. Wildes, N. Mori, T. Takagi, V. Raman and Z. M. Bhujwalla, Noninvasive detection of lentiviral-mediated choline kinase targeting in a human breast cancer xenograft. Cancer Res **69**, 3464–3471 (2009).

120. N. M. Al-Saffar, H. Troy, A. Ramirez de Molina, L. E. Jackson, B. Madhu, J. R. Griffiths, M. O. Leach, P. Workman, J. C. Lacal, et al., Noninvasive magnetic resonance spectroscopic pharmacodynamic markers of the choline kinase inhibitor MN58b in human carcinoma models. Cancer Res **66**, 427–434 (2006).

121. P. E. Sijens, M. J. van den Bent, P. J. Nowak, P. van Dijk and M. Oudkerk, 1H chemical shift imaging reveals loss of brain tumor choline signal after administration of Gd-contrast. Magn Reson Med **37**, 222–225 (1997).

122. A. P. Lin and B. D. Ross, Short-echo time proton MR spectroscopy in the presence of gadolinium. J Comput Assist Tomogr **25**, 705–712 (2001).

123. B. Madhu, S. P. Robinson, F. A. Howe and J. R. Griffiths, Effect of Gd-DTPA-BMA on choline signals of HT29 tumors detected by in vivo 1H MRS. J Magn Reson Imaging **28**, 1201–1208 (2008).

124. R. E. Lenkinski, X. Wang, M. Elian and S. N. Goldberg, Interaction of gadolinium-based MR contrast agents with choline: implications for MR spectroscopy (MRS) of the breast. Magn Reson Med **61**, 1286–1292 (2009).

125. D. L. Morse, N. Raghunand, P. Sadarangani, S. Murthi, C. Job, S. Day, C. Howison and R. J. Gillies, Response of choline metabolites to docetaxel therapy is quantified in vivo by localized (31)P MRS of human breast cancer xenografts and in vitro by high-resolution (31)P NMR spectroscopy of cell extracts. Magn Reson Med **58**, 270–280 (2007).

126. L. R. Jensen, E. M. Huuse, T. F. Bathen, P. E. Goa, A. M. Bofin, T. B. Pedersen, S. Lundgren and I. S. Gribbestad, Assessment of early docetaxel response in an experimental model of human breast cancer using DCE-MRI, ex vivo HR MAS, and in vivo 1H MRS. NMR Biomed **23**, 56–65 (2010).

127. J. M. Hakumaki, H. Poptani, A. M. Sandmair, S. Yla-Herttuala and R. A. Kauppinen, 1H MRS detects polyunsaturated fatty acid accumulation during gene therapy of glioma: implications for the in vivo detection of apoptosis. Nat Med **5**, 1323–1327 (1999).

128. C. E. Mountford and L. C. Wright, Organization of lipids in the plasma membranes of malignant and stimulated cells: a new model. Trends Biochem Sci **13**, 172–177 (1988).

129. C. Remy, N. Fouilhe, I. Barba, E. Sam-Lai, H. Lahrech, M. G. Cucurella, M. Izquierdo, A. Moreno, A. Ziegler, et al., Evidence that mobile lipids detected in rat brain glioma by 1H nuclear magnetic resonance correspond to lipid droplets. Cancer Res **57**, 407–414 (1997).

130. K. S. Opstad, B. A. Bell, J. R. Griffiths and F. A. Howe, An investigation of human brain tumor lipids by high-resolution magic angle spinning 1H MRS and histological analysis. NMR Biomed **21**, 677–685 (2008).

131. J. E. Schmitz, M. I. Kettunen, D. E. Hu and K. M. Brindle, 1H MRS-visible lipids accumulate during apoptosis of lymphoma cells in vitro and in vivo. Magn Reson Med **54**, 43–50 (2005).

132. S. Zoula, G. Herigault, A. Ziegler, R. Farion, M. Decorps and C. Remy, Correlation between the occurrence of 1H-MRS lipid signal, necrosis and lipid droplets during C6 rat glioma development. NMR Biomed **16**, 199–212 (2003).

133. A. Knijn, A. Ferretti, P. J. Zhang, M. Giambenedetti, A. Molinari, S. Meschini, S. Pulciani and F. Podo, Lower levels of 1H MRS-visible mobile lipids in H-ras transformed tumorigenic fibroblasts with respect to their untransformed parental cells. Cell Mol Biol (Noisy-le-grand) **43**, 691–701 (1997).

134. M. M. Mahon, N. M. deSouza, R. Dina, W. P. Soutter, G. A. McIndoe, A. D. Williams and I. J. Cox, Preinvasive and invasive cervical cancer: an ex vivo proton magic angle spinning magnetic resonance spectroscopy study. NMR Biomed **17**, 144–153 (2004).

135. V. Righi, A. Mucci, L. Schenetti, M. R. Tosi, W. F. Grigioni, B. Corti, A. Bertaccini, A. Franceschelli, F. Sanguedolce, et al., Ex vivo HR-MAS magnetic resonance spectroscopy of normal and malignant human renal tissues. Anticancer Res **27**, 3195–3204 (2007).

136. J. Griffitts, Y. Tesiram, G. E. Reid, D. Saunders, R. A. Floyd and R. A. Towner, In vivo MRS assessment of altered fatty acyl unsaturation in liver tumor formation of a TGF alpha/c-myc transgenic mouse model. J Lipid Res **50**, 611–622 (2009).

137. V. Righi, A. Mucci, L. Schenetti, A. Bacci, R. Agati, M. Leonardi, R. Schiavina, G. Martorana, G. Liguori, et al., Identification of mobile lipids in human cancer tissues by ex vivo diffusion edited HR-MAS MRS. Oncol Rep **22**, 1493–1496 (2009).

138. K. Stenman, J. B. Hauksson, G. Grobner, P. Stattin, A. Bergh and K. Riklund, Detection of polyunsaturated omega-6 fatty acid in human malignant prostate tissue by 1D and 2D high-resolution magic angle spinning NMR spectroscopy. MAGMA **22**, 327–331 (2009).

139. J. R. Griffiths, D. J. McIntyre, F. A. Howe and M. Stubbs, Why are cancers acidic? A carrier-mediated diffusion model for H+ transport in the interstitial fluid. Novartis Found Symp **240**, 46–62; discussion 62-47, 152–153 (2001).

140. R. J. Gillies, Z. Liu and Z. Bhujwalla, 31P-MRS measurements of extracellular pH of tumors using 3-aminopropylphosphonate. Am J Physiol **267**, C195–203 (1994).

141. R. van Sluis, Z. M. Bhujwalla, N. Raghunand, P. Ballesteros, J. Alvarez, S. Cerdan, J. P. Galons and R. J. Gillies, In vivo imaging of extracellular pH using 1H MRSI. Magn Reson Med **41**, 743–750 (1999).

142. R. A. Gatenby and R. J. Gillies, Why do cancers have high aerobic glycolysis? Nat Rev Cancer **4**, 891–899 (2004).

143. A. Roos and W. F. Boron, Intracellular pH. Physiol Rev **61**, 296–434 (1981).

144. W. H. Moolenaar, Effects of growth factors on intracellular pH regulation. Annu Rev Physiol **48**, 363–376 (1986).

145. S. S. Ober and A. B. Pardee, Intracellular pH is increased after transformation of Chinese hamster embryo fibroblasts. Proc Natl Acad Sci U S A **84**, 2766–2770 (1987).

146. S. J. Reshkin, A. Bellizzi, S. Caldeira, V. Albarani, I. Malanchi, M. Poignee, M. Alunni-Fabbroni, V. Casavola and M. Tommasino, Na+/H+ exchanger-dependent intracellular alkalinization is an early event in malignant transformation and plays an essential role in the development of subsequent transformation-associated phenotypes. FASEB J **14**, 2185–2197 (2000).

147. P. Swietach, R. D. Vaughan-Jones and A. L. Harris, Regulation of tumor pH and the role of carbonic anhydrase 9. Cancer Metastasis Rev **26**, 299–310 (2007).

148. B. A. Webb, M. Chimenti, M. P. Jacobson and D. L. Barber, Dysregulated pH: a perfect storm for cancer progression. Nature Reviews Cancer **11**, 671–677 (2011).

149. S. K. Parks, J. Chiche and J. Pouyssegur, pH control mechanisms of tumor survival and growth. Journal of Cellular Physiology **226**, 299–308 (2011).

150. Y. Ihara, Y. Kihara, F. Hamano, K. Yanagida, Y. Morishita, A. Kunita, T. Yamori, M. Fukayama, H. Aburatani, et al., The G protein-coupled receptor T-cell death-associated gene 8 (TDAG8) facilitates tumor development by serving as an extracellular pH sensor. Proc Natl Acad Sci U S A **107**, 17309–17314 (2010).

151. D. Fukumura, L. Xu, Y. Chen, T. Gohongi, B. Seed and R. K. Jain, Hypoxia and acidosis independently up-regulate vascular endothelial growth factor transcription in brain tumors in vivo. Cancer Res **61**, 6020–6024 (2001).

152. L. Xu, D. Fukumura and R. K. Jain, Acidic extracellular pH induces vascular endothelial growth factor (VEGF) in human glioblastoma cells via ERK1/2 MAPK signaling pathway: mechanism of low pH-induced VEGF. J Biol Chem **277**, 11368–11374 (2002).

153. J. Rozhin, M. Sameni, G. Ziegler and B. F. Sloane, Pericellular pH affects distribution and secretion of cathepsin B in malignant cells. Cancer Res **54**, 6517–6525 (1994).

154. I. F. Robey, B. K. Baggett, N. D. Kirkpatrick, D. J. Roe, J. Dosescu, B. F. Sloane, A. I. Hashim, D. L. Morse, N. Raghunand, et al., Bicarbonate increases tumor pH and inhibits spontaneous metastases. Cancer Res **69**, 2260–2268 (2009).

155. M. Stubbs, Z. M. Bhujwalla, G. M. Tozer, L. M. Rodrigues, R. J. Maxwell, R. Morgan, F. A. Howe and J. R. Griffiths, An assessment of 31P MRS as a method of measuring pH in rat tumors. NMR Biomed **5**, 351–359 (1992).

156. G. E. Soto, Z. Zhu, J. L. Evelhoch and J. J. Ackerman, Tumor 31P NMR pH measurements in vivo: a comparison of inorganic phosphate and intracellular 2-deoxyglucose-6-phosphate as pHnmr indicators in murine radiation-induced fibrosarcoma-1. Magn Reson Med **36**, 698–704 (1996).

157. J. S. Taylor, D. B. Vigneron, J. Murphy-Boesch, S. J. Nelson, H. B. Kessler, L. Coia, W. Curran and T. R. Brown, Free magnesium levels in normal human brain and brain tumors: 31P chemical-shift imaging measurements at 1.5 T. Proc Natl Acad Sci U S A **88**, 6810–6814 (1991).

158. D. Maintz, W. Heindel, H. Kugel, R. Jaeger and K. J. Lackner, Phosphorus-31 MR spectroscopy of normal adult human brain and brain tumors. NMR Biomed **15**, 18–27 (2002).

159. T. A. Cadoux-Hudson, M. J. Blackledge, B. Rajagopalan, D. J. Taylor and G. K. Radda, Human primary brain tumor metabolism in vivo: a phosphorus magnetic resonance spectroscopy study. Br J Cancer **60**, 430–436 (1989).

160. K. Glunde and Z. M. Bhujwalla, Metabolic tumor imaging using magnetic resonance spectroscopy. Semin Oncol **38**, 26–41 (2011).

161. S. He, R. P. Mason, S. Hunjan, V. D. Mehta, V. Arora, R. Katipally, P. V. Kulkarni and P. P. Antich, Development of novel 19F NMR pH indicators: synthesis and evaluation of a series of fluorinated vitamin B6 analogues. Bioorg Med Chem **6**, 1631–1639 (1998).

162. R. P. Mason, Transmembrane pH gradients in vivo: measurements using fluorinated vitamin B6 derivatives. Curr Med Chem **6**, 481–499 (1999).

163. A. S. Ojugo, P. M. McSheehy, D. J. McIntyre, C. McCoy, M. Stubbs, M. O. Leach, I. R. Judson and J. R. Griffiths, Measurement of the extracellular pH of solid tumors in mice by magnetic resonance spectroscopy: a comparison of exogenous (19)F and (31)P probes. NMR Biomed **12**, 495–504 (1999).

164. R. J. Gillies and D. L. Morse, In vivo magnetic resonance spectroscopy in cancer. Annu Rev Biomed Eng **7**, 287–326 (2005).

165. D. L. Rabenstein and A. A. Isab, Determination of the intracellular pH of intact erythrocytes by 1H NMR spectroscopy. Anal Biochem **121**, 423–432 (1982).

166. S. Gil, P. Zaderenzo, F. Cruz, S. Cerdan and P. Ballesteros, Imidazol-1-ylalkanoic acids as extrinsic 1H NMR probes for the determination of intracellular pH, extracellular pH and cell volume. Bioorg Med Chem **2**, 305–314 (1994).

167. M. L. Garcia-Martin, G. Herigault, C. Remy, R. Farion, P. Ballesteros, J. A. Coles, S. Cerdan and A. Ziegler, Mapping extracellular pH in rat brain gliomas in vivo by 1H magnetic resonance spectroscopic imaging: comparison with maps of metabolites. Cancer Res **61**, 6524–6531 (2001).

168. P. Provent, M. Benito, B. Hiba, R. Farion, P. Lopez-Larrubia, P. Ballesteros, C. Remy, C. Segebarth, S. Cerdan, et al., Serial in vivo spectroscopic nuclear magnetic resonance imaging of lactate and extracellular pH in rat gliomas shows redistribution of protons away from sites of glycolysis. Cancer Res **67**, 7638–7645 (2007).

169. D. W. Hoffman and R. W. Henkens, The rates of fast reactions of carbon dioxide and bicarbonate in human erythrocytes measured by carbon-13 NMR. Biochem Biophys Res Commun **143**, 67–73 (1987).

170. C. Arus, Y. C. Chang and M. Barany, The separation of phosphocreatine from creatine, and pH determination in frog muscle by natural abundance 13C-NMR. Biochim Biophys Acta **844**, 91–93 (1985).

171. F. A. Gallagher, M. I. Kettunen, S. E. Day, D. E. Hu, J. H. Ardenkjaer-Larsen, R. Zandt, P. R. Jensen, M. Karlsson, K. Golman, et al., Magnetic resonance imaging of pH in vivo using hyperpolarized 13C-labeled bicarbonate. Nature **453**, 940–943 (2008).

172. E. O. Aboagye, R. J. Maxwell, M. R. Horsman, A. D. Lewis, P. Workman, M. Tracy and J. R. Griffiths, The relationship between tumor oxygenation determined by oxygen electrode measurements and magnetic resonance spectroscopy of the fluorinated 2-nitroimidazole SR-4554. Br J Cancer **77**, 65–70 (1998).

173. B. M. Seddon, G. S. Payne, L. Simmons, R. Ruddle, R. Grimshaw, S. Tan, A. Turner, F. Raynaud, G. Halbert, et al., A phase I study of SR-4554 via intravenous administration for noninvasive investigation of tumor hypoxia by magnetic resonance spectroscopy in patients with malignancy. Clin Cancer Res **9**, 5101–5112 (2003).

174. R. P. Mason, W. Rodbumrung and P. P. Antich, Hexafluorobenzene: a sensitive 19F NMR indicator of tumor oxygenation. NMR Biomed **9**, 125–134 (1996).

175. B. J. Dardzinski and C. H. Sotak, Rapid tissue oxygen tension mapping using 19F inversion-recovery echo-planar imaging of perfluoro-15-crown-5-ether. Magn Reson Med **32**, 88–97 (1994).

176. L. Bogin, M. Z. Papa, S. Polak-Charcon and H. Degani, TNF-induced modulations of phospholipid metabolism in human breast cancer cells. Biochim Biophys Acta **1392**, 217–232 (1998).

177. N. W. Lutz, M. E. Tome and P. J. Cozzone, Early changes in glucose and phospholipid metabolism following apoptosis induction by IFN-gamma/TNF-alpha in HT-29 cells. FEBS Lett **544**, 123–128 (2003).

178. J. I. Johnsen, M. Lindskog, F. Ponthan, I. Pettersen, L. Elfman, A. Orrego, B. Sveinbjornsson and P. Kogner, Cyclooxygenase-2 is expressed in neuroblastoma, and nonsteroidal anti-inflammatory drugs induce apoptosis and inhibit tumor growth in vivo. Cancer Res **64**, 7210–7215 (2004).

179. M. Lindskog, C. Spenger, J. Jarvet, A. Graslund and P. Kogner, Predicting resistance or response to chemotherapy by proton magnetic resonance spectroscopy in neuroblastoma. J Natl Cancer Inst **96**, 1457–1466 (2004).

180. M. Muruganandham, A. A. Alfieri, C. Matei, Y. Chen, G. Sukenick, I. Schemainda, M. Hasmann, L. B. Saltz and J. A. Koutcher, Metabolic signatures associated with a NAD synthesis inhibitor-induced tumor apoptosis identified by 1H-decoupled-

31P magnetic resonance spectroscopy. Clin Cancer Res **11**, 3503–3513 (2005).

181. J. E. Schmitz, M. I. Kettunen, D. E. Hu and K. M. Brindle, H-1 MRS-visible lipids accumulate during apoptosis of lymphoma cells in vitro and in vivo. Magn Reson Med **54**, 43–50 (2005).

182. K. S. Opstad, B. A. Bell, J. R. Griffiths and F. A. Howe, Taurine: a potential marker of apoptosis in gliomas. Br J Cancer **100**, 789–794 (2009).

183. T. Liimatainen, J. M. Hakumaki, R. A. Kauppinen and M. Ala-Korpela, Monitoring of gliomas in vivo by diffusion MRI and H-1 MRS during gene therapy-induced apoptosis: interrelationships between water diffusion and mobile lipids. Nmr in Biomedicine **22**, 272–279 (2009).

184. A. C. Kuesel, G. R. Sutherland, W. Halliday and I. C. Smith, 1H MRS of high grade astrocytomas: mobile lipid accumulation in necrotic tissue. NMR Biomed **7**, 149–155 (1994).

185. F. A. Howe and K. S. Opstad, H-1 MR spectroscopy of brain tumors and masses. NMR Biomed **16**, 123–131 (2003).

186. A. R. Tate, J. Underwood, D. M. Acosta, M. Julia-Sape, C. Majos, A. Moreno-Torres, F. A. Howe, M. V. Graaf, V. Lefournier, et al., Development of a decision support system for diagnosis and grading of brain tumors using in vivo magnetic resonance single voxel spectra. NMR Biomed **19**, 411–434 (2006).

187. M. Julià-Sapé, I. Coronel, C. Majós, A. P. Candiota, M. Serrallonga, M. Cos, C. Aguilera, J. J. Acebes, J. R. Griffiths and C. Arús, Prospective diagnostic performance evaluation of single-voxel (1) H MRS for typing and grading of brain tumors. NMR Biomed (2011).

188. J. Kurhanewicz and D. B. Vigneron, Advances in MR spectroscopy of the prostate. Magn Reson Imaging Clin N Am **16**, 697–710, ix-x (2008).

189. M. T. Nelson, L. I. Everson, M. Garwood, T. Emory and P. J. Bolan, MR Spectroscopy in the diagnosis and treatment of breast cancer. Semin Breast Dis **11**, 100–105 (2008).

190. F. S. De Edelenyi, C. Rubin, F. Esteve, S. Grand, M. Decorps, V. Lefournier, J. F. Le Bas and C. Remy, A new approach for analyzing proton magnetic resonance spectroscopic images of brain tumors: nosologic images. Nature Medicine **6**, 1287–1289 (2000).

191. T. C. Ng, W. T. Evanochko, R. N. Hiramoto, V. K. Ghanta, M. B. Lilly, A. J. Lawson, T. H. Corbett, J. R. Durant and J. D. Glickson, 31P NMR spectroscopy of in vivo tumors. Journal of Magnetic Resonance **49**, 271–286 (1982).

192. G. M. Tozer, Z. M. Bhujwalla, J. R. Griffiths and R. J. Maxwell, Phosphorus-31 magnetic resonance spectroscopy and blood perfusion of the RIF-1 tumor following X-irradiation. International Journal of Radiation Oncology Biology and Physics **16**, 155–164 (1989).

193. W. T. Evanochko, T. C. Ng, M. B. Lilly, A. J. Lawson, T. H. Corbett, J. R. Durant and J. D. Glickson, In vivo P31 NMR study of the metabolism of murine mammary 16/C adenocarcinoma and its response to chemotherapy, x-radiation, and hyperthermia. Proceedings of the National Academy of Sciences of the United States of America-Biological Sciences **80**, 334–338 (1983).

194. J. A. Koutcher, P. Okunieff, L. Neuringer, H. Suit and T. Brady, Size dependent changes in tumor phosphate metabolism after radiation therapy as detected by P31 NMR spectroscopy. International Journal of Radiation Oncology Biology Physics **13**, 1851–1855 (1987).

195. U. Mahmood, A. A. Alfieri, H. Thaler, D. Cowburn and J. A. Koutcher, Radiation dose-dependent changes in tumor metabolism measured by P31 nuclear magnetic resonance spectroscopy. Cancer Res **54**, 4885–4891 (1994).

196. U. Mahmood, A. A. Alfieri, D. Ballon, F. Traganos and J. A. Koutcher, In-vitro and in-vivo P31 nuclear magnetic resonance measurements of metabolic changes post radiation. Cancer Res **55**, 1248–1254 (1995).

197. P. E. Sijens, W. Bovee, D. Seijkens, G. Los and D. H. Rutgers, In vivo P31 nuclear magnetic resonance study of the response of a murine mammary tumor to different doses of gamma-radiation. Cancer Res **46**, 1427–1432 (1986).

198. E. K. Rofstad, P. Demuth, B. M. Fenton, T. L. Ceckler and R. M. Sutherland, P31 NMR spectroscopy and HbO_2 cryospectrophotometry in prediction of tumor radioresistance caused by hypoxia. International Journal of Radiation Oncology Biology Physics **16**, 919–923 (1989).

199. K. K. Fu, M. F. Wendland, S. B. Iyer, K. N. Lam, H. Engeseth and T. L. James, Correlations between in vivo 31P NMR spectroscopy measurements, tumor size, hypoxic fraction and cell survival after radiotherapy. Int J Radiat Oncol Biol Phys **18**, 1341–1350 (1990).

200. J. A. Koutcher, A. A. Alfieri, A. B. Kornblith, M. L. Devitt, D. Cowburn, D. Ballon and J. H. Kim, Changes in Radiation Sensitization Induced by Fluosol-DA as Measured by 31P Nuclear Magnetic Resonance Spectroscopy. Cancer Res **50**, 7252–7256 (1990).

201. W. Semmler, G. Gademann, P. Bachertbaumann, H. J. Zabel, W. J. Lorenz and G. Vankaick, Monitoring human tumor response to therapy by means of P31 MR spectroscopy. Radiology **166**, 533–539 (1988).

202. T. C. Ng, S. Grundfest, S. Vijayakumar, N. J. Baldwin, A. W. Majors, I. Karalis, T. F. Meaney, K. H. Shin, F. J. Thomas and R. Tubbs, Therapeutic response of breast carcinoma monitored by P31 MRS in situ. Magn Reson Med **10**, 125–134 (1989).

203. M. O. Leach, M. Verrill, J. Glaholm, T. A. D. Smith, D. J. Collins, G. S. Payne, J. C. Sharp, S. M. Ronen, V. R. McCready, et al., Measurements of human breast cancer using magnetic resonance spectroscopy: a review of clinical measurements and a report of localized P-31 measurements of response to treatment. NMR Biomed **11**, 314–340 (1998).

204. D. M. Prescott, H. C. Charles, H. D. Sostman, R. K. Dodge, D. E. Thrall, R. L. Page, J. A. Tucker, J. M. Harrelson, K. A. Leopold, et al., Therapy monitoring in human and canine soft-tissue sarcomas using magnetic resonance imaging and spectroscopy. International Journal of Radiation Oncology Biology Physics **28**, 415–423 (1994).

205. S. K. Szigety, P. S. Allen, D. Huyserwierenga and R. C. Urtasun, The effect of radiation on normal human CNS as detected by NMR spectroscopy. International Journal of Radiation Oncology Biology Physics **25**, 695–701 (1993).

206. D. Brandsma, L. Stalpers, W. Taal, P. Sminia and M. van den Bent, Clinical features, mechanisms, and management of pseudoprogression in malignant gliomas. Lancet Oncology **9**, 453–461 (2008).

207. J. D. Rabinov, P. L. Lee, F. G. Barker, D. N. Louis, G. R. Harsh, G. R. Cosgrove, E. A. Chiocca, A. F. Thornton, J. S. Loeffler, et al., In vivo 3-T MR spectroscopy in the distinction of recurrent glioma versus radiation effects: Initial experience. Radiology **225**, 871–879 (2002).

208. M. C. Preul, R. Leblanc, Z. Caramanos, R. Kasrai, S. Narayanan and D. L. Arnold, Magnetic resonance spectroscopy guided brain tumor resection: Differentiation between recurrent glioma and radiation change in two diagnostically difficult cases. Canadian Journal of Neurological Sciences **25**, 13–22 (1998).

209. H. P. Schlemmer, P. Bachert, K. K. Herfarth, I. Zuna, J. Debus and G. van Kaick, Proton MR spectroscopic evaluation of suspicious brain lesions after stereotactic radiotherapy. American Journal of Neuroradiology **22**, 1316–1324 (2001).

210. M. A. Heesters, R. L. Kamman, E. L. Mooyaart and K. G. Go, Localized proton spectroscopy of inoperable brain gliomas. Response to radiation therapy. J Neurooncol **17**, 27–35 (1993).

211. A. Bizzi, B. Movsas, G. Tedeschi, C. L. Phillips, P. Okunieff, J. R. Alger and G. Dichiro, Response of non-Hodgkin lymphoma to radiation therapy - early and long-term assessment with H1 MR spectroscopic imaging. Radiology **194**, 271–276 (1995).

212. T. Usenius, J. P. Usenius, M. Tenhunen, P. Vainio, R. Johansson, S. Soimakallio and R. Kauppinen, Radiation-induced changes in human brain metabolites as studied by H1 nuclear magnetic resonance spectroscopy in vivo. International Journal of Radiation Oncology Biology Physics **33**, 719–724 (1995).

213. J. S. Taylor, J. W. Langston, W. E. Reddick, P. B. Kingsley, R. J. Ogg, M. H. Pui, L. E. Kun, J. J. Jenkins, G. Chen, et al., Clinical value of proton magnetic resonance spectroscopy for differentiating recurrent or residual brain tumor from delayed cerebral necrosis. International Journal of Radiation Oncology Biology Physics **36**, 1251–1261 (1996).

214. L. L. Wald, S. J. Nelson, M. R. Ray, S. E. Noworolski, R. G. Henry, S. L. Huhn, S. Chang, M. D. Prados, P. K. Sneed, et al., Serial proton magnetic resonance spectroscopy imaging of glioblastoma multiforme after brachytherapy. Journal of Neurosurgery **87**, 525–534 (1997).

215. F. Esteve, C. Rubin, S. Grand, H. Kolodie and J. F. Le Bas, Transient metabolic changes observed with proton MR spectroscopy in normal human brain after radiation therapy. International Journal of Radiation Oncology Biology Physics **40**, 279–286 (1998).

216. S. M. Waldrop, P. C. Davis, C. A. Padgett, M. B. Shapiro and R. Morris, Treatment of brain tumors in children is associated with abnormal MR spectroscopic ratios in brain tissue remote from the tumor site. American Journal of Neuroradiology **19**, 963–970 (1998).

217. J. A. Lazareff, R. K. Gupta and J. Alger, Variation of post-treatment H-MRSI choline signal intensity in pediatric gliomas. Journal of Neuro-Oncology **41**, 291–298 (1999).

218. Y. L. Chan, D. K. W. Yeung, S. F. Leung and G. Cao, Proton magnetic resonance spectroscopy of late delayed radiation-induced injury of the brain. Journal of Magnetic Resonance Imaging **10**, 130–137 (1999).

219. V. F. H. Chong, H. Rumpel, Y. F. Fan and S. K. Mukherji, Temporal lobe changes following radiation therapy: imaging and proton MR spectroscopic findings. European Radiology **11**, 317–324 (2001).

220. H. P. Schlemmer, P. Bachert, M. Henze, R. Buslei, K. K. Herfarth, J. Debus and G. van Kaick, Differentiation of radiation necrosis from tumor progression using proton magnetic resonance spectroscopy. Neuroradiology **44**, 216–222 (2002).

221. E. E. Graves, S. J. Nelson, D. B. Vigneron, L. Verhey, M. McDermott, D. Larson, S. Chang, M. D. Prados and W. P. Dillon, Serial proton MR spectroscopic imaging of recurrent malignant gliomas after gamma knife radiosurgery. AJNR Am J Neuroradiol **22**, 613–624 (2001).

222. C. Dowling, A. W. Bollen, S. M. Noworolski, M. W. McDermott, N. M. Barbaro, M. R. Day, R. G. Henry, S. M. Chang, W. P. Dillon, et al., Preoperative proton MR spectroscopic imaging of brain tumors: correlation with histopathologic analysis of resection specimens.[see comment]. Ajnr: American Journal of Neuroradiology **22**, 604–612 (2001).

223. J. P. Rock, D. Hearshen, L. Scarpace, D. Croteau, J. Gutierrez, J. L. Fisher, M. L. Rosenblum and T. Mikkelsen, Correlations between magnetic resonance spectroscopy and image-guided histopathology, with special attention to radiation necrosis. Neurosurgery **51**, 912–919 (2002).

224. R. Tarnawski, M. Sokol, P. Pieniazek, B. Maciejewski, J. Walecki, L. Miszczyk and T. Krupska, H-1-MRS in vivo predicts the early treatment outcome of postoperative radiotherapy for malignant gliomas. International Journal of Radiation Oncology Biology Physics **52**, 1271–1276 (2002).

225. P. Weybright, P. C. Sundgren, P. Maly, D. G. Hassan, B. Nan, S. Rohrer and L. Junck, Differentiation between brain tumor recurrence and radiation injury using MR spectroscopy. American Journal of Roentgenology **185**, 1471–1476 (2005).

226. A. Pirzkall, T. R. McKnight, E. E. Graves, M. P. Carol, P. K. Sneed, W. W. Wara, S. J. Nelson, L. J. Verhey and D. A. Larson, MR-spectroscopy guided target delineation for high-grade gliomas. International Journal of Radiation Oncology Biology Physics **50**, 915–928 (2001).

227. A. Pirzkall, S. J. Nelson, T. R. McKnight, M. M. Takahashi, X. J. Li, E. E. Graves, L. J. Verhey, W. W. Wara, D. A. Larson and P. K. Sneed, Metabolic imaging of low-grade gliomas with three-dimensional magnetic resonance spectroscopy. International Journal of Radiation Oncology Biology Physics **53**, 1254–1264 (2002).

228. A. Pirzkall, X. J. Li, J. M. Oh, S. Chang, M. S. Berger, D. A. Larson, L. J. Verhey, W. P. Dillon and S. J. Nelson, 3D MRSI for resected high-grade gliomas before RT: Tumor extent according to metabolic activity in relation to MRI. International Journal of Radiation Oncology Biology Physics **59**, 126–137 (2004).

229. A. Laprie, A. Pirzkall, D. A. Haas-Kogan, S. Cha, A. Banerjee, T. P. Le, Y. Lu, S. Nelson and T. R. McKnight, Longitudinal multivoxel MR spectroscopy study of pediatric diffuse brainstem gliomas treated with radiotherapy. International Journal of Radiation Oncology Biology Physics **62**, 20–31 (2005).

230. F. V. Coakley, H. S. Teh, A. Qayyum, M. G. Swanson, Y. Lu, M. Roach, B. Pickett, K. Shinohara, D. B. Vigneron and J. Kurhanewicz, Endorectal MR imaging MR spectroscopic imaging for locally recurrent prostate cancer after external beam radiation therapy: Preliminary experience. Radiology **233**, 441–448 (2004).

231. J. Pouliot, Y. Kim, E. Lessard, I. C. Hsu, D. B. Vigneron and J. Kurhanewicz, Inverse planning for HDR prostate brachytherapy used to boost dominant intraprostatic lesions defined by magnetic resonance spectroscopy imaging. International Journal of Radiation Oncology Biology Physics **59**, 1196–1207 (2004).

232. J. A. Jung, F. V. Coakley, D. B. Vigneron, M. G. Swanson, A. Qayyum, V. Weinberg, K. D. Jones, P. R. Carroll and J. Kurhanewicz, Prostate depiction at endorectal MR spectroscopic imaging: Investigation of a standardized evaluation system. Radiology **233**, 701–708 (2004).

233. B. Pickett, R. K. Ten Haken, J. Kurhanewicz, A. Qayyum, K. Shinohara, B. Fein and M. Roach, Time to metabolic atrophy after permanent prostate seed implantation based on magnetic resonance spectroscopic imaging. International Journal of Radiation Oncology Biology Physics **59**, 665–673 (2004).

234. B. Pickett, J. Kurhanewicz, F. Coakley, K. Shinohara, B. Fein and M. Roach, Use of MRI and spectroscopy in evaluation of external beam radiotherapy for prostate cancer. International Journal of Radiation Oncology Biology Physics **60**, 1047–1055 (2004).

235. D. Pucar, A. Shukla-Dave, H. Hricak, C. S. Moskowitz, K. Kuroiwa, S. Olgac, L. E. Ebora, P. T. Scardino, J. A. Koutcher and K. L. Zakian, Prostate cancer: Correlation of MR Imaging and MR spectroscopy with pathologic findings after radiation therapy - Initial experience. Radiology **236**, 545–553 (2005).

236. C. Menard, I. C. P. Smith, R. L. Somorjai, L. Leboldus, R. Patel, C. Littman, S. J. Robertson and T. Bezabeh, Magnetic resonance spectroscopy of the malignant prostate gland after radiotherapy: A histopathologic study of diagnostic validity. International Journal of Radiation Oncology Biology Physics **50**, 317–323 (2001).

237. A. D. King, D. K. W. Yeung, K. H. Yu, F. K. F. Mo, K. S. Bhatia, G. M. K. Tse, A. C. Vlantis, J. K. T. Wong, C. W. Hu and A. T. Ahuja, Pre-treatment and Early Intratreatment Prediction of Clinicopathologic Response of Head and Neck Cancer to Chemoradiotherapy Using H-1-MRS. Journal of Magnetic Resonance Imaging **32**, 199–203 (2010).

238. Z. M. Bhujwalla and J. D. Glickson, Detection of tumor response to radiation therapy by in vivo proton MR spectroscopy. International Journal of Radiation Oncology Biology Physics **36**, 635–639 (1996).

239. D. C. Shungu and J. D. Glickson, Band-selective spin echoes for in vivo localized 1H NMR spectroscopy. Magn Reson Med **32**, 277–284 (1994).

240. E. O. Aboagye, Z. M. Bhujwalla, Q. H. He and J. D. Glickson, Evaluation of lactate as a H-1 nuclear magnetic resonance spectroscopy index for noninvasive prediction and early detection of tumor response to radiation therapy in EMT6 tumors. Radiation Research **150**, 38–42 (1998).

241. V. Quennet, A. Yaromina, D. Zips, A. Rosner, S. Walenta, M. Baumann and W. Mueller-Klieser, Tumor lactate content predicts for response to fractionated irradiation of human squamous cell carcinomas in nude mice. Radiotherapy and Oncology **81**, 130–135 (2006).

242. J. P. Dyke, K. L. Zakian, W. M. Spees, C. Matei, Y. C. Chen, M. L. Mao, D. C. Shungu and J. A. Koutcher, Metabolic response of the CWR22 prostate tumor xenograft after 20 Gy of radiation studied by H-1 spectroscopic imaging. Clin Cancer Res **9**, 4529–4536 (2003).

243. S. E. Day, M. I. Kettunen, M. K. Cherukuri, J. B. Mitchell, M. J. Lizak, H. D. Morris, S. Matsumoto, A. P. Koretsky and K. M. Brindle, Detecting Response of Rat C6 Glioma Tumors to Radiotherapy Using Hyperpolarized 1-(13)C Pyruvate and (13)C Magnetic Resonance Spectroscopic Imaging. Magn Reson Med **65**, 557–563 (2011).

244. W. Semmler, G. Gademann, P. Schlag, P. Bachertbaumann, H. J. Zabel, W. J. Lorenz and G. Vonkaick, Impact of hyperthermic regional perfusion therapy on cell metabolism of malignant melanoma monitored by P31 MR spectroscopy. Magnetic Resonance Imaging **6**, 335–340 (1988).

245. C. Kettelhack, M. V. Wickede, T. Vogl, U. Schneider and P. Hohenberger, (31)phosphorus-magnetic resonance spectroscopy to assess histologic tumor response noninvasively after isolated limb perfusion for soft tissue tumors. Cancer **94**, 1557–1564 (2002).

246. A. Shukla-Dave, H. Poptani, L. A. Loevner, A. Mancuso, H. Serrai, D. I. Rosenthal, A. M. Kilger, D. S. Nelson, K. L. Zakian, et al., Prediction of treatment response of head and neck cancers with P-31 MR spectroscopy from pre-treatment relative phosphomonoester levels. Academic Radiology **9**, 688–694 (2002).

247. E. Proietti, G. Carpinelli, M. Divito, F. Belardelli, I. Gresser and F. Podo, P31-nuclear magnetic-resonance analysis of interferon-induced alterations of phospholipid metabolites in interferon-sensitive and interferon-resistant Friend-leukemia cell tumors in mice. Cancer Res **46**, 2849–2857 (1986).

248. C. Allavena, J. L. Guerquin-Kern and J. M. Lhoste, Follow-up by 31P NMR spectroscopy of the energy metabolism of malignant tumor in rats during treatment. Radiother Oncol **21**, 48–52 (1991).

249. D. A. Beauregard, P. E. Thelwall, D. J. Chaplin, S. A. Hill, G. E. Adams and K. M. Brindle, Magnetic resonance imaging and spectroscopy of combretastatin A(4) prodrug-induced disruption of tumor perfusion and energetic status. British Journal of Cancer **77**, 1761–1767 (1998).

250. D. A. Beauregard, R. B. Pedley, S. A. Hill and K. M. Brindle, Differential sensitivity of two adenocarcinoma xenografts to the anti-vascular drugs combretastatin A4 phosphate and 5,6-dimethylxanthenone-4-acetic acid, assessed using MRI and MRS. NMR Biomed **15**, 99–105 (2002).

251. L. D. McPhail, Y. L. Chung, B. Madhu, S. Clark, J. R. Griffiths, L. R. Kelland and S. P. Robinson, Tumor dose response to the vascular disrupting agent, 5,6-dimethylxanthenone-4-acetic acid, using in vivo magnetic resonance spectroscopy. Clin Cancer Res **11**, 3705–3713 (2005).

252. J. A. Koutcher, M. Motwani, K. L. Zakian, X. K. Li, C. Matei, J. P. Dyke, D. Ballon, H. H. Yoo and G. K. Schwartz, The in vivo effect of bryostatin-1 on paclitaxel-induced tumor growth, mitotic entry, and blood flow. Clin Cancer Res **6**, 1498–1507 (2000).

253. G. R. Silberhumer, K. Zakian, S. Malhotra, P. Brader, M. Gonen, J. Koutcher and Y. Fong, Relationship between P-31 metabolites and oncolytic viral therapy sensitivity in human colorectal cancer xenografts. British Journal of Surgery **96**, 809–816 (2009).

254. J. Klawitter, D. J. Kominsky, J. L. Brown, U. Christians, D. Leibfritz, J. V. Melo, S. G. Eckhardt and N. J. Serkova, Metabolic characteristics of imatinib resistance in chronic myeloid leukaemia cells. British Journal of Pharmacology **158**, 588–600 (2009).

255. J. A. Koutcher, A. A. Alfieri, C. Matei, K. L. Meyer, J. C. Street and D. S. Martin, Effect of 6-aminonicotinamide on the pentose phosphate pathway: P-31 NMR and tumor growth delay studies. Magn Reson Med **36**, 887–892 (1996).

256. N. M. S. Al-Saffar, L. E. Jackson, F. I. Raynaud, P. A. Clarke, A. R. de Molina, J. C. Lacal, P. Workman and M. O. Leach, The Phosphoinositide 3-Kinase Inhibitor PI-103 Downregulates Choline Kinase a Leading to Phosphocholine and Total Choline Decrease Detected by Magnetic Resonance Spectroscopy. Cancer Res **70**, 5507–5517 (2010).

257. Y. L. Chung, H. Troy, U. Banerji, L. E. Jackson, M. I. Walton, M. Stubbs, J. R. Griffiths, I. R. Judson, M. O. Leach, et al., Magnetic resonance spectroscopic pharmacodynamic markers of the heat shock protein 90 inhibitor 17-allylamino,17-demethoxygeldanamycin (17AAG) in human colon cancer models. Journal of the National Cancer Institute **95**, 1624–1633 (2003).

258. A. H. Brandes, C. S. Ward and S. M. Ronen, 17-allyamino-17-demethoxygeldanamycin treatment results in a magnetic resonance spectroscopy-detectable elevation in choline-containing metabolites associated with increased expression of choline transporter SLC44A1 and phospholipase A2. Breast Cancer Research **12**, R84 (2010).

259. Y. L. Chung, H. Troy, R. Kristeleit, W. Aherne, E. Jackson, P. Atadja, J. R. Griffiths, I. R. Judson, P. Workman, et al., Noninvasive magnetic resonance spectroscopic pharmacodynamic markers of a novel histone deacetylase inhibitor, LAQ824, in human colon carcinoma cells and xenografts. Neoplasia **10**, 303–313 (2008).

260. M. Sankaranarayanapillai, W. P. Tong, D. S. Maxwell, A. Pal, J. H. Pang, W. G. Bornmann, J. G. Gelovani and S. M. Ronen, Detection of histone deacetylase inhibition by noninvasive magnetic resonance spectroscopy. Molecular Cancer Therapeutics **5**, 1325–1334 (2006).

261. M. Sterin, J. S. Cohen, Y. Mardor, E. Berman and I. Ringel, Levels of phospholipid metabolites in breast cancer cells treated with antimitotic drugs: A P-31-magnetic resonance spectroscopy study. Cancer Res **61**, 7536–7543 (2001).

262. L. M. Rodrigues, R. J. Maxwell, P. M. McSheehy, C. R. Pinkerton, S. P. Robinson, M. Stubbs and J. R. Griffiths, In vivo detection of ifosfamide by 31P-MRS in rat tumors: increased uptake and cytotoxicity induced by carbogen breathing in GH3 prolactinomas. Br J Cancer **75**, 62–68 (1997).

263. L. M. Rodrigues, S. P. Robinson, P. M. J. McSheehy, M. Stubbs and J. R. Griffiths, Enhanced uptake of ifosfamide into GH3 prolactinomas with hypercapnic hyperoxic gases monitored in vivo by P-31 MRS. Neoplasia **4**, 539–543 (2002).

264. G. S. Payne, C. R. Pinkerton, E. Bouffet and M. O. Leach, Initial measurements of ifosfamide and cyclophosphamide in patients using P-31 MRS: Pulse-and-acquire, decoupling, and polarization transfer. Magn Reson Med **44**, 180–184 (2000).

265. L. Mancini, G. S. Payne, A. S. K. Dzik-Jurasz and M. O. Leach, Ifosfamide pharmacokinetics and hepatobiliary uptake in vivo investigated using single- and double-resonance P-31 MRS. Magn Reson Med **50**, 249–255 (2003).

266. G. S. Payne, A. S. K. Dzik-Jurasz, L. Mancini, B. Nutley, F. Raynaud and M. O. Leach, Identification of biliary metabolites of ifosfamide using P-31 magnetic resonance spectroscopy and mass spectrometry. Cancer Chemotherapy and Pharmacology **56**, 409–414 (2005).

267. S. T. Fricke, O. Rodriguez, J. VanMeter, L. E. Dettin, M. Casimiro, C. D. Chien, T. Newell, K. Johnson, L. Ileva, et al., In vivo magnetic resonance volumetric and spectroscopic analysis of mouse prostate Cancer Models. The Prostate **66**, 708–717 (2006).

268. D. C. Shungu, Z. M. Bhujwalla, J. P. Wehrle and J. D. Glickson, 1H NMR spectroscopy of subcutaneous tumors in mice: preliminary studies of effects of growth, chemotherapy and blood flow reduction. NMR Biomed **5**, 296–302 (1992).

269. Y. Mardor, O. Kaplan, M. Sterin, J. Ruiz-Cabello, E. Ash, Y. Roth, I. Ringel and J. S. Cohen, Noninvasive real-time monitoring of intracellular cancer cell metabolism and response to lonidamine treatment using diffusion weighted proton magnetic resonance spectroscopy. Cancer Res **60**, 5179–5186 (2000).

270. P. C. M. van Zijl, C. T. W. Moonen, P. Faustino, J. Pekar, O. Kaplan and J. S. Cohen, Complete separation of intracellular and extracellular information in NMR spectra of perfused cells by diffusion-weighted spectroscopy. Proceedings of the National Academy of Sciences of the United States of America **88**, 3228–3232 (1991).

271. K. Natarajan, N. Mori, D. Artemov and Z. M. Bhujwalla, Exposure of human breast cancer cells to the anti-inflammatory agent indomethacin alters choline phospholipid metabolites and Nm23 expression. Neoplasia **4**, 409–416 (2002).

272. M. Q. Huang, D. S. Nelson, S. Pickup, H. Qiao, E. J. Delikatny, H. Poptani and J. D. Glickson, In vivo monitoring response to chemotherapy of human diffuse large B-cell lymphoma xenografts in SCID mice by 1H and 31P MRS. Acad Radiol **14**, 1531–1539 (2007).

273. S. C. Lee, M. Q. Huang, D. S. Nelson, S. Pickup, S. Wehrli, O. Adegbola, H. Poptani, E. J. Delikatny and J. D. Glickson, In vivo MRS markers of response to CHOP chemotherapy in the WSU-DLCL2 human diffuse large B-cell lymphoma xenograft. NMR Biomed **21**, 723–733 (2008).

274. A. J. Schwarz, N. R. Maisey, D. J. Collins, D. Cunningham, R. Huddart and M. O. Leach, Early in vivo detection of metabolic response: a pilot study of 1H MR spectroscopy in extracranial lymphoma and germ cell tumors. **75**, 959–966 (2002).

275. J. R. Griffiths, A. R. Tate, F. A. Howe, M. Stubbs and G. Multi Inst, Magnetic Resonance Spectroscopy of cancer - practicalities of multi-centre trials and early results in non-Hodgkin's lymphoma. European Journal of Cancer **38**, 2085–2093 (2002).

276. S. C. Lee, E. J. Delikatny, H. Poptani, S. Pickup and J. D. Glickson, In vivo H-1 MRS of WSU-DLCL2 human non-Hodgkin's lymphoma xenografts: response to rituximab and rituximab plus CHOP. NMR Biomed **22**, 259–265 (2009).

277. H. M. Baek, J. H. Chen, K. Nie, H. J. Yu, S. Bahri, R. S. Mehta, O. Nalcioglu and M. Y. Su, Predicting pathologic response to neoadjuvant chemotherapy in breast cancer by using MR imaging and quantitative 1H MR spectroscopy. Radiology **251**, 653–662 (2009).

278. M. Tozaki, M. Sakamoto, Y. Oyama, T. O'Uchi, N. Kawano, T. Suzuki, N. Yamashiro, S. Ozaki, N. Sakamoto, et al., Monitoring of early response to neoadjuvant chemotherapy in breast cancer with H-1 MR spectroscopy: Comparison to sequential 2- 18F - fluorodeoxyglucose positron emission tomography. Journal of Magnetic Resonance Imaging **28**, 420–427 (2008).

279. U. Sharma, H. M. Baek, M. Y. Su and N. R. Jagannathan, In vivo (1)H MRS in the assessment of the therapeutic response of breast cancer patients. NMR Biomed **24**, 700–711 (2011).

280. C. Balmaceda, D. Critchell, X. L. Mao, K. Cheung, S. Pannullo, R. L. DeLaPaz and D. C. Shungu, Multisection H-1 magnetic resonance spectroscopic imaging assessment of glioma response to chemotherapy. Journal of Neuro-Oncology **76**, 185–191 (2006).

281. J. P. Dyke, P. C. Sanelli, H. U. Voss, J. V. Serventi, P. E. Stieg, T. H. Schwartz, D. Ballon, D. C. Shungu and S. C. Pannullo, Monitoring the effects of BCNU chemotherapy Wafers (Gliadel (R)) in glioblastoma multiforme with proton magnetic resonance spectroscopic imaging at 3.0 Tesla. Journal of Neuro-Oncology **82**, 103–110 (2007).

282. T. Sankar, Z. Caramanos, R. Assina, J. G. Villemure, R. Leblanc, A. Langleben, D. L. Arnold and M. C. Preul, Prospective serial proton MR spectroscopic assessment of response to tamoxifen for recurrent malignant glioma. Journal of Neuro-Oncology **90**, 63–76 (2008).

283. M. C. Preul, Z. Caramanos, J. G. Villemure, G. Shenouda, R. LeBlanc, A. Langleben and D. L. Arnold, Using proton magnetic resonance spectroscopic imaging to predict in vivo the response of recurrent malignant gliomas to tamoxifen chemotherapy. Neurosurgery **46**, 306–318 (2000).

284. N. R. Jagannathan, M. Singh, V. Govindaraju, P. Raghunathan, O. Coshic, P. K. Julka and G. K. Rath, Volume localized in vivo proton MR spectroscopy of breast carcinoma: variation of water-fat ratio in patients receiving chemotherapy. NMR Biomed **11**, 414–422 (1998).

285. D. J. Manton, A. Chaturvedi, A. Hubbard, M. J. Lind, M. Lowry, A. Maraveyas, M. D. Pickles, D. J. Tozer and L. W. Turnbull, Neoadjuvant chemotherapy in breast cancer: early response prediction with quantitative MR imaging and spectroscopy. Br J Cancer **94**, 427–435 (2006).

286. P. E. G. Kristjansen, B. Quistorff, M. Spangthomsen and H. H. Hansen, Intratumoral pharmacokinetic analysis by F19 magnetic resonance spectroscopy and cytostatic in-vivo activity of gemcitabine (DFDC) in 2 small-cell lung-cancer xenografts. Annals of Oncology **4**, 157–160 (1993).

287. A. W. Blackstock, H. Lightfoot, L. D. Case, J. E. Tepper, S. K. Mukherji, B. S. Mitchell, S. G. Swarts and S. M. Hess, Tumor uptake and elimination of 2′,2′-difluoro-2′-deoxycytidine (gemcitabine) after deoxycytidine kinase gene transfer: correlation with in vivo tumor response. Clin Cancer Res **7**, 3263–3268 (2001).

288. G. O. Cron, N. Beghein, R. Ansiaux, P. Martinive, O. Feron and B. Gallez, F-19 NMR in vivo spectroscopy reflects the effectiveness of perfusion-enhancing vascular modifiers for improving gemcitabine chemotherapy. Magn Reson Med **59**, 19–27 (2008).

289. K. P. Olive, M. A. Jacobetz, C. J. Davidson, A. Gopinathan, D. McIntyre, D. Honess, B. Madhu, M. A. Goldgraben, M. E. Caldwell, et al., Inhibition of Hedgehog Signaling Enhances Delivery of Chemotherapy in a Mouse Model of Pancreatic Cancer. Science **324**, 1457–1461 (2009).

290. H. Pinedo and G. Peters, Fluorouracil: biochemistry and pharmacology. J Clin Oncol **6**, 1653–1664 (1988).

291. P. M. J. McSheehy, M. T. Seymour, A. S. E. Ojugo, L. M. Rodrigues, M. O. Leach, I. R. Judson and J. R. Griffiths, A pharmacokinetic and pharmacodynamic study in vivo of human HT29 tumors using F-19 and P-31 magnetic resonance spectroscopy. European Journal of Cancer **33**, 2418–2427 (1997).

292. N. W. Lutz, B. Naser-Hijazi, S. Koroma, M. R. Berger and W. E. Hull, Fluoropyrimidine chemotherapy in a rat model: comparison of fluorouracil metabolite profiles determined by high-field F-19-NMR spectroscopy of tissues ex vivo with therapy response and toxicity for locoregional vs systemic infusion protocols. NMR Biomed **17**, 101–131 (2004).

293. Y. Doi, T. Shimmura, H. Kuribayashi, Y. Tanaka and Y. Kanazawa, Quantitative 19F imaging of nmol-level F-nucleotides/-sides from 5-FU with T2 mapping in mice at 9.4T. Magn Reson Med **62**, 1129–1139 (2009).

294. A. S. K. Dzik-Jurasz, D. J. Collins, M. O. Leach and I. J. Rowland, Gallbladder localization of 19F MRS catabolite signals in patients receiving bolus and protracted venous infusional 5-fluorouracil. Magn Reson Med **44**, 516–520 (2000).

295. M.-C. Malet-Martino, R. Martino, A. Lopez, J.-P. Béteille, M. Bon, J. Bernadou and J.-P. Armand, New approach to metabolism of 5′-deoxy-5-fluorouridine in humans with fluorine-19 NMR. Cancer Chemotherapy and Pharmacology **13**, 31–35 (1984).

296. A. N. Stevens, P. G. Morris, R. A. Iles, P. W. Sheldon and J. R. Griffiths, 5-fluorouracil metabolism monitored in vivo by 19F NMR. Br J Cancer **50**, 113–117 (1984).

297. W. Wolf, M. J. Albright, M. S. Silver, H. Weber, U. Reichardt and R. Sauer, Fluorine-19 NMR spectroscopic studies of the metabolism of 5-fluorouracil in the liver of patients undergoing chemotherapy. Magn Reson Imaging **5**, 165–169 (1987).

298. W. Wolf, C. A. Presant, K. L. Servis, A. El-Tahtawy, M. J. Albright, P. B. Barker, Ring R, III, D. Atkinson, R. Ong, et al., Tumor Trapping of 5-Fluorouracil: In vivo 19F NMR Spectroscopic Pharmacokinetics in Tumor-Bearing Humans and Rabbits. Proceedings of the National Academy of Sciences **87**, 492–496 (1990).

299. C. A. Presant, W. Wolf, V. Waluch, C. Wiseman, P. Kennedy, D. Blayney and R. R. Brechner, Association of intratumoral pharmacokinetics of fluorouracil with clinical response. The Lancet **343**, 1184–1187 (1994).

300. W. Wolf, V. Waluch and C. A. Presant, Non-invasive F-19-NMRS of 5-fluorouracil in pharmacokinetics and pharmacodynamic studies. NMR Biomed **11**, 380–387 (1998).

301. W. Wolf, C. A. Presant and V. Waluch, 19F-MRS studies of fluorinated drugs in humans. Advanced Drug Delivery Reviews **41**, 55–74 (2000).

302. C. A. Presant, W. Wolf, V. Waluch, C. L. Wiseman, I. Weitz and J. Shani, Enhancement of Fluorouracil Uptake in Human Colorectal and Gastric Cancers by Interferon or by High-Dose Methotrexate: An In Vivo Human Study Using Noninvasive 19F-Magnetic Resonance Spectroscopy. Journal of Clinical Oncology **18**, 255–000 (2000).

303. C. A. Presant, J. Jacobson, W. Wolf, V. Waluch, I. C. Weitz and J. S. Macdonald, Does Leucovorin Alter the Intratumoral Pharmacokinetics of 5-Fluorouracil (5-FU)? A Southwest Oncology Group Study. Investigational New Drugs **20**, 369–376 (2002).

304. A. El-Tahtawy and W. Wolf, In Vivo Measurements of Intratumoral Metabolism, Modulation, and Pharmacokinetics of 5-Fluorouracil, Using 19F Nuclear Magnetic Resonance Spectroscopy. Cancer Res **51**, 5806–5812 (1991).

305. J.-L. Guerquin-Kern, F. Leteurtre, A. Croisy and J.-M. Lhoste, pH Dependence of 5-Fluorouracil Uptake Observed by in Vivo 31P and 19F Nuclear Magnetic Resonance Spectroscopy. Cancer Res **51**, 5770–5773 (1991).

306. L. E. Gerweck, J. G. Rhee, A. K. Jason, C. W. Song and M. Urano, Regulation of pH in Murine Tumor and Muscle. Radiation Research **126**, 206–209 (1991).

307. A. S. E. Ojugo, P. M. J. McSheehy, M. Stubbs, G. Alder, C. L. Bashford, R. J. Maxwell, M. O. Leach, I. R. Judson and J. R. Griffiths, Influence of pH on the uptake of 5-fluorouracil into isolated tumor cells. Br J Cancer **77**, 873–879 (1998).

308. P. M. J. McSheehy, H. Troy, L. R. Kelland, I. R. Judson, M. O. Leach and J. R. Griffiths, Increased tumor extracellular pH induced by Bafilomycin A(1) inhibits tumor growth and mitosis in vivo and alters 5-fluorouracil pharmacokinetics. European Journal of Cancer **39**, 532–540 (2003).

309. L. P. Lemaire, P. M. J. McSheehy and J. R. Griffiths, Pre-treatment energy status of primary rat tumors as the best predictor of response to 5-fluorouracil chemotherapy: a magnetic resonance spectroscopy study in vivo. Cancer Chemotherapy and Pharmacology **42**, 201–209 (1998).

310. W. Semmler, P. Bachert-Baumann, F. Gückel, F. Ermark, P. Schlag, W. J. Lorenz and G. van Kaick, Real-time follow-up of 5-fluorouracil metabolism in the liver of tumor patients by means of F-19 MR spectroscopy. Radiology **174**, 141–145 (1990).

311. M. P. N. Findlay, M. O. Leach, D. Cunningham, D. J. Collins, G. S. Payne, J. Glaholm, J. L. Mansi and V. R. McCready, The non-invasive monitoring of low dose, infusional 5-fluorouracil and its modulation by interferon-α using in vivo 19F magnetic resonance spectroscopy in patients with colorectal cancer: A pilot study. Annals of Oncology **4**, 597–602 (1993).

312. H. P. Schlemmer, P. Bachert, W. Semmler, P. Hohenberger, P. Schlag, W. J. Lorenz and G. van Kaick, Drug monitoring of 5-fluorouracil: in vivo 19F NMR study during 5-FU chemotherapy in patients with metastases of colorectal adenocarcinoma. Magn Reson Imaging **12**, 497–511 (1994).

313. C. W. Li, W. G. Negendank, K. A. Padavic-Shaller, P. J. O'Dwyer, J. Murphy-Boesch and T. R. Brown, Quantitation of 5-fluorouracil catabolism in human liver in vivo by three-dimensional localized 19F magnetic resonance spectroscopy. Clin Cancer Res **2**, 339–345 (1996).

314. J. Murphy-Boesch, C.-W. Li, L. He, K. A. Padavic-Shaller, W. Negendank and T. R. Brown, Proton-decoupled ^{19}F spectroscopy of 5-FU catabolites in human liver. Magn Reson Med **37**, 321–326 (1997).

315. C. W. Li and O. Gonen, Simultaneous 3D NMR spectroscopy of fluorine and phosphorus in human liver during 5-fluorouracil chemotherapy. Magn Reson Med **35**, 841–847 (1996).

316. D. W. Klomp, H. W. Van Laarhoven, A. P. Kentgens and A. Heerschap, Optimization of localized 19F magnetic resonance spectroscopy for the detection of fluorinated drugs in the human liver. Magn Reson Med **50**, 303–308 (2003).

317. H. W. M. van Laarhoven, D. W. J. Klomp, M. Rijpkema, Y. L. P. Kamm, D. J. T. Wagener, J. O. Barentsz, C. J. A. Punt and A. Heerschap, Prediction of chemotherapeutic response of colorectal liver metastases with dynamic gadolinium-DTPA-enhanced MRI and localized F-19 MRS pharmacokinetic studies of 5-fluorouracil. NMR Biomed **20**, 128–140 (2007).

318. P. S. Tofts, G. Brix, D. L. Buckley, J. L. Evelhoch, E. Henderson, M. Knopp, H. B. W. Larsson, T. Y. Lee, N. A. Mayr, et al., Estimating kinetic parameters from dynamic contrast-enhanced T- 1-weighted MRI of a diffusable tracer: Standardized quantities and symbols. Journal of Magnetic Resonance Imaging **10**, 223–232 (1999).

319. J. R. Griffiths, D. J. O. McIntyre, F. A. Howe, P. M. J. McSheehy, A. S. E. Ojugo, L. M. Rodrigues, P. Wadsworth, N. M. Price, F. Lofts, et al., Issues of normal tissue toxicity in patient and animal studies - Effect of carbogen breathing in rats after 5-fluorouracil treatment. Acta Oncologica **40**, 609–614 (2001).

320. D. J. O. McIntyre, F. A. Howe, C. Ladroue, F. Lofts, M. Stubbs and J. R. Griffiths, Can localised 19F magnetic resonance spectroscopy pharmacokinetics of 5FU in colorectal metastases predict clinical response? Cancer Chemotherapy and Pharmacology **68**, 29–36 (2011).

321. P. M. J. McSheehy, S. P. Robinson, A. S. E. Ojugo, E. O. Aboagye, M. B. Cannell, M. O. Leach, I. R. Judson and J. R. Griffiths, Carbogen breathing increases 5-fluorouracil uptake and cytotoxicity in hypoxic murine RIF-1 tumors: A magnetic resonance study in vivo. Cancer Res **58**, 1185–1194 (1998).

322. P. M. J. McSheehy, R. E. Port, L. M. Rodrigues, S. P. Robinson, M. Stubbs, K. van der Borns, G. J. Peters, I. R. Judson, M. O. Leach and J. R. Griffiths, Investigations in vivo of the effects of carbogen breathing on 5-fluorouracil pharmacokinetics and physiology of solid rodent tumours. Cancer Chemotherapy and Pharmacology **55**, 117–128 (2005).

323. Y. J. L. Kamm, A. Heerschap and D. J. T. Wagener, Effect of carbogen breathing on the pharmacodynamics of 5-fluorouracil in a murine colon carcinoma. European Journal of Cancer **36**, 1180–1186 (2000).

324. Y. J. L. Kamm, G. J. Peters, W. E. Hull, C. J. A. Punt and A. Heerschap, Correlation between 5-fluorouracil metabolism and treatment response in two variants of C26 murine colon carcinoma. Br J Cancer **89**, 754–762 (2003).

325. H. W. M. van Laarhoven, G. Gambarota, J. Lok, M. Lammens, Y. L. M. Kamm, T. Wagener, C. J. A. Punt, A. J. van der Kogelz and A. Heerschap, Carbogen breathing differentially enhances blood plasma volume and 5-fluorouracil uptake in two murine colon tumor models with a distinct vascular structure. Neoplasia **8**, 477–487 (2006).

326. P. M. McSheehy, M. J. Prior and J. R. Griffiths, Prediction of 5-fluorouracil cytotoxicity towards the Walker carcinosarcoma using peak integrals of fluoronucleotides measured by MRS in vivo. Br J Cancer **60**, 303–309 (1989).

327. P. McSheehy, M. Prior and J. Griffiths, Enhanced 5-fluorouracil cytotoxicity and elevated 5-fluoronucleotides in the rat Walker carcinosarcoma following methotrexate pre-treatment: a 19F-MRS study in vivo. Br J Cancer **65**, 369–375 (1992).

328. M. J. Prior, R. J. Maxwell and J. R. Griffiths, In vivo 19F NMR spectroscopy of the antimetabolite 5-fluorouracil and its analogues. An assessment of drug metabolism. Biochemical Pharmacology **39**, 857–863 (1990).

329. S. K. Holland, A. M. Bergman, Y. Zhao, E. R. Adams and G. Pizzorno, 19F NMR monitoring of in vivo tumor metabolism after biochemical modulation of 5-fluorouracil by the uridine phosphorylase inhibitor 5-benzylacyclouridine. Magn Reson Med **38**, 907–916 (1997).

330. H. W. M. van Laarhoven, D. W. J. Klomp, Y. J. L. Kamm, C. J. A. Punt and A. Heerschap, In Vivo Monitoring of Capecitabine Metabolism in Human Liver by 19Fluorine Magnetic Resonance Spectroscopy at 1.5 and 3 Tesla Field Strength. Cancer Res **63**, 7609–7612 (2003).

331. D. Klomp, H. van Laarhoven, T. Scheenen, Y. Kamm and A. Heerschap, Quantitative 19F MR spectroscopy at 3 T to detect heterogeneous capecitabine metabolism in human liver. NMR Biomed **20**, 485–492 (2007).

332. Y.-L. Chung, H. Troy, I. R. Judson, R. Leek, M. O. Leach, M. Stubbs, A. L. Harris and J. R. Griffiths, Noninvasive Measurements of Capecitabine Metabolism in Bladder Tumors Overexpressing Thymidine Phosphorylase by Fluorine-19 Magnetic Resonance Spectroscopy. Clin Cancer Res **10**, 3863–3870 (2004).

333. H. Poptani, N. Bansal, W. T. Jenkins, D. Blessington, A. Mancuso, D. S. Nelson, M. Feldman, E. J. Delikatny, B. Chance and J. D. Glickson, Cyclophosphamide treatment modifies tumor oxygenation and glycolytic rates of RIF-1 tumors: 13C magnetic resonance spectroscopy, Eppendorf electrode, and redox scanning. Cancer Res **63**, 8813–8820 (2003).

334. D. Rivenzon-Segal, S. Boldin-Adamsky, D. Seger, R. Seger and H. Degani, Glycolysis and glucose transporter 1 as markers of response to hormonal therapy in breast cancer. International Journal of Cancer **107**, 177–182 (2003).

335. T. H. Witney, M. I. Kettunen, S. E. Day, D. E. Hu, A. A. Neves, F. A. Gallagher, S. M. Fulton and K. M. Brindle, A Comparison between Radiolabeled Fluorodeoxyglucose Uptake and Hyperpolarized C-13-Labeled Pyruvate Utilization as Methods for Detecting Tumor Response to Treatment. Neoplasia **11**, 574–U588 (2009).

336. P. Seth, A. Grant, J. Tang, E. Vinogradov, X. Wang, R. Lenkinski and V. P. Sukhatme, On-target inhibition of tumor fermentative glycolysis as visualized by hyperpolarized pyruvate. Neoplasia **13**, 60–71 (2011).

337. I. Park, R. Bok, T. Ozawa, J. J. Phillips, C. D. James, D. B. Vigneron, S. M. Ronen and S. J. Nelson, Detection of Early Response to Temozolomide Treatment in Brain Tumors Using Hyperpolarized (13)C MR Metabolic Imaging. Journal of Magnetic Resonance Imaging **33**, 1284–1290 (2011).

338. F. A. Gallagher, M. I. Kettunen, D. E. Hu, P. R. Jensen, R. in't Zandt, M. Karlsson, A. Gisselsson, S. K. Nelson, T. H. Witney, et al., Production of hyperpolarized 1,4-(13)C(2) malate from 1,4-(13)C(2) fumarate is a marker of cell necrosis and treatment response in tumors. Proceedings of the National Academy of Sciences of the United States of America **106**, 19801–19806 (2009).

339. S. E. Bohndiek, M. I. Kettunen, D. E. Hu, T. H. Witney, B. W. C. Kennedy, F. A. Gallagher and K. M. Brindle, Detection of Tumor Response to a Vascular Disrupting Agent by Hyperpolarized C-13 Magnetic Resonance Spectroscopy. Molecular Cancer Therapeutics **9**, 3278–3288 (2010).

340. T. H. Witney, M. I. Kettunen, D. E. Hu, F. A. Gallagher, S. E. Bohndiek, R. Napolitano and K. M. Brindle, Detecting treatment response in a model of human breast adenocarcinoma using hyperpolarised 1-C-13 pyruvate and 1,4-C-13(2) fumarate. British Journal of Cancer **103**, 1400–1406 (2010).

341. C. S. Ward, H. S. Venkatesh, M. M. Chaumeil, A. H. Brandes, M. Vancriekinge, H. Dafni, S. Sukumar, S. J. Nelson, D. B. Vigneron, et al., Noninvasive detection of target modulation following phosphatidylinositol 3-kinase inhibition using hyperpolarized 13C magnetic resonance spectroscopy. Cancer Res **70**, 1296–1305 (2010).